Determination of Energy Band Parameters of Phosphorus Doped Carbon/Silicon Heterojunction

A thesis submitted to

the Department of Electrical and Electronic Engineering of

Bangladesh University of Engineering and Technology

in partial fulfillment of the requirement

for the degree of

MASTER OF SCIENCE IN ELECTRICAL AND ELECTRONIC ENGINEERING

by

Mohammad Hasanuzzaman

DEPARTMENT OF ELECTRICAL AND ELECTRONIC ENGINEERING

BANGLADESH UNIVERSITY OF ENGINEERING AND TECHNOLOGY

2003

The thesis titled **"Determination of Energy Band Parameters of Phosphorus Doped Carbon/Silicon Heterojunction"** submitted by Mohammad Hasanuzzaman, Roll no.: 100106236P, Session: October 2001 has been accepted as satisfactory in partial fulfillment of the requirement for the degree of MASTER OF SCIENCE IN ELECTRICAL AND ELECTRONIC ENGINEERING on July 15, 2003.

BOARD OF EXAMINERS

1. ______________________________

Dr. Sharif Mohammad Mominuzzaman — **Chairman** (Supervisor)
Assistant Professor
Department of Electrical and Electronic Engineering
Bangladesh University of Engineering and Technology
Dhaka-1000, Bangladesh

2. ______________________________ 15/7/2003

Dr. Mohammad Ali Choudhury — **Member** (Ex-Officio)
Professor and Head
Department of Electrical and Electronic Engineering
Bangladesh University of Engineering and Technology
Dhaka-1000, Bangladesh

3. ______________________________ 15/7/2003

Dr. Quazi Deen Mohd Khosru — **Member**
Professor
Department of Electrical and Electronic Engineering
Bangladesh University of Engineering and Technology
Dhaka-1000, Bangladesh

4. ______________________________

Dr. Md. Abu Hashan Bhuiyan — **Member (External)**
Professor
Department of Physics
Bangladesh University of Engineering and Technology
Dhaka-1000, Bangladesh

Declaration

It is hereby declared that this thesis or any part of it has not been submitted elsewhere for the award of any degree or diploma.

Signature of the candidate

(Mohammad Hasanuzzaman)

Dedication

To My Parents

Contents

Declaration ii

Dedication iii

List of Figures v

List of Tables ix

Acknowledgements xi

Abstract xii

1 Introduction 1

1.1 Background 2

1.2 Objective of the work 5

1.3 Thesis Layout 5

2 Review of Carbon Research, Introduction to Camphoric Carbon Films for its Device Applications and Heterojunction Device Modeling 7

2.1 Various Forms of Carbon. 8

2.2 Present Status of Carbon Research 10

2.3 Un-doped Camphoric Carbon Films........ 21

2.3.1 Target Preparation 22

2.3.2 Un-doped Camphoric Carbon Film Deposition by Pulsed Laser Deposition 23

2.4 P-doped Camphoric Carbon Film and its Deposition by PLD .. 24

2.5 P-doped n-DLC/p-Si Heterostructure and its Deposition Procedure........ 25

2.6 Theory of Constructing Energy Band Diagram for Heterojunction Device........ 26

3 Results and Discussions 34

3.1 Analysis of Capacitance-Voltage Characteristics........ 34

3.2 Analysis of Current Density-Voltage Characteristics........ 59

3.3 Results and Discussions........ 67

4 Conclusions 85

4.1 Conclusions........ 85

4.2 Suggestions for Future Works........ 87

References 88

List of Figures

2.1	The structure of hexagonal single crystal graphite......................	9
2.2	The ideal diamond structure...	9
2.3	Chemical structure of camphor molecule ($C_{10}H_{16}O$)..................	22
2.4	Schematic representation of camphor burning system.................	23
2.5	Experimental setup of pulsed laser deposition (PLD) technique for the deposition of thin film..	25
2.6	Schematic view of the n-C/p-Si heterojunction........................	26
2.7	Energy band diagram of an ideal n-p heterojunction at equilibrium.	28
2.8	Current-voltage characteristics of a practical Si diode.................	33
3.1	Capacitance versus voltage characteristics for n-DLC/p-Si heterojunction where, DLC thin film has been deposited from the target containing 1% phosphorus...	37
3.2	Capacitance versus voltage characteristics for n-DLC/p-Si heterojunction where, DLC thin film has been deposited from the target containing 3% phosphorus...	37
3.3	Capacitance versus voltage characteristics for n-DLC/p-Si heterojunction where, DLC thin film has been deposited from the target containing 5% phosphorus...	38
3.4	Capacitance versus voltage characteristics for n-DLC/p-Si heterojunction where, DLC thin film has been deposited from the target containing 7% phosphorus...	38
3.5	Capacitance versus voltage characteristics for n-DLC/p-Si heterojunction where, DLC film has been deposited from target containing 1%, 3%, 5% and 7% phosphorus...........................	39
3.6	C^{-2} vs V characteristics for n-DLC/p-Si heterojunction where, carbon thin films are deposited from the target containing 1%, 3%, 5% and 7% phosphorus and the extrapolation of the linear part of the characteristics for the low reverse bias voltage....................	40

3.7 Variation of carrier concentration in n-DLC and the built-in potential of the heterojunction with % phosphorus in the target material from where the films are grown 42

3.8 Optical band gap and activation energy for silicon.................... 42

3.9 ln(σ) vs T^{-1} to calculate activation energy and conductivity prefactor for different phosphorus contents in the target............. 45

3.10 Variation of activation energy of DLC with dopant content in the target material.. 46

3.11 Variation of conductivity prefactor with the change in dopant content in the target material.. 47

3.12 Variation of room temperature conductivity with the change in dopant content in the target material.................................... 47

3.13 Variation of optical transmittance with wavelength.................. 49

3.14 Variation of optical reflectance with wavelength..................... 49

3.15 Variation of extinction coefficient with photon energy.............. 51

3.16 Variation of refractive index with photon energy.................... 51

3.17 Variation of relative permittivity with photon energy................ 52

3.18 Variation of optical gap as a function of %P content in the target. 53

3.19 Energy band diagram constructed from practical data for heterojunction where, the carbon thin film is deposited from target containing 1% phosphorus.. 56

3.20 Energy band diagram constructed from practical data for heterojunction where, the carbon thin film is deposited from target containing 3% phosphorus.. 56

3.21 Energy band diagram constructed from practical data for heterojunction where, the carbon thin film is deposited from target containing 5% phosphorus.. 57

3.22 Energy band diagram constructed from practical data for heterojunction where, the carbon thin film is deposited from target containing 7% phosphorus.. 57

3.23	Variation of electron affinity for the experimental data with dopant contents in the target material from where the films are grown..	58
3.24	Variation of conduction band discontinuity and valance band discontinuity for the experimental data with dopant contents in the target from where the films are grown................................	58
3.25	Current density-voltage characteristics for the heterojunction for the films grown from targets containing different dopant contents..	59
3.26	Current density-voltage characteristics to calculate the built-in potential for the heterojunction for different dopant contents (1%, 3%, 5% and 7% phosphorus) in the target material.................	60
3.27	Variation of built-in potential calculated from current density-voltage characteristics with dopant content in the target material...	61
3.28	ln(J) vs V characteristics to calculate the diode quality factor for films deposited from target containing different dopant contents...	62
3.29	Extrapolation of ln(J) vs V characteristics to calculate J_0............	64
3.30	Variation of reverse saturation current with dopant content in the target from where the films are grown.................................	65
3.31	Variation of intrinsic carrier concentration in carbon thin film with dopant content in the target material..................................	69
3.32	Variation of donor carrier concentration in carbon thin film with dopant content in target material..	69
3.33	Variation of electron mobility in carbon thin film with dopant content in the target..	71
3.34	Variation of ESR spin density of the carbon film as a function of % P in the target..	72
3.35	Variation of hole diffusion length in carbon thin film with the variation of dopant content in the target...............................	74
3.36	Variation of minority carrier life time in carbon thin film with the variation of dopant content in the target...............................	74

3.37 Proposed energy band diagram constructed for n-carbon/p-silicon heterojunction where, the carbon thin film is deposited from target containing 1% P.. 76
3.38 Proposed energy band diagram constructed for n-carbon/p-silicon heterojunction where, the carbon thin film is deposited from target containing 3% P.. 76
3.39 Proposed energy band diagram constructed for n-carbon/p-silicon heterojunction where, the carbon thin film is deposited from target containing 5% P.. 77
3.40 Proposed energy band diagram constructed for n-carbon/p-silicon heterojunction where, the carbon thin film is deposited from target containing 7% P.. 77
3.41 Variation of depletion width in carbon thin film with the applied voltage in the junction.. 78
3.42 Variation of depletion width in silicon substrate with the applied voltage in the junction.. 78
3.43 Variation of total depletion width in the heterostructure with the applied voltage in the junction.. 79
3.44 Revised C-V characteristics determined from the fitted data......... 80
3.45 C-V characteristics from experiment and from fitted data............ 80
3.46 Junction capacitance as a function of reverse bias voltage for diodes with different nitrogen-doping levels (0.7, 1.0 and 1.5 at % nitrogen) in the ta-C reported by Veerasamy *et al.* [5]................ 84

List of Tables

3.1	Capacitance versus voltage data for the films deposited from the target containing various amounts (1%, 3%, 5% and 7%) of phosphorus by mass	35
3.2	Carrier concentration and built-in potential calculated for the heterojunction where carbon thin film is deposited from target containing 1%, 3%, 5% and 7% phosphorus	41
3.3	Conductivity of the films deposited from the target containing various amounts of phosphorus (1%, 3%, 5% and 7% by mass) for different temperatures	43
3.4	Values of activation energy, conductivity prefactor and room temperature conductivity for different dopant contents	48
3.5	Calculated energy band parameters for the constructed energy band diagram	55
3.6	Built-in potential calculated from current density-voltage characteristics	60
3.7	Calculated diode quality factors from ln(J) vs V characteristics	63
3.8	Reverse saturation current density for the heterojunctions for the thin films grown from targets containing different dopant contents (1%, 3%, 5% and 7% phosphorus)	64
3.9	Intrinsic carrier concentration and donor carrier concentration calculated for films deposited from targets containing different dopant contents	68
3.10	Electron mobility calculated from room temperature conductivity and calculated donor carrier concentration	70
3.11	Calculated diffusion length and minority carrier life time in carbon thin film	73
3.12	Revised built-in potential, electron affinity of carbon thin films, conduction band discontinuity and valance band discontinuity with the variation of dopant content	75

3.13 Carrier concentration in carbon thin film, conduction band and valance band discontinuity and built-in potential in the heterojunction with the variation in dopant content in the target material.. 81

Acknowledgements

I wish to offer my heartiest gratitude and profound respect to my thesis supervisor Dr. Sharif Mohammad Mominuzzaman, Assistant Professor, Department of Electrical and Electronic Engineering (EEE), Bangladesh University of Engineering and Technology (BUET), Bangladesh, for giving me the opportunity to work with him and for his continuous guidance, suggestions and wholehearted supervision throughout the progress of this work. I am indebted to him for acquainting me with the world of advanced research.

I am grateful to Dr. Mohammad Ali Choudhury, Professor and Head of the Department of EEE, BUET, who provided all the research facilities of the department accessible all the time and encouraged completing the work. I would like to express my special thanks to Dr. M. M. Shahidul Hassan, Professor and former Head, Department of EEE, BUET who always encouraged and advised me to complete the work. Also I want to offer thanks to Professor T. Soga and all other personnel involved with "Soga laboratory", Dept. of EEE, Nagoya Institute of Technology, Japan for providing experimental data.

I want to thank my parents for their support and encouragement to complete the work. I also like to thank my wife for her inspiration to finish this work. I want to thank my friends and colleagues, who were directly or indirectly related to this work and gave fruitful suggestions. I thank all the personnel at the faculty library and BUET central reference library for providing me with the valuable journals and thesis papers to complete the work.

Finally, I am grateful to Almighty Allah for giving me strength and courage to complete the work.

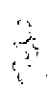

Abstract

Energy band parameters of n-Carbon/p-Silicon heterojunction have been determined using experimental observations. The heterojunction was fabricated by depositing phosphorus (P) doped carbon thin film on p-type silicon substrate by pulsed laser deposition (PLD) technique. Camphor ($C_{10}H_{16}O$), a natural source is used as a starting precursor for the carbon layer of the heterojunction. Carbon layer of the heterojunction was obtained using target containing various amounts of phosphorus (1%, 3%, 5% and 7% by mass). The capacitance-voltage (C-V) characteristics are analyzed. From the C-V characteristics, the carrier concentration in carbon thin film is calculated and it is seen that the carrier concentration in the thin film carbon decreases gradually for films grown from target containing 1%, 3% and 5% P and then increases for 7% P. The built-in potential (V_{bi}) determined from the C-V characteristics shows the same trend. Later, temperature dependent conductivity data analysis shows that with the increase in dopant content in the target material from where the films are grown, the value of activation energy decreases, which indicates that the increase in dopant content activates the carbon thin film in greater amount and thus the carrier concentration in carbon thin film and the built-in potential of the heterojunctions obtained from C-V characteristics are not consistent with the results obtained from temperature dependent conductivity data analyses. Thus later it is attempted to calculate the intrinsic carrier concentration and donor carrier concentration in the thin film carbon by fitting the parameters with the reverse saturation current determined from the current density-voltage (J-V) characteristics of the heterojunction. The calculated parameters show acceptable trends and are consistent with the activation energy values calculated from the temperature dependent conductivity data analyses. The revised built-in potential is calculated by using the activation energy calculated from temperature dependent conductivity analysis and data fitting with standard equations. Then the energy band diagrams for the heterojunctions with carbon thin films grown from targets containing different amounts of dopant contents are proposed. The extracted parameters are then compared with the previously reported results.

Chapter 1

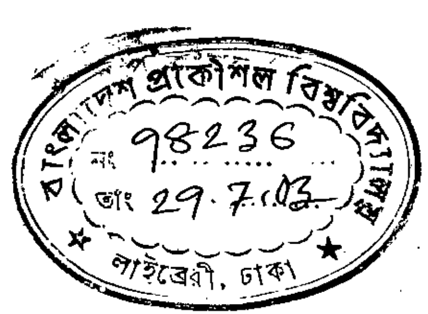

Introduction

Silicon (Si) has been dominating the field of semiconductor industry for many years. Researchers are always looking for alternative materials for semiconductor devices. Carbon has shown very interesting properties and scientists are now trying to implement carbon materials for device fabrication purposes. Some heterojunction devices based on carbon materials have already been reported [1]-[4]. These devices show a potential scope of using carbon as a material in the device research. Carbon shows outstanding electrical, physical and optical properties. All these properties can be varied in a wide range by changing the optical gap of the material. This unique characteristic has got a lot of attractions of the researchers now a days. Carbon is available in the nature in wide varities of forms, from graphite to diamond, whose behaviors are wide apart from each other. Besides these, carbon is found in the nature in numerous amorphous forms [5]. These amorphous forms of carbon have now received a great interest of the device researchers. Chapter one covers the background along with the objective of the work. The organization of the thesis is also presented at the end of this chapter.

1.1 Background

The world wide electronic market is governed by silicon. Si is an easily available material, and it provides a high-quality natural oxide that enables a high degree of monolithic integration. The semiconductor industry is forced to shrink the device dimensions and increase the package density in order to make the chips faster and cheaper. Though silicon and compound semiconductor based materials have dominated the market for the last few decades, low cost, stable and high efficient semiconductor devices are yet to be commercially realized due to high material and production cost. In search of alternative low cost materials, carbon has attracted attention of the researchers for its unique properties. Carbon based heterostructures such as, metal insulator semiconductor (MIS) diodes [1], Schottky diodes [2], metal insulator semiconductor field effect transistors (MISFET) [3], heterojunction diodes [4] on silicon have already been reported and thereby demonstrate the potentiality of carbon materials in electronic devices. Diamond like carbon offers opportunities to create novel electro-optic devices owing to its high refractive index and its ability to be deposited directly on to silicon substrates.

Heterojunctions and multi planer structures in compound semiconductors create a wide range of possibilities for device development. Thus scientists are trying to introduce new materials for heterojunction device fabrication and are trying to develop low cost, stable and highly efficient semiconductor devices. Recently carbon has attracted attention of researchers for device application for its wide range of properties.

Over the past few years carbon based materials have become increasingly interesting for the use in electronic applications. These range from the rather unsophisticated heat sink requirements for power semiconductors, through disposable electronics for consumer goods, to UV sensors and dosimeters and the highly sophisticated large

area flat panel displays. Each one of these potential applications depends upon the production of high quality, reproducible and well-characterized material, each particular application being determined by the material available. Of these potential materials thin film amorphous carbon has many attractive features for electronic use: a band gap which can be varied in a wide range, potential to produce n, p and intrinsic material, and large area deposition at room temperature. Carbon exhibits outstanding physical, electrical and optical properties such as chemical inertness, high hardness, high electrical resistivity, high dielectric strength and infrared (IR) optical transparency. Interestingly, these properties can be tailored over an unusual wide range from that of semi metallic graphite (~0.0 eV) to that of insulating diamond (~5.5 eV). All these properties make growing interest in DLC thin films for device fabrication purpose and carbon has been emerging as an important material for the application in the field of electronic and optical devices. Hence more interests are growing towards the research on carboneous films and the device based on carbon thin films. Appreciable works have already been done on amorphous thin film carbon grown on Si substrate [4],[6]-[8].

Veerasamy *et al.* [4] analyzed electronic and photoresponse properties of n-type (nitrogen doped) tetrahedral amorphous carbon (ta-C) deposited by filtered cathodic vacuum arc (FCVA) onto p-type crystalline Si. Secondary ion mass spectroscopy (SIMS) measurements showed the junction to be abrupt in nature. Interface state density at the abrupt heterojunction between ta-C and Si was calculated. Dark forward current density-voltage-temperature (J-V-T) characteristics were found to be consistent with current tunneling-recombination process through states at the ta-C/Si interface. The photoresponse and photovoltaic behavior were also presented as a function of doping in tbe ta-C.

Chan *et al.* [6] deposited semiconducting diamond-like carbon-diamond (DLC-diamond) at room temperature by r.f plasma-enhanced chemical vapour deposition (PECVD) technique on n-type silicon. The deposited films were found to be semiconducting with a variable band gap that could be controlled by changing the deposition conditions. Also, the undoped films were found to be intrinsically p-type

in nature. Photoresponse characteristic of the heterojunction diode was also characterized.

Konofaos *et al.* [7] examined electronic properties of amorphous DLC and their capability of application to electronic devices. MIS diodes and p-n heterojunction devices were created and characterized. The films were grown by PECVD of methane and their structural composition was obtained by Raman spectroscopy, ellipsometry and X-rays. Conductance technique was used to measure the density of trapping states at the carbon/silicon interface. The ion implantation technique was used to transform the insulating DLC film into semiconducting by adding boron ions as dopants at different doses to achieve p-type conductivity. The device performed like Schottky diode for low boron doses and like p-n diodes for high doses.

Mominuzzaman *et al.* [8] deposited thin films of carbon on n-type single-crystal silicon and quartz substrates by simple ion beam sputtering of camphoric carbon, obtained from camphor, a natural source. Optical absorption coefficients were obtained for as-deposited and annealed films. The optical band gap energies of the as-deposited and annealed films were measured. Temperature dependence of conductivity of camphoric thin films was also observed.

Pulsed laser deposition (PLD) technique was used for the first time to obtain phosphorus (P) doped n-type Camphoric Carbon (CC) films [9]. Some optical and electrical properties were studied with the variation of P content in the film. Recently, P-doped CC film has been developed by PLD on p-type silicon to obtain n-Carbon/p-Silicon heterostructure [10]. The detailed characteristics of phosphorus doped carbon thin films grown on silicon substrate are yet to be reported so far. Therefore, there is a wide scope to work on the detailed characteristics of these kinds of devices.

1.2 Objective of the Work

The objective of this work is to determine the characteristics of phosphorus doped carbon on silicon heterostructure (n-C/p-Si). The energy band diagrams for the given heterostructure with the variation of dopant concentration (P doping) in carbon region will be determined. Further, the device characteristics will be correlated with the optoelectronic properties of the P doped carbon films obtained from ultraviolet visible infrared (UV-VIS-IR) spectroscopy and temperature dependence conductivity analyses.

The capacitance versus voltage (C-V) characteristics of the n-C/p-Si device has been measured practically for different dopant concentration in the thin film. The current density versus voltage (J-V) characteristics has also been measured for the device. Carrier concentration in the thin film of the device is calculated from the reverse saturation current and is compared with the carrier concentration obtained from C-V characteristics. The band gap for the carbon thin film is determined from UV-VIS-IR spectroscopy for different dopant concentrations. The activation energy for the thin film is determined from the temperature dependence conductivity analyses. With all of these calculated parameters, the energy band parameters for the n-C/p-Si heterojunction for different dopant concentration are calculated.

1.3 Thesis Layout

Organization of this thesis is divided into four chapters.

Chapter one gives general introduction followed by the background and the objective of the work.

Chapter two deals with the review on carbon materials, carbon thin film based heterojunction, theory of heterojunction energy band modeling, growth procedure of our n-carbon/p-silicon heterojunction device. The experimental details of the deposition of undoped and P doped carbon thin films from the camphoric target are

described. Also, the experimental procedure of the fabrication of the n-C/p-Si heterostructure is described.

Chapter three deals with the determination of energy band parameters of phosphorus doped n-C/p-Si heterostructure. The experimental data are obtained from the "Soga Laboratory", Department of Electrical and Electronic Engineering, Nagoya Institute of Technology, Japan. The detailed procedures for the determination of the energy band parameters for the heterojunctions are shown, the problems faced to do that is mentioned and the procedure to overcome those problems are described there.

Conclusive discussions and remarks are given in chapter four. Some scopes to the future works are also presented there.

Chapter 2

Review of Carbon Research, Introduction to Camphoric Carbon Films for its Device Application and Heterojunction Device Modeling

Carbon is abundantly available in the nature and is available both in amorphous and crystalline structure. Besides amorphous structure, graphite and diamond are two allotropes of carbon having wide difference in their properties. Under ambient condition, graphite has strong inplane trigonal bonding and it is a stable state of carbon. Graphite can be converted to diamond under high pressure (6000 atms) and temperature (2000 K). But the converted diamond quickly transforms back to more stable form of carbon i.e, to graphite when it is exposed to irradiation or heat. When carbon thin films are grown, special conditions must be achieved to deposit diamond like carbon (DLC) films, otherwise graphitic films are grown. DLC has unique optical, electronic and mechanical properties for which it has got a lot of attractions of the scientists now a days for device applications. These properties include chemical inertness, extreme hardness, high dielectric strength, high electrical resistivity, optical transparency and high thermal conductivity. Interestingly, these properties can be tuned over an unusual wide range from that of semi metallic graphite (~0.0 eV) to that of insulating diamond (~5.5 eV). There are various techniques used to obtain high quality diamond like carbon thin films. In this chapter, various forms of carbon are described and the present status of amorphous and diamond like carbon research is reviewed. The theoretical descriptions of heterojunction device modeling are also presented here. Also the experimental details

of the deposition of undoped and phosphorus doped carbon thin films and n-carbon/p-silicon heterostructure using camphor precursor is presented.

2.1 Various Forms of Carbon

A neutral carbon atom has 6 protons and 6 neutrons in its nucleus, balanced by 6 electrons. The electron shell configuration of carbon is $1s^2 2s^2 2p^2$. Carbon has a valence of 4, since 4 electrons can be accepted to fill the 2p orbital. The four electrons in the outer orbital may arrange themselves in different hybridization bonding configurations (sp^1, sp^2, sp^3). Carbon is found free in nature in three allotropic forms: amorphous (lampblack, boneblack), graphite, and diamond. A fourth form, 'white' carbon, is thought to exist. Graphite or diamond structure is dictated by the trigonal (sp^2) and tetrahedral (sp^3) configurations.

Graphite has a sheet like structure where the atoms all lie in a plane and are only weakly bonded to the graphite sheets above and below. The 3 fold coordinated sp^2 configuration in graphite has three of four valance electrons assigned to trigonally directed sp^2 hybrid orbitals which form strong intra-layer σ bonds. The fourth electron lies in a $p\pi$ orbital, which lies normal to this bonding plane. This orbital forms weak π bonds with neighboring π orbitals. The structure of graphite (Fig. 2.1) is described as layers of carbon atoms with an inter-atomic distance of 0.1415 nm in the basal plane. Graphite shows properties like good electrical conductivity, lubricity, lower density, a grayish-black appearance and softness.

Diamond is one of the hardest substances, with a high melting point and index of refraction. The Mohs hardness scale shows the hardness of diamond to be '10'. Diamond is also the least compressible and stiffest substance. It is an exceptional thermal conductor - 4 times better than copper. Diamond has an extremely low thermal expansion, is chemically inert with respect to most acids and alkalis, is transparent from the far infrared through the deep ultraviolet. Diamonds do not conduct electricity well, although some are semiconductors. Diamond can burn if subjected to a high temperature in the presence of oxygen. Diamond has a high specific gravity; it is amazingly dense given the low atomic weight of carbon.

Diamond has the highest reflectance and index of refraction of any transparent substances. Diamond is made up of repeating units of carbon atoms joined to four other carbon atoms via the strongest chemical linkage, covalent bonds. Each carbon atom is in a rigid tetrahedral network where it is equidistant from its neighboring carbon atoms. The structural unit of diamond consists of 8 atoms, fundamentally arranged in a cube. This network is very stable and rigid, and that is why diamonds are so very hard and have a high melting point. In Diamond, the carbon atom's four valance electrons are assigned to a tetrahedrally directed sp^3 hybrid orbital, which makes a strong σ bond with an adjacent atom. The diamond structure (Fig 2.2) is face centered cubic with inter-atomic distance of 0.154 nm [11]. Since none of the outer shell electrons are weakly bonded like graphite structure, diamond exhibits most of the properties quite different from that of graphite.

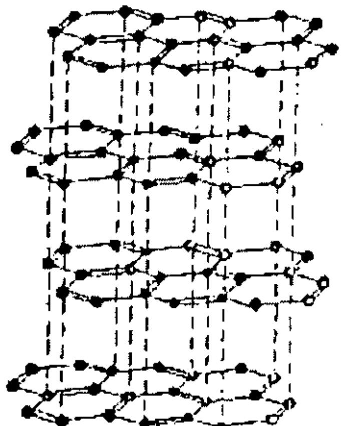

Figure 2.1: The structure of hexagonal single crystal graphite.

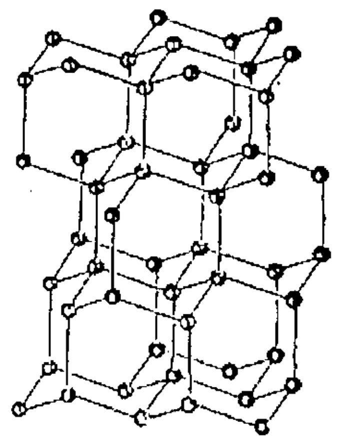

Figure 2.2: The ideal diamond structure.

Besides graphite and diamond, there are other forms of carbon. There exist numerous forms of amorphous carbons, which are characterized as imperfect graphite structures i.e., the layers planes are not oriented with respect to their common axis, the angular displacement of layers is random and the layers overlap one another irregularly [11]. Among those diamond like carbon (DLC), amorphous carbon (a-C) and hydrogenated amorphous carbon (a-C:H) have mixture of sp^2 and sp^3 bonded carbon of different fractions. At present, research on DLC, a-C and a-C:H has found

great interest to researchers and scientists are working to understand the properties of these elements and trying to implement these in device fabrication.

2.2 Present Status of Carbon Research

At present many scientists have shown keen interest in diamond like carbon (DLC), amorphous carbon (a-C) and hydrogenated amorphous carbon (a-C:H). DLC has unique optical, electronic and mechanical properties. These properties include chemical inertness, extreme hardness, high dielectric strength, high electrical resistivity, optical transparency and high thermal conductivity. Interestingly, these properties can be tuned over an unusual wide range from that of semi metallic graphite (~0.0 eV) to that of insulating diamond (~5.5 eV). All these properties make growing interest in DLC thin films for device fabrication purpose. DLC thin films are prepared by several methods such as ion beam deposition, sputtering, rf plasma deposition and pulsed laser deposition [5]. The properties of the film strongly depend on the precursor material, method and the condition of deposition. The optical and electronic properties of these films are of much interest because of their potential application in semiconductor technologies including photonic devices. Carbon based heterostructures [1]-[4] have already been reported and thereby demonstrate the potentiality of carbon materials in electronic devices. The semiconducting carbon thin films can be intrinsic or can be converted to extrinsic during or after the growth process [1], [6], [12]-[13]. However, undoped carbon is weakly p-type in nature [12]. The carbon films doped with various phosphorus (P) contents are reported to be n-type [9], [12]. The detailed characteristics of phosphorus doped carbon thin films grown on silicon substrate are yet to be reported so far. Therefore, the study of this type of device is very important for practical implementations.

The first diamond-like carbon was prepared by Aisenberg and Chabot [14] and later confirmed by Spencer *et al.* [15]. At present wide variety of methods are used for their deposition. In all the processes the film is subjected to ion bombardment during the growth process. This produces sp^3 bonding in the film.

Properties of amorphous carbons deposited under ion bombardment conditions were studied by Weissmantel *et al.* [16] and Angus *et al.* [17]. They showed that unsaturated a-C deposited at low ion energy is essentially graphitic in nature and similar to evaporated a-C. It changes to hard a-C at moderate ion energies and it then becomes less hard again at high ion energies. This happens as its structure adopts a highly disordered, defected graphitic structure.

Koidl *et al.* [18] showed that a-C:H at low ion energies is soft and polymeric in nature due to predominance of $=CH_2$ groups. Its hardness becomes maximum at moderate ion energies and the hardness declines at high ion energies as it then adopts defect graphitic structure.

Angus *et al.* [20] showed that the diamond-like forms of a-C:H has much higher atomic density than the conventional hydrocarbon polymers. Graphite has a lower density and lower atomic density than diamond. The atom densities of diamond-like hydrocarbons are above 0.19 gram-atom cm^{-3}. The hard amorphous carbon formed from filtered ion beams or from laser plasmas are seen to have densities and atomic densities above graphite and below diamond.

Robertson *et al.* [21] suggested that defect configurations of a-C are more complicated than those of a-Si. The main cause of defect of a-Si is the dangling bond, a trivalent Si site, formed by breaking a σ bond, while a defect in a-C can be formed by breaking a σ or a π bond. As the π bonding is weaker, π defects predominate in the defect creation. The dangling bond in a-C has π character and not the sp^3 character as in a-Si.

Meyerson *et al.* [22] discovered that a-C:H could be substitutionally doped by B_2H_6 or PH_3. Meyerson showed the typical change in the activation energy of conduction at room temperature and compared them with the analogous changes found for a-Si:H by Spear *et al.* [23]. It was found that a substitutional change in conductivity occurred in a-C:H, but its doping efficiency is lower than that of a-Si:H.

Jones *et al.* [24] showed that a-C:H could be doped to n-type with nitrogen (N). It was shown that doping efficiency of N in a-C:H is low and true substitutional doping mechanism was not involved there. The higher N contents promote sp^2 coordination of carbon was shown by Amir *et al.* [25]. Increased sp^2 C bonding narrows the gap and increases the conductivity, which could be confused with doping.

High defect densities arise from low deposition temperatures, rapid deposition rates or strong ion bombardment. Low defect density can reflect a gentle growth process or some annealing of damage. Defect densities can be measured directly by electron spin resonance (ESR). Orzeszko *et al.* [26] found a spin density of about 10^{18} cm^{-3} in evaporated a-C, which was relatively independent of annealing temperature. A similar value was calculated for sputtered a-C from conductivity data by Hauser *et al.*, [27]. Wada *et al.* [28] found 2 x 10^{19} cm^{-3} spins in the sputtered a-C. A much higher density of 2 x 10^{20} cm^{-3} was found in the sputtered a-C of Pan *et al.* [29], deposited at 77 K. Higher values of spin density have been found in reactively sputtered a-C and a-C:H [30].

Vogel *et al.* [31] deposited amorphous carbon layers (a-C, a-C:H) with hydrogen content between 3 % and 25 % by d.c. plasma decomposition process of benzene, ion beam sputtering and thermal evaporation. The purpose was to investigate the middle infrared (MIR) / near infrared (NIR) / visible (VIS) absorption picture and the d.c. conductivity as a function of the temperature of amorphous carbon layers with the variation of hydrogen content and to compare the obtained results with those obtained from e-beam evaporated, microwave plasma deposited and r.f. sputtered layers [32]-[33]. On the basis of the experimental results found by Vogel *et al.* [31], the carbon layers were classified into three groups. The first group included the insulating carbon layers whose temperature dependent conductivity leads to a thermally activated hopping in band tails in the temperature range 150-300 K with activation energies between 0.06 and 0.21 eV. Their absorption picture exhibited an Urbach tail (Urbach tail width values 1600~2500 cm^{-1}) and a power law absorption region (E_0 = 0.5-1.1 eV). Their electrical and dielectric properties were interpreted by Davis-Mott model. The second group contained the high absorbing and conducting

carbon layers and was deposited by evaporation and ion beam sputtering. The layers showed vanishing gaps with no Urbach tailing. Their absorption picture was found to be close to that of graphite. The conductivity data of these layers could be explained by assuming a defective graphite model. The third group included carbon layers with medium room temperature conductivity. Their optical gap was found to be near of 0.3 eV and no Urbach tailing was observed. The dispersion behaviour of these layers was found to be close to that of insulating films. The temperature dependent conductivity could be explained by the two conduction mechanism of the previous two groups. It was explained that the different extension of sp^2 hybridization areas in the network layers caused these type of differences in the behaviour of the carbon layers.

Veerasamy *et al.* [34] deposited highly tetrahedral amorphous carbon (ta-C) and its hydrogenated form (ta-C:H) on fused silica and silicon substrates using filtered cathodic arc process. The optical and electrical band gaps of amorphous diamond and its hydrogenated form a-C:H were found to be near of 2 eV. The H content of the ta-C:H was found to be about 3 % using elastic recoil detection analysis (ERDA) and electron energy loss spectroscopy (EELS) was used to show that ta-C:H was tetrahedral structure in nature. Both materials were found to be stable at room temperatures up to 1000 K. The room temperature conductivity of 10^{-7}-10^{-8} $\Omega^{-1}cm^{-1}$ was shown to be thermally active. The activation energy was found in the range of 0.2-0.3 eV. Analysis of current-voltage characteristics of ta-C/p-Si heterojunction showed that there was space-charge limited current in the system and that was influenced by bulk traps. The density of state profile in the range of quasi-Fermi level was calculated and was found in the range of 10^{18} $cm^{-3}eV^{-1}$. Optical absorption data was coupled with the electrical results to confirm that the valance band density of states was of the order 10^{20} $cm^{-3}eV^{-1}$. It was also shown that there was reduction of nearly one order of magnitude at the quasi-Fermi level upon hydrogenation.

Zeisel *et al.* [35] worked with type IIb diamond, a p-type semiconducting diamond species. The Fermi level for this species was found to be 0.37 eV above the valance band edge. The species used here was doped with boron. From capacitance-voltage

(C-V) profiling, the acceptor concentration was found to be 2.5 x 10^{16} cm^{-3}. The radiation damage was created by implantation of C^+ ions with an energy of 160 keV at room temperature. It was shown that the C-V characteristics of the unimplanted diode exhibited a normal behaviour while the implanted sample showed a Schottky behaviour.

Liu *et al.* [36] investigated tetrahedral amorphous carbon (ta-C) film based metal-semiconductor-metal (MSM) structures for high temperature applications. The ta-C films were deposited in a filtered cathodic vacuum arc (FCVA) process. During deposition, the nitrogen gas was introduced into the deposition chamber through an r. f. ion beam source with the ion energy of 120 eV and ion density of 20 mA. The nitrogen partial pressure was varied between 2.6 x 10^{-5} and 1.3 x 10^{-4} Torr. The N content was found to be in the range 3-34 % with nitrogen flow rate changing from 0.5 to 10 sccm. They showed that the Tauc gap increases from 2.56 eV for the ta-C film without nitrogen doping to 2.62 eV for the film deposited at 0.5 sccm nitrogen flow rate and then decreases from 2.62 to 1.1 eV with the increase of nitrogen flow rate from 0.5 to 10 sccm during deposition. All the films show a linear relationship between the log(conductivity) and the reciprocal of temperature above 100°C, indicating a thermally activated conduction mechanism in the extended state in the high temperature range. The activation energy was found to increase from 0.9 eV to 1.18 eV when the nitrogen flow rate increased from null to 1 sccm and then decreased to 0.17 eV when the nitrogen flow rate was further increased to 10 sccm. The high-temperature performance of MSM structure was evaluated by measuring their I-V characteristics at different temperatures up to 300° C. Further Al/n-ta-C/Al structure showed Schottky behaviour, while Ti/n-ta-C/Ti and Cr/n-ta-C/Cr showed typical ohmic contact behaviour in the testing temperature range.

Veerasamy *et al.* [37] reported successful control of the conductivity of tetrahedral bonded amorphous carbon (ta-C) by incorporation of N during film growth. N is introduced into the films during the growth by injecting N_2 gas into a plasma stream formed by a carbon cathodic vacuum arc. The films were grown on quartz and silicon (100) substrates. X-ray-photoemission-spectroscopy studies of films prepared

over a range of N_2 partial pressures showed that the N concentration varies from 2% to below detection limit. Spectroscopy studies using electron-energy-loss spectroscopy confirmed that the ta-C films with N contents up to 1 at % retain their predominantly tetrahedral amorphous structure. The as-deposited ta-C, with no intentional N incorporation, was found p-type in nature with resistivity of 10^7 Ω cm and an activation energy of 0.22 eV. The addition of N under varying injection levels from 10^{-3} to 10 standard cubic cm caused the resistivity to initially go through a maximum at 10^9 Ω cm and then decrease monotonically to 10 Ω cm. The optical band gap was found to be slightly decreased to 1.8 eV with up to 1.5% N. With 10% N incorporation, the optical band gap reduced to 1.5 eV.

Weiler *et al.* [38] deposited highly tetrahedral bonded hydrogenated amorphous carbon (ta-C:H) from an acetylene-fed plasma beam source. The resulting films were characterized in terms of sp^3 content, mass density, intrinsic stress, surface roughness, radial distribution function, C-H bonding, Raman spectra, optical gap, electrical conductivity, gap states, Young's modulus and hardness. The sp^3 content was found to reach the maximum value of 75% at an ion energy of 200 eV or 92 eV per C ion. The density and the stress also reached the maximum value at this ion energy. The formation of ta-C:H was interpreted in terms of the subplantation of C^+ that produced a densified sp^3 bonded network. From the C-H vibration spectrum it was shown that C sp^2 sites form C=C alkene group. The maximum value of optical gap was found to be 2.85 eV and that was found to increase with the sp^3 fraction. The spin density due to defects showed a high value and was shown a decreasing trend with increasing ion energy. The Young's modulus and hardness was measured by microindenter and was found the maximum value of 290 and 61 GPa respectively. These values were found consistent with the high sp^3 bonding.

However, the optical and electrical properties of the thin film are mainly dictated by two dominating factors-precursors and the method of deposition. Thus finding alternative precursor materials and simple method of deposition have been always getting the priority of the researchers. In recent days, camphor ($C_{10}H_{16}O$) has been found as an alternative precursor material because of its additional advantages over

graphite. Camphor consists of both sp^2 and sp^3 hybridization, whereas, graphite consists of only sp^2 hybridization. Hydrogen in a-C films modifies the properties of the films and introduces many sp^3 sites. Hydrogen passivates the dangling bonds in the gap states and also tailors the optoelectronic properties of the film. Thus while graphite is used as a precursor, additional hydrogen gas/ions have to be supplied whereas camphor has abundant hydrogen in its structure. Further, the presence of sp^3 hybridized bonds in the camphor molecule plays an important role in the deposition of carbon films especially for diamond like carbon (DLC) films.

It is reported that the fullerenes [39] , Carbon tubules [40] and semiconducting carbon [40] have been successfully generated from the soot of this natural precursor, camphor ($C_{10}H_{16}O$) . It is found from the study that in order to obtain DLC films, graphite has been commonly used as a target material for the physical vapor deposition system such as sputtering [41], filtered cathodic vacuum arc (FCVA) [42] and pulsed laser arc deposition (PLD) [4], etc. Mominuzzaman *et al.* [7] recently successfully deposited carbon thin film by simple ion beam sputtering (IBS) of camphoric carbon, obtained from camphor- a natural source. They also studied various optoelectronic properties and the effects of annealing on these properties. They reported that the optoelectronic characteristics of carbon thin films deposited by ion beam sputtering of a camphoric carbon target without any H_2 gas precursor are observed to be similar to those of hydrogenated a-C films. The optical absorption coefficient of as-deposited film was found in the order of 10^4-10^5 cm^{-1} and the optical gap was calculated to be equal to about 0.5 eV. While annealed up to 400° C, the optical and electrical properties of these films remained stable, but there were abrupt changes at annealing temperature greater than 400° C. The room temperature conductivity of the as-deposited film was found in the order of 10^{-1} $(\Omega\text{-cm})^{-1}$ and upon annealing up to 800° C, it showed a graphitic nature and the conductivity increased and reached at the order of 10^1 $(\Omega\text{-cm})^{-1}$. Based on these observations of camphoric carbon thin films they suggested that camphor and camphor like other precursors might be the best-suited candidates as starting materials for semiconducting carbon thin films for electronic applications.

Inspired by the previous results, Mominuzzaman *et al.* [43] successfully used camphor as a precursor material in the deposition methods other than IBS. They first used camphor in the PLD method. Along with the undoped camphoric carbon (CC) film, they incorporated phosphorus (P) in the CC films. Various optoelectrical properties of these films were later studied [8],[44]. It was shown that the optical gap remains relatively unchanged to 0.85 eV for the films deposited using targets containing 1%, 3% and 5% P and then decreases to 0.75 eV for target containing 7% P. This decline in optical gap indicated the increase in sp^2 fraction due to graphitization of the CC film. The resistivity of the undoped CC film was found to be 2×10^4 Ω-cm and increased to 3.7×10^4 Ω-cm for the film deposited from the target containing 1% P. But for the films whose target contained higher percentage of P showed a sharp decrease in resistivity at first and gradual decrease thereafter. This trend of resistivity is different from that reported by Veerasamy *et al.* [12], where, the authors found only a decrease in resistivity with P content in their films. The undoped CC film is slightly p-type due to the presence of acceptor like defect states and Fermi level lies close to the valance band edge. Small amount of P addition compensates/passivates the acceptor like defect states by ionized electrons from P atoms and Fermi level moves upwards through the mid gap and result in an increase in resistivity for the film deposited from the target containing 1% P. With further increase in P content, the Fermi level moves towards the conduction band edge and resistivity decreases.

Maldei *et al.* [2] deposited hydrogenated amorphous carbon (a-C:H) employing two methods-electric arc evaporation and dc magnetron sputtering, and applied them to fabricate Schottky diode and heterojunction solar cell. They reported there are several parameters that control the band gap of a-C:H, such as, 1. kinetic energy of ionized particle, 2. substrate temperature and 3. partial pressure of existing hydrogen. Kinetic energy of the impinging particles can be varied by bias voltage. An increase in substrate temperature yields a-C:H films with decreasing band gap. An increase of partial pressure of H_2 during deposition of a-C:H causes widening of band gap. The increase of band gap width is attributed to two mechanisms. The first is the passivation of the dangling bonds by hydrogen while the second mechanism is the

hydrogenation of unsaturated bonds in a-C:H. This is in contrast to a-Si:H, where, the incorporation of hydrogen leads only to a removal of dangling bonds. With the films obtained from the electric arc evaporation, they observed that the absorption coefficient of a-C:H films increased with photon energy, because, for a fixed band gap, the probability of electron transfer across the mobility gap rises with photon energy. However, at high photon energy (> 3.5 eV) the absorption coefficient became increasingly independent of photon energy. With increasing pressure of hydrogen in the vacuum chamber, the absorption coefficient of a-C:H films decreased because of widening of the band gap with H_2 pressure. Absorption coefficient of a-C:H films deposited by dc magnetron sputtering increased with photon energy and became independent of photon energy at higher value (> 3.5 eV).. However, absorption coefficient decreased with H_2 content in the gas phase from 10% to 80% and increased thereafter because the band gap increased and reached at a maximum value at 80% H_2 content and then decreased. Then they fabricated glass/Cr/Au/a-C:H/Au sandwich structure deposited in the vacuum chamber with gold and chromium being thermally evaporated. These structures showed a linear I-V relationship. The ohmic contact was used for the back contact of each fabricated device.

Veerasamy *et al.* [4] deposited n-type (nitrogen doped) tetrahedral amorphous carbon (ta-C) on p-type crystalline silicon by filtered cathodic vacuum arc (FCVA) process. The cathodic vacuum arc is a low voltage and high current density type of discharge with the voltage drop being approximately equal to the potential of the cathodic material. The N content in the ta-C films was found to be varied from 0.7 to 2.0 %. The resistivity of the doped ta-C films varied from 1000 to 1 Ω cm. Activation energy measured for the resistivity revealed that the Fermi levels in the N-doped ta-C used to make the junctions varied from 0.15 to 0.10 eV with respect to the conduction band edge, whereas, the Fermi level of the p-type Si was 0.2-0.3 eV above the valance band edge. Experimentally it has been found that undoped ta-C is p-type in nature [45] and is ascribed to unpaired dangling bonds. Veerasamy found the electron affinity of the ta-C to be in the range of 2.9 – 3.0 eV from the photoemission spectroscopy measurements performed on doped ta-C films. The

interfacial density of states at the ta-C/Si heterojunction was found to be in the order of 10^{11} cm^{-2}. The doping level in the ta-C had negligible effect of the conduction band discontinuity (constant at ~ 1 eV). The carrier concentration at the Si substrate was found to be 1.0-1.1 x 10^{15} cm^{-3}, whereas, the carrier concentration in ta-C thin film increased with the increase of percentage doping. The carrier concentration was calculated in the range of 0.35 x10^{15} – 18.2 x 10^{15} cm^{-3}. The built-in potential of the heterojunction was seen to increase with the increase in carrier concentration in the thin film. Equilibrium energy band model was also proposed for the heterojunction device. The dark forward current density-voltage-temperature (J-V-T) characteristics for 1 % N at low voltage region (≤ 0.2 eV) showed that the current density to be recombination limited with the diode quality factor to be varying from 1.68 to 1.94 with the temperature varying from 115-265° K. In the high voltage region tunneling limited current was found. The J-V-T characteristics at 2 % N showed an weaker current-voltage characteristics variation with temperature. The total current was found to be limited by tunneling mechanism only. Dark reverse current densities were also measured as a function of reverse bias voltage up to –2V in the same temperature range (115-265° K). It was shown that under reverse bias condition, two possible tunneling mechanism dominated- (i) tunneling of electrons from the Si valance band through the depletion region to the ta-C conduction band via its states. (ii) a Zener type tunneling of electrons from the Si valance band into the ta-C conduction band.

Chan *et al.* [6] deposited DLC-diamond films on n-type silicon with resistivity of 1-5 Ω-cm using 13.56 MHz, capacitively coupled r. f. plasma deposition chamber at room temperature. The source gas was typically a mixture of 6% methane and 94% argon, making a total flow of 160 standard cm^3 min^{-1} at a pressure of 300 mTorr. The DLC-diamond/silicon heterojunction diodes were fabricated by thermally evaporating 25 mm thick gold contacts onto the DLC diamond at a pressure of 10^{-6} Torr. A rectifying I-V characteristic was obtained for the DLC-diamond/silicon heterojuncion diodes. The forward to reverse rectification ratio was typically about 3-4 orders in magnitude. The diode turn on voltage was found about 1.5 V and the forward current characteristics was found to be resistance limited. The typical

resistivity was of the order of 10^{6}-10^{8} Ω-cm. The activation energy was found to be 0.34 eV. A plot of $\log_e$(conductivity) against temperature$^{-1/4}$ showed an approximate linear relationship, which suggests that electrical transport by hopping at the Fermi level. The built-in potential of the junction was found to be 0.49 eV. A.C. conductance of the diodes was also investigated. It was found that at low frequencies up to 1 kHz, the conductance was constant and similar to d.c case. At higher frequencies the conductance curve corresponded to the hopping of trapped carriers between the filled and the empty states near the quasi-Fermi level. It was also mentioned that the half of the trapping states were empty in that case. Under forward bias, the capacitance for the device was found to be constant and the diodes behaved like metal/insulator/semiconductor (MIS) structure as the DLC-diamond layer was undoped and acted like an insulator. It was also shown that the optical band gap of the r.f. deposited DLC diamond could be varied from 1.2 eV to 4.0 eV by changing the d.c. self bias during deposition.

Konofaos *et al.* [1] deposited amorphous diamond like carbon (DLC) thin films on n-type (100) silicon substrate. The method used to grow the films was plasma enhanced chemical vapor deposition of methane gas as the source for the carbon ions and the silicon was kept at 350° C. A texture camera was used to determine the crystallinity of the films. It was found that the films to be amorphous in nature. The samples were annealed at higher temperatures to observe any possible change to a polycrystalline form. The x-ray pictures after annealing were exactly the same as those produced by the as-deposited films indicating that there were no change in the film structure. The optical gaps for the deposited films were found to be 1.9 eV for as-deposited films and 1.7 eV for the annealed films. The density of trapping states at the silicon/carbon interface were measured. The values of the density of state were found in the order of 10^{11}-10^{12} cm^{-2} eV^{-1}. It was also shown that annealing has the effect of reducing the magnitude of the density of states. The films were doped with four different doses of boron atom. Ion implantation technique was used to transform the insulating DLC films into semiconducting by adding boron ions as dopants to achieve p-type conductivity. Thus p-n heterojunction devices were made, having silicon as one of the elements and DLC as the other element. The current-voltage

(I-V) characteristics of the undoped film grown on silicon substrate behaved like MIS device containing a defect insulator. The I-V characteristics of the devices containing four different doses of dopant were studied. Doping of the films showed a substantial increase in the forward bias region of the I-V characteristics and it was shown that doping had a dramatic effect on the conducting properties of the DLC films. The devices performed like Schottky diodes for low boron doses and like p-n diodes for high doses.

Our target in this work is to determine the energy band parameters of phosphorus doped n-C/p-Si heterojunction device. The experimental data obtained with n-C/p-Si heterojunction was fabricated at Soga laboratory, Department of Electrical and Electronic Engineering, Nagoya Institute of Technology, Japan. The obtained results are then compared with the previous reported ones. Some experimental details of deposition of CC films and n-C/p-Si heterostructure are discussed in the next section.

2.3 Un-doped Camphoric Carbon Films

Graphite had been commonly used as a target material for depositing carbon thin films for a long time. Scientists are always looking for alternative materials for this purpose. Recently camphor ($C_{10}H_{16}O$) has shown a lot of potentials for this purpose and to be used as alternative of graphite. Graphite consists of only sp^2 hybridized bonds, whereas, camphor ($C_{10}H_{16}O$) consists of both sp^2 and sp^3 hybridized bonds in its structure (Fig. 2.3). The existence of sp^3 bond helps to deposit diamond like carbon (DLC) films. DLC possess improved version of thin film quality. When hydrogenising of film is needed to change the thin film property, camphor gives an advantage over graphite. As the camphor structure has abundant hydrogen in it, no additional supply of hydrogen to the film growing system is needed, whereas, for graphite, additional hydrogen need to be supplied to the process. This advantage of camphor over graphite has introduced camphor as an alternative precursor material for deposition of carbon thin films.

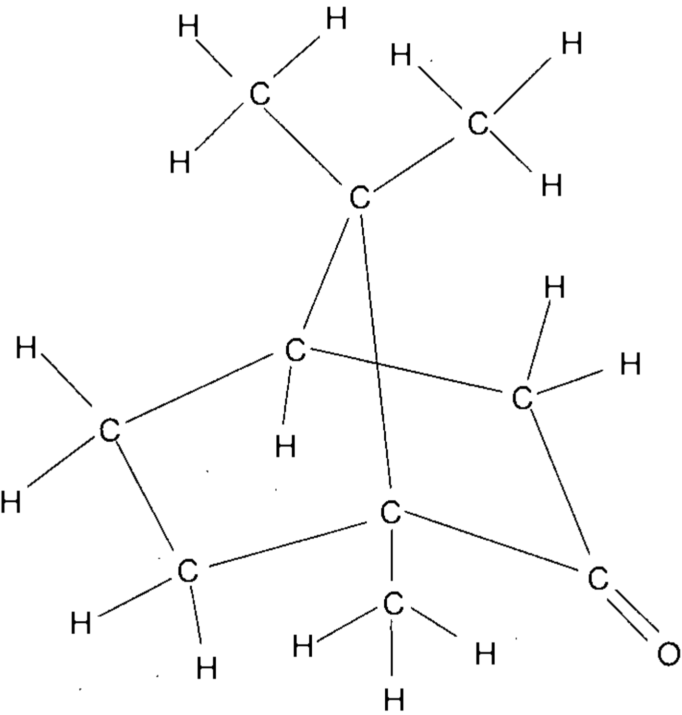

Figure 2.3: Chemical structure of camphor molecule ($C_{10}H_{16}O$).

2.3.1 Target Preparation

To prepare the target, camphor was burnt in a 1-meter long and 11 cm diameter quartz tube. A schematic representation of the experimental setup constructed for the generation of carbon soot by burning camphor is shown in Fig. 2.4. The soot deposited on the wall of the tube was collected, dried in the oven for an hour and pressed into pellets of about 1 cm in diameter and 2mm in thickness. These films were used as targets for carboneous thin films by ion beam sputtering. To facilitate the burning of camphor, an aspiration pump is used to maintain continuous circulation of air and to suck the gas from the burning system. Cold water flow is maintained to keep the inside wall of the quartz tube cool.

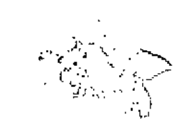

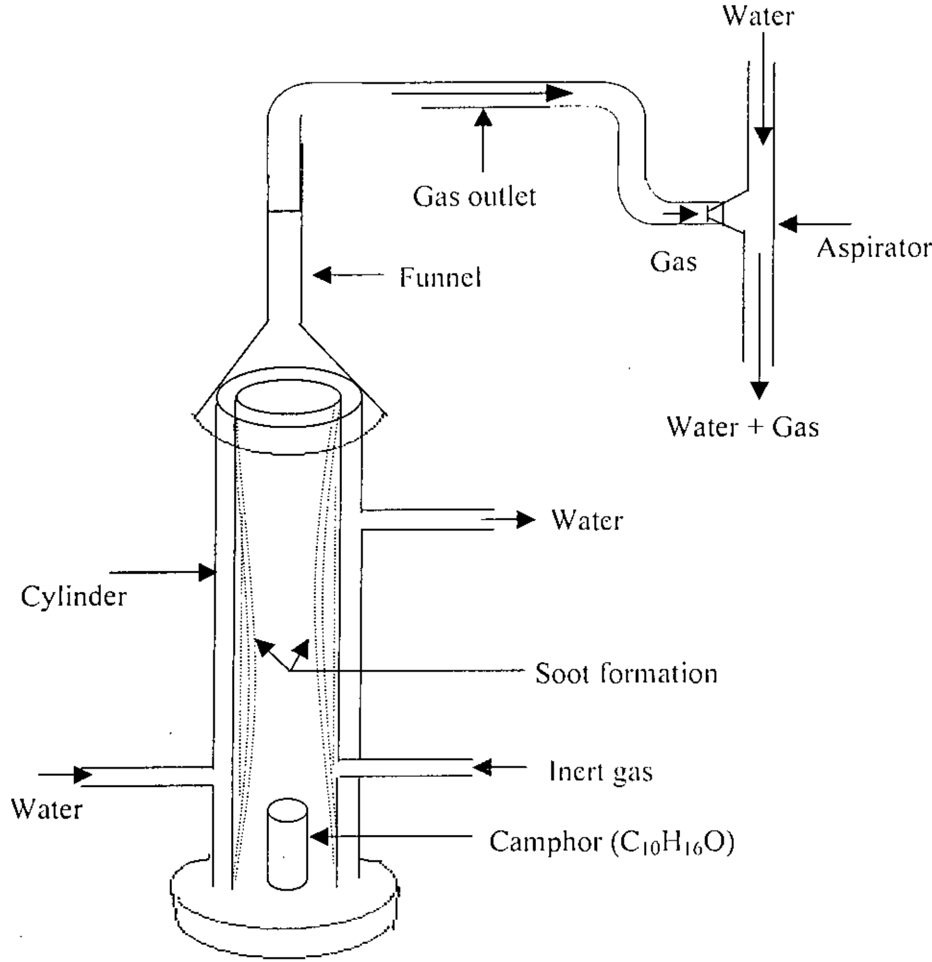

Figure 2.4: Schematic representation of camphor burning system.

2.3.2 Un-doped Camphoric Carbon Film Deposition by Pulsed Laser Deposition (PLD)

The properties of carbon thin film can be changed by controlling the relative amounts of sp^2 and sp^3 hybridized bonds in the film. The sp^3/ sp^2 in the thin film can be controlled by the energy of carbon species generated by various film deposition methods and the nature of the precursor materials. Pulsed laser deposition (PLD) process has the ability to generate highly energetic carbon species and thus even at low temperature can form a high percentage of sp^3 bonding in the film. PLD system is thus a very efficient method to deposit high quality diamond like carbon (DLC) thin film. Fig. 2.5 shows the arrangements for PLD system. DLC films are deposited

on silicon and quartz by excimer laser (NISSIN 10X, XeCl, λ = 308 nm, τ = 20 ns, repetition rate = 2 Hz, spot size = 5.5 mm^2), which is focused on the target at an incident angle of 45° to the target normal. The deposition system has a high vacuum chamber that is evacuated by a turbo molecular pump. The substrate is mounted parallel to the target at a distance of 45 mm. The films are deposited at room temperature at a base pressure of 10^{-6} Torr. The laser pulse energy is 150 mJ on the window.

2.4 P-doped Camphoric Carbon Film and its Deposition by PLD

As mentioned earlier, precursor materials and the method of deposition of carbon thin films dictate the properties of the film. Scientists are always searching for new precursors materials to deposit films in the efficient way. It was also mentioned that camphor gives some attractive advantage over graphite as a precursor material for depositing carbon thin films. It is found that undoped carbon is p-type in nature [12] and scientists in recent days are working on successful doping on carbon films. Attempts have been made to dope carbon films using various elements [12], [51]-[54]. Phosphorus (P) is widely used as an n-type impurity in silicon and phosphorus is a possible alternative to nitrogen (N) in carbon [56]. Veerasamy *et al.* [12] succeeded in obtaining n-type carbon using solid phosphorous. Nitrogen is the best atom for n-type doping because it is a shallow donor compared with phosphorus [37]. The atomic radius of nitrogen is less than that of phosphorus. However, very recently, successful electronic doping of camphoric carbon using a P target has been performed employing pulsed laser deposition (PLD) technique [9],[44]. The experimental procedure of deposition of the P-doped film is similar to that is used for the deposition of undoped film with a slight difference in the preparation of the target. For that, camphor is burnt in quartz tube and the soot deposited along the walls of the tube is collected, dried in the oven for approximately an hour. But before compressing into pallets, the dried CC soot is mixed with varying amounts of red phosphorus powder (1%, 3%, 5% and 7% by mass). Then using this target containing phosphorus, the films are deposited on silicon and quartz substrates by PLD system.

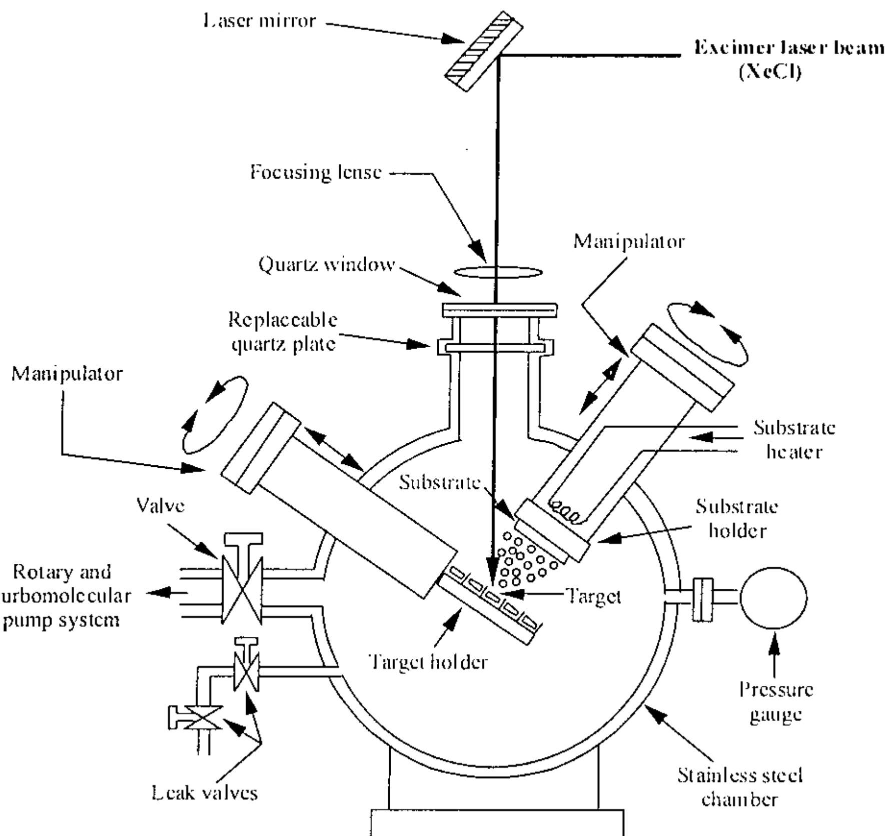

Figure 2.5: Experimental setup of pulsed laser deposition (PLD) technique for the deposition of thin film.

2.5 P-doped n-DLC/p-Si Heterostructure and its Deposition Procedure

In early stages of carbon/silicon heterojunction fabrication, most of the scientists deposited undoped carbonaceous film on n-type silicon substrate. As undoped carbonaceous film is p-type in nature, that kind of heterojunction was in fact p-carbon/ n-silicon heterostructure. Later some researchers tried to dope carbon with nitrogen and phosphorus and they were successful to do that and the materials thus prepared were n-type in nature. Inspired by that, P-doped n-type carbon films have been deposited on p-type silicon to obtain n-C/p-Si heterostructure. The schematic

view of the n-C/p-Si studied here is shown in Fig 2.6. Since undoped CC film shows p-type nature, carbon films obtained from the CC target is deposited on n-Si substrate. Similarly, P incorporated CC films are deposited on p-Si substrate because of n-type nature of P doped CC films. The resistivity of the substrate is about 5-10 Ω-cm [10]. A gold (Au) electrode of about 15 nm is deposited on carbon film for the top contact. For the bulk contact, about 100 nm antimony-gold electrode on n-Si substrate and gold electrode on p-Si substrate is deposited by conventional electron beam evaporation method. The contacts are found to be ohmic in nature.

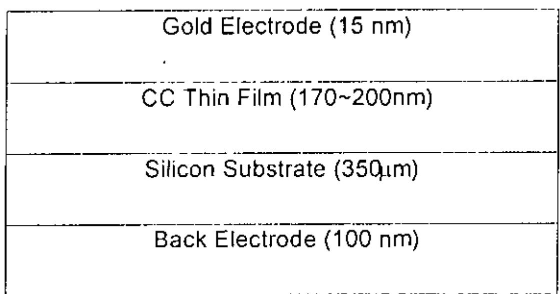

Figure 2.6: Schematic view of the n-C/p-Si heterojunction.

2.6 Theory of Constructing Energy Band Diagram for Heterojunction Device

A heterojunction is a junction formed between two semiconductors having different energy band gaps. Shockley [46] in 1951 first proposed the abrupt heterojunction to be used as emitter-base junction in a transistor. Kroemer [47] later analyzed the same for a wide-gap emitter of a transistor. A perfect match of the lattice constants and thermal expansion coefficients, however, are not normally possible in heterojunctions. Thus interface dislocations are usually present at the heterojunction interface [48]. While constructing the heterojunction, it is always tried to make the interface between the two semiconductors virtually free of defects. Recent development of heterojuntions and multiple heterojunctions have opened a broad range of prospects for device applications.

When semiconductors of different band gaps and electron affinities are brought together to form a heterojunction, the optical band gaps between the two materials are accommodated in the conduction band discontinuity ΔE_c and the valance band discontinuity ΔE_v. The conduction band discontinuity is always the differences between the electron affinities of the two materials constructing the heterojunction and the value of electron affinity is always constant for a particular material [63].

$$\Delta E_c = \chi_1 - \chi_2 \qquad \text{.....................................(2.1)}$$

where, χ_1 and χ_2 are the electron affinities of the two materials.

Change in doping in the material does not alter the value of its electron affinity. Valance band discontinuity ΔE_v is always related with the conduction band discontinuity ΔE_c and with the differences of optical gaps by the relation [63],

$$\Delta E_C + \Delta E_V = E_{g2} - E_{g1} \text{.....................................(2.2)}$$

where, E_{g2} and E_{g1} are the band gap energies of each semiconductor constructing the heterojunction. By using this relation the value of ΔE_v is calculated.

The built-in potential (V_{bi}) is always equal to the differences of work functions of the materials constructing the junction [63] as seen from Fig 2.3.

$$V_{bi} = \phi_{m2} - \phi_{m1} \qquad \text{.................................(2.3)}$$

where, ϕ_{m2} and ϕ_{m1} are the work functions of materials constructing the junction.

The built-in potential is divided between the two materials as required to align the Fermi levels at equilibrium. The resulting depletion region of each side of the heterojunction and the amount of built-in potential on each side are found by solving Poisson's equation with the boundary condition of continuous flux density at the junction. The barrier height that the electron must overcome to cross the junction is usually different from the barrier height the holes must overcome.

The energy band model of an ideal abrupt heterojunction was proposed by Anderson [49] based on the previous work of Shockley [46]. The model of Anderson is adequate to explain all the transport processes in the heterojuction devices. Anderson considered that the semiconductors which make the heterojunction have different band gaps (E_g), different dielectric constants (ε), different work functions (Φ) and different electron affinities (θ). Work function and electron affinity are defined, respectively, as that energy required to remove an electron from the Fermi level (E_F) and from the bottom of a conduction band (E_c) to a position just outside of the material (vacuum level). The top of the valance band is represented by E_v. The difference in the conduction band edges in the two materials is represented by ΔE_c and that in the valance band edges ΔE_v. Figure 2.7 shows the energy band diagram of n-p heterojunction at equilibrium. The difference in work functions of the two materials is the built-in voltage (V_D). V_D is equal to the sum of the partial built-in voltages ($V_{D1} + V_{D2}$), where, V_{D1} and V_{D2} are the electrostatic potentials supported at the equilibrium by semiconductor 1 and 2 respectively.

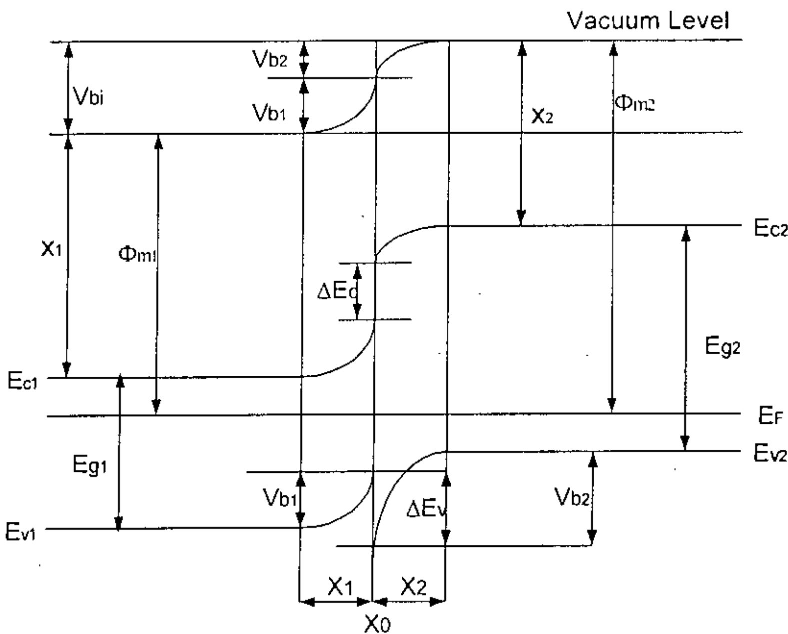

Figure 2.7: Energy band diagram of an ideal n-p heterojunction at equilibrium [63].

For non-degenerate materials, the discontinuity in the conduction band edges (ΔE_c) and the valance band edges (ΔE_v) are invariant with doping as in those cases the

electron affinity and band gap are not function of doping. The depletion widths and the transition capacitance are obtained by solving Poisson's equation for the step junction on either side of the interface. The expressions for depletion widths are [63],

$$X_1 = \sqrt{\frac{2N_{A2}\varepsilon_1\varepsilon_2(V_{bi} - V)}{qN_{D1}(\varepsilon_1 N_{D1} + \varepsilon_2 N_{A2})}} \quad \text{.............................(2.4)}$$

$$X_2 = \sqrt{\frac{2N_{D1}\varepsilon_1\varepsilon_2(V_{bi} - V)}{qN_{A2}(\varepsilon_1 N_{D1} + \varepsilon_2 N_{A2})}} \quad \text{.............................(2.5)}$$

And the transition capacitance is [63],

$$C = \sqrt{\frac{qN_{D1}N_{A2}\varepsilon_1\varepsilon_2}{2(\varepsilon_1 N_{D1} + \varepsilon_2 N_{A2})(V_{bi} - V)}} \quad \text{.............................(2.6)}$$

Here q is the charge of electron and V_{bi} is the built-in potential of the heterojunction.

The relative voltages supported in each of the semiconductors are given by the relation [63],

$$\frac{V_{D1} - V_1}{V_{D2} - V_2} = \frac{N_{A2}\varepsilon_2}{N_{D1}\varepsilon_1} \quad \text{.................................(2.7)}$$

where, V_1 and V_2 are the portions of the applied voltage V supported by materials 1 and 2 respectively.

According to Anderson's model for an abrupt heterojunction, C^{-2} is usually a linear function of the applied reverse bias out to at least a few volts in the reverse direction. From the slope of this linear part of C^{-2} versus V characteristics, it is possible to calculate the carrier concentration in any of the materials constructing the junction using Eqn. 2.6. The interception of the extrapolated part of the C^{-2} versus V characteristics to the voltage axis gives the total built-in potential in the heterojunction. Once the carrier concentration in each of the materials constructing the heterojuction and the built-in potential of the junction are known, it is possible to

calculate the depletion widths from Eqns. 2.4 and 2.5 and the separation of built-in voltage in the two materials from Eqn. 2.7.

To construct the energy band diagram, it is also necessary to calculate the optical gaps of the materials constructing the junction. To do that optical absorption coefficient (α) is calculated from the measurements of optical reflectance and transmittance data using the relation [57],

$$T=(1-R)^2 e^{-\alpha d} \quad \text{.....................................(2.8)}$$

where, T is optical transmittance, R is optical reflectance, α is absorption coefficient and d is thickness of the film.

Then $(\alpha h\nu)^{1/2}$ is plotted as a function of photon energy ($h\nu$). The optical gap is then obtained from the extrapolation of the linear part of the curve, $(\alpha h\nu)^{1/2}$ vs ($h\nu$) at the absorption coefficient α=0, using Tauc relation [8],

$$(\alpha h\nu)^{1/2} = B(E_g - h\nu) \quad \text{..............................(2.9)}$$

where, B is the Tauc parameter.

It is then necessary to calculate the positions of Fermi energy levels in each materials. To do that, activation energy of each materials constructing the heterojunction is calculated by analyzing the conductivity data for the materials using the relation [8],

$$\sigma = \sigma_0 \exp\left(-\frac{E_a}{kT}\right) \quad \text{............................(2.10)}$$

where, σ is the conductivity at temperature T (given in K), σ_0 is the conductivity prefactor, k is the Boltzmann's constant and E_a is the activation energy.

When all the parameters thus calculated are known, the energy band diagram can be drawn by aligning the Fermi energy levels of the materials constructing the heterojunction. In case of heterojunctions, the junction properties depend on both the properties of the materials constructing the junction. The current voltage characteristics in the heterojunction depends on the band discontinuities in the junction. If the barrier to holes is much higher than that of electrons, then the current consists almost all of electrons. Both the forward current and the reverse current strongly depend on the behaviours of the junction constructing materials. The expression for total current in the junction is given by [63],

$$I = I_0(e^{\frac{qV}{\eta kT}} - 1) \quad \text{.....(2.11)}$$

where,

I is the total junction current

I_0 is the reverse saturation current in the junction

q is the charge of electron

V is the applied voltage to the junction

η is the diode quality factor

k is the Boltzmann's constant

T is the temperature given in K

The reverse saturation current is given by [63],

$$I_0 = qA\left(\frac{D_p}{L_p}\frac{n_{iN}^2}{N_D} + \frac{D_n}{L_n}\frac{n_{iP}^2}{N_A}\right) \quad \text{.....(2.12)}$$

where,

q is the charge of electron

A is the cross section area of the junction

D_p is the hole diffusivity in the n-type material

D_n is the electron diffusivity in the p-type material

L_p is the hole diffusion length in the n-type material

L_n is the electron diffusion length in the p-type material

n_{iN} is the intrinsic carrier concentration in the n-type material

n_{iP} is the intrinsic carrier concentration in the p-type material

Thus knowing the value of reverse saturation current, it is possible to calculate some of the parameters for the heterojunction using Eqn. 2.12.

Fig. 2.8 shows current-voltage characteristics of a practical Si diode. J_s represents the saturation current density in the junction. In the figure region (a) represents generation-recombination current. Because of the reduction in carrier concentration under the reverse bias, the dominant recombination-generation process is due to emission. The generation current is given by [63],

$$J_{gen} = \frac{qn_iW}{\tau_e} \quad \text{.............................(2.13)}$$

where, q is the charge of electron, n_i is the intrinsic carrier concentration, W is the total depletion width and τ_e is the effective carrier life time.

At a given temperature, generation current is proportional to the depletion-layer width, which is dependent on the applied reverse bias voltage. If the effective life time is a slowly varying function of temperature, the generation current will then have the same temperature dependence as n_i. For semiconductors with large values of n_i the diffusion component will dominate at room temperature, but if n_i is small the generation current may dominate. At sufficiently high temperatures, however, the diffusion current will dominate. At forward bias, the major recombination-generation processes in the depletion region are the capture processes, there exists a recombination current in addition to the diffusion current. The recombination current is given by [63],

$$J_{rec} \sim n_i N_t \quad \text{.............................(2.14)}$$

where, N_t is the trap density.

Similar to generation current in the reverse bias, the recombination current in the forward bias is also proportional to n_i.

In the Fig. 2.8, region (b) represents diffusion current in the bulk of the semiconductor.

Region (c) indicates high injection current. At high current densities under the forward bias condition such that the injected minority carrier density is comparable with the majority concentration, both drift and diffusion current components must be considered.

At region (d) series resistance effect is introduced to the current voltage characteristics of the diode.

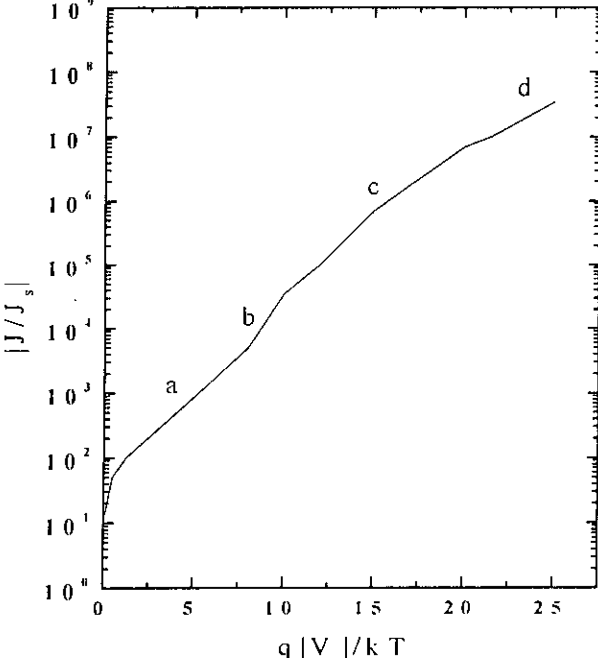

Figure 2.8: Current-voltage characteristics of a practical Si diode [61].

Chapter 3

Results and Discussions

Since long, silicon is dominating the market of semiconductor devices. Scientists are always searching for alternative materials for this purpose. They are also looking for element that will give a much more advantage over silicon in device fabrication process and will give a much more flexibility to alter the properties of the fabricated devices with simpler means. In recent days carbon has shown a great potentiality in device fabrication technology. Very recently, P-doped camphoric carbon film has been deposited on p-type silicon to obtain n-C/p-Si heterostructure. Some of the electrical and optical characteristics of this heterostructure have been studied. In this chapter we shall study the behaviour of this heterostructure and shall propose energy band diagrams for the device using the experimental observations [56]. The results obtained here will then be correlated with the previously reported results.

3.1 Analyses of Capacitance-Voltage (C-V) Characteristics

Phosphorus (P)-doped n-DLC/p-Si heterojunction has been fabricated and experimented at the "Soga Laboratory", Department of Electrical and Electronic Engineering, Nagoya Institute of Technology, Japan [56]. The deposition procedure and the details of the fabricated device is described in chapter two. The capacitance versus voltage (C-V) data have been obtained and are shown in Table 3.1.

Table 3.1: Capacitance versus voltage data for the films deposited from the target containing various amounts (1%, 3%, 5% and 7%) of phosphorus by mass

Applied Voltage (volts)	Capacitance (F/cm^2)			
	1% P	3% P	5% P	7% P
-2.00	6.01709E-10	5.18691E-10	4.11920E-10	5.75688E-10
-1.95	6.04598E-10	5.47696E-10	4.13867E-10	5.78581E-10
-1.90	6.07486E-10	5.49628E-10	4.15814E-10	5.81474E-10
-1.85	6.09411E-10	5.54457E-10	4.18734E-10	5.83402E-10
-1.80	6.12299E-10	5.57354E-10	4.20680E-10	5.86294E-10
-1.75	6.15186E-10	5.67006E-10	4.22627E-10	5.90149E-10
-1.70	6.18073E-10	5.67006E-10	4.24573E-10	5.93040E-10
-1.65	6.20959E-10	5.68936E-10	4.26518E-10	5.95930E-10
-1.60	6.23844E-10	5.71830E-10	4.29437E-10	5.98820E-10
-1.55	6.27691E-10	5.73759E-10	4.31382E-10	6.01709E-10
-1.50	6.30575E-10	5.77617E-10	4.34299E-10	6.05561E-10
-1.45	6.33459E-10	5.80510E-10	4.36244E-10	6.08449E-10
-1.40	6.37304E-10	5.86294E-10	4.39161E-10	6.12299E-10
-1.35	6.42108E-10	5.88222E-10	4.42077E-10	6.16148E-10
-1.30	6.44991E-10	5.91113E-10	4.44021E-10	6.19997E-10
-1.25	6.48833E-10	5.95930E-10	4.46936E-10	6.22882E-10
-1.20	6.52674E-10	6.04598E-10	4.50822E-10	6.27691E-10
-1.15	6.57474E-10	6.14224E-10	4.53737E-10	6.32498E-10
-1.10	6.61313E-10	6.13261E-10	4.56650E-10	6.36343E-10
-1.05	6.65152E-10	6.16148E-10	4.59563E-10	6.41148E-10
-1.00	6.69949E-10	6.20959E-10	4.63447E-10	6.45951E-10
-0.95	6.74744E-10	6.25768E-10	4.67329E-10	6.50753E-10
-0.90	6.79538E-10	6.30575E-10	4.71211E-10	6.55554E-10
-0.85	6.85290E-10	6.35382E-10	4.75092E-10	6.62273E-10
-0.80	6.91039E-10	6.40187E-10	4.79942E-10	6.68030E-10
-0.75	6.96787E-10	6.44030E-10	4.83821E-10	6.73785E-10
-0.70	7.02532E-10	6.43069E-10	4.89637E-10	6.81456E-10
-0.65	7.09233E-10	6.50753E-10	4.94483E-10	6.88165E-10
-0.60	7.16888E-10	6.57474E-10	5.00296E-10	6.95829E-10
-0.55	7.24540E-10	6.64192E-10	5.06107E-10	7.04447E-10
-0.50	7.33144E-10	6.84331E-10	5.12884E-10	7.14018E-10
-0.45	7.42699E-10	6.90081E-10	5.20626E-10	7.24540E-10
-0.40	7.53203E-10	6.91997E-10	5.28365E-10	7.36011E-10
-0.35	7.65610E-10	7.02532E-10	5.39000E-10	7.49384E-10
-0.30	7.78960E-10	7.13061E-10	5.49628E-10	7.64656E-10
-0.25	7.95158E-10	7.24540E-10	5.63146E-10	7.82773E-10
-0.20	8.14196E-10	7.39833E-10	5.79546E-10	8.03728E-10
-0.15	8.37013E-10	7.78007E-10	5.99783E-10	8.31312E-10
-0.10	8.64545E-10	8.08487E-10	6.24806E-10	8.64545E-10
-0.05	8.98663E-10	8.38914E-10	6.57474E-10	9.08128E-10
0.00	9.41218E-10	8.79717E-10	7.00617E-10	9.63871E-10

The variation of capacitance with reverse bias voltage of the n-DLC/p-Si heterojunction device for the n-DLC thin film grown from the targets containing different amounts of P (1%, 3%, 5% and 7%) are shown in Figs. 3.1, 3.2, 3.3 and 3.4 respectively. Fig 3.5 shows a comparative picture of the variation of capacitance with reverse bias voltage with different P contents in the target material from where the films are grown.

For the device, the C-V characteristics show interesting characteristics. From Fig. 3.5 it is seen that with the increase in the P content, the value of capacitance in the high reverse bias region decreases from 1% to 3% P and then increases for 7% P. Whereas, reports from the findings of others scientists show that, the value of the capacitance increases with the increase in dopant percentage in the target from where the films are grown [4]. Under reverse bias, the capacitance decreases with the increase in reverse bias. This happens as the reverse bias voltage is increased, the depletion width both in carbon thin film and silicon increases and there is a decrease in the total capacitance of the heterojunction. The total depletion capacitance of the junction is in fact a series combination of two capacitances, one is the depletion capacitance for the Si side and the other is the depletion capacitance for the C side. As the reverse bias voltage is increased, a situation attains when the DLC thin film becomes fully depleted. After that, when the reverse voltage is increased further, the depletion capacitance on the Si side just remain a function of the applied voltage, while on the DLC side, the capacitance reaches a limit equal to $\varepsilon A/d$, where, ε is the permittivity of the DLC thin film, A is the device cross sectional area and d is the film thickness. In the latter regime, the slopes of the C^{-2} versus reverse V characteristics only depend on the Si substrate. Thus the depletion on the Si substrate will give a common slope for the C^{-2} versus V characteristics only on the high reverse bias for all the n-DLC/p-Si heterojunction devices having varying amounts of P (1% to 7% by mass) in carbon layer.

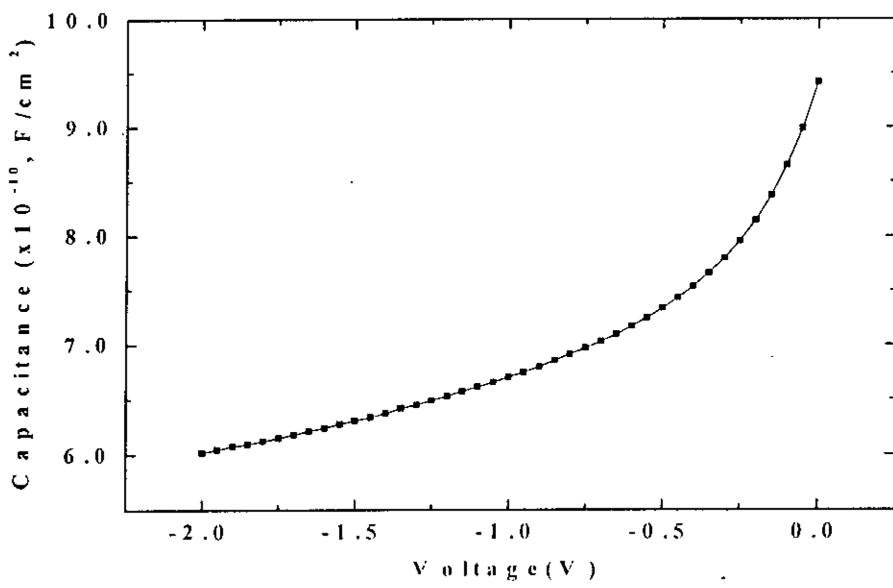

Figure 3.1: Capacitance versus voltage characteristics for n-DLC/p-Si heterojunction where, DLC thin film has been deposited from the target containing 1% phosphorus.

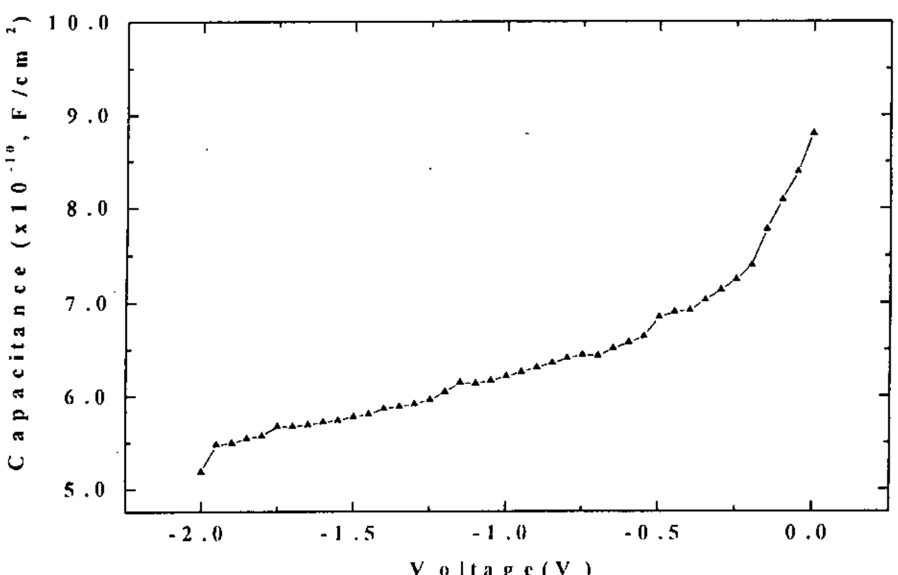

Figure 3.2: Capacitance versus voltage characteristics for n-DLC/p-Si heterojunction where, DLC thin film has been deposited from the target containing 3% phosphorus.

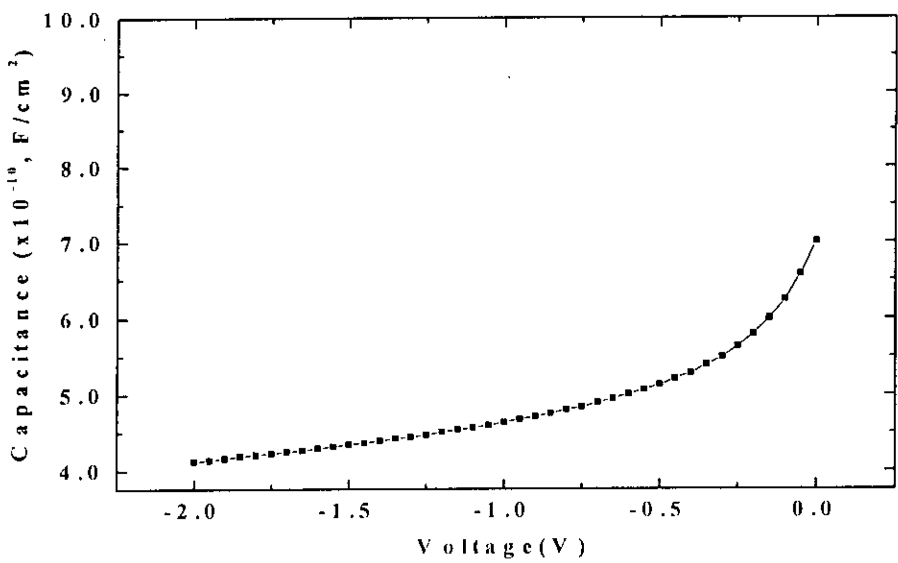

Figure 3.3: Capacitance versus voltage characteristics for n-DLC/p-Si heterojunction where, DLC thin film has been deposited from the target containing 5% phosphorus.

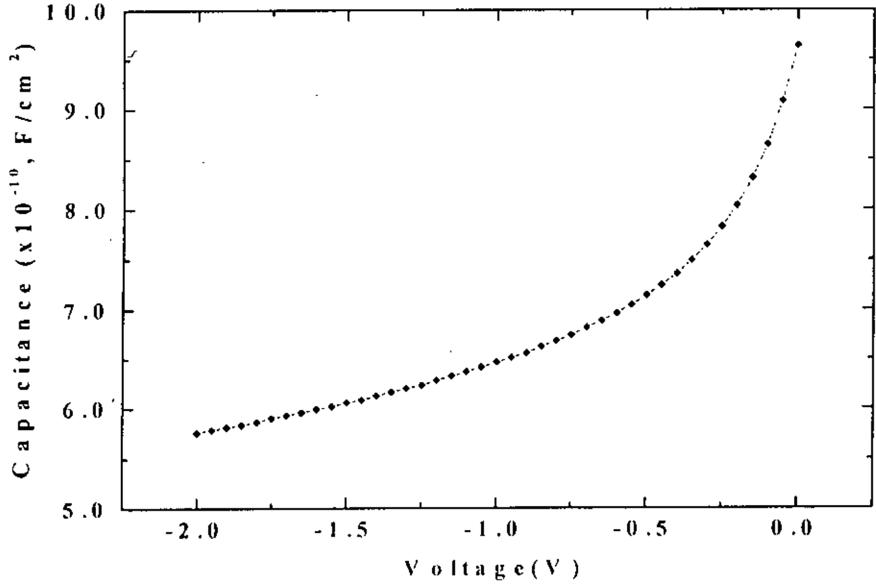

Figure 3.4: Capacitance versus voltage characteristics for n-DLC/p-Si heterojunction where, DLC thin film has been deposited from the target containing 7% phosphorus.

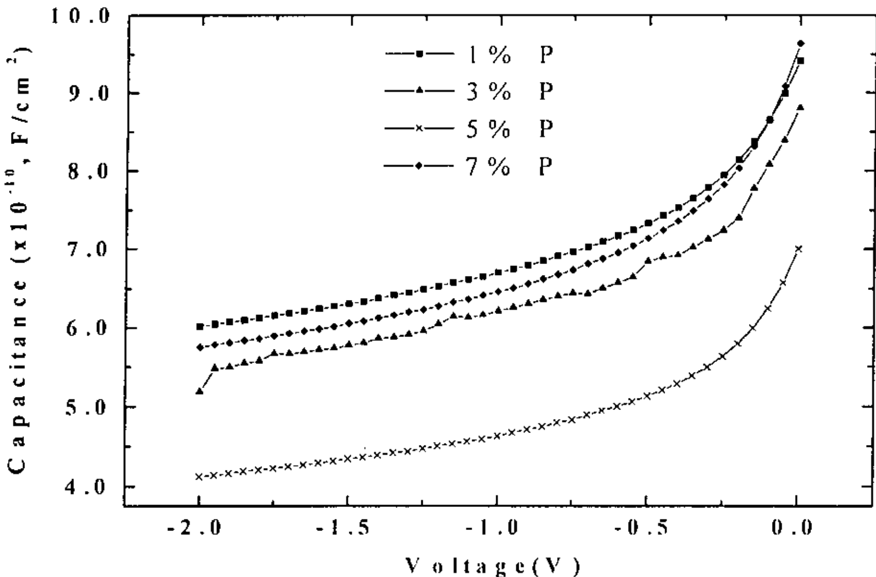

Figure 3.5: Capacitance versus voltage characteristics for n-DLC/p-Si heterojunction where, DLC film has been deposited from target containing 1%, 3%, 5% and 7% phosphorus.

The substrate of heterojunction as mentioned earlier is silicon with thickness of 350 μm. The silicon substrate is doped with boron with constant carrier concentration of 1.5×10^{15} cm^{-3} for all the cases. The capacitance and the bias voltage are related to the parameters of heterojunction with the Eqn. 2.6 given in chapter two. Actually the voltage dependence of the junction capacitance contains information regarding the heterojunction. For a plot of C^{-2} versus the reverse bias voltage, the slope depends on the doping levels of the acceptor carrier concentration (N_A) in p-Si and donor carrier concentration (N_D) in n-DLC. The permittivity of carbon is considered to be $5.5\varepsilon_0$ [62] and that of silicon is $11.8\varepsilon_0$, where, ε_0 is the permittivity of free space. The extrapolation of linear C^{-2} versus reverse V characteristics for low reverse bias region intercepting on the voltage axis gives the value of built-in potential (V_{bi}) for the heterojunction for different dopant concentrations. The C^{-2} versus V characteristics for different P dopant contents are shown in Fig. 3.6. From the slope of the characteristics, knowing the values of N_A, the values of permittivies for both in Si and DLC, the carrier concentration in DLC is calculated from Eqn. 3.1, which is evaluated from Eqn. 2.6.

efficiently done, then it is unrealistic to find any decrease in carrier concentration with the increase in P in the target materials from where the films are grown. Further we calculated the depletion width for both in carbon and silicon region using Eqn. 2.4 and Eqn. 2.5. These equations are repeated here for our device. Eqns 3.2 and 3.3 give the depletion widths in DLC and Si respectively.

$$X_C = \sqrt{\frac{2N_A\varepsilon_1\varepsilon_2(V_{bi}-V)}{qN_D(\varepsilon_1 N_D+\varepsilon_2 N_A)}} \quad \text{.....(3.2)}$$

$$X_{Si} = \sqrt{\frac{2N_D\varepsilon_1\varepsilon_2(V_{bi}-V)}{qN_A(\varepsilon_1 N_D+\varepsilon_2 N_A)}} \quad \text{.....(3.3)}$$

where, V is the applied voltage to the heterojunction.

Using the values of parameters of Eqn. 3.2, the value of depletion widths in carbon thin film is calculated for films deposited from targets containing different amounts of P. It is found that even at zero bias, the carbon thin film is fully depleted. It is calculated that the depletion width at zero bias in carbon is of the order 10^3 nm, whereas, the total width of the thin film is 170-200 nm. As the carrier concentration in the DLC film is found to be appreciably small with respect to that in Si, the depletion width in the DLC film penetrates much greater than in Si substrate and the calculated depletion width in DLC is found much greater than its film thickness.

Table 3.2: Carrier concentration and built-in potential calculated for the heterojunction where, carbon thin film is deposited from target containing 1%, 3%, 5% and 7% phosphorus

% P	Carrier concentration in n-DLC (N_D), cm^{-3}	Built-in potential of the heterojunction (V_{bi}), volt
1	1.23×10^{13}	0.56
3	1.08×10^{13}	0.55
5	4.90×10^{12}	0.41
7	9.85×10^{12}	0.47

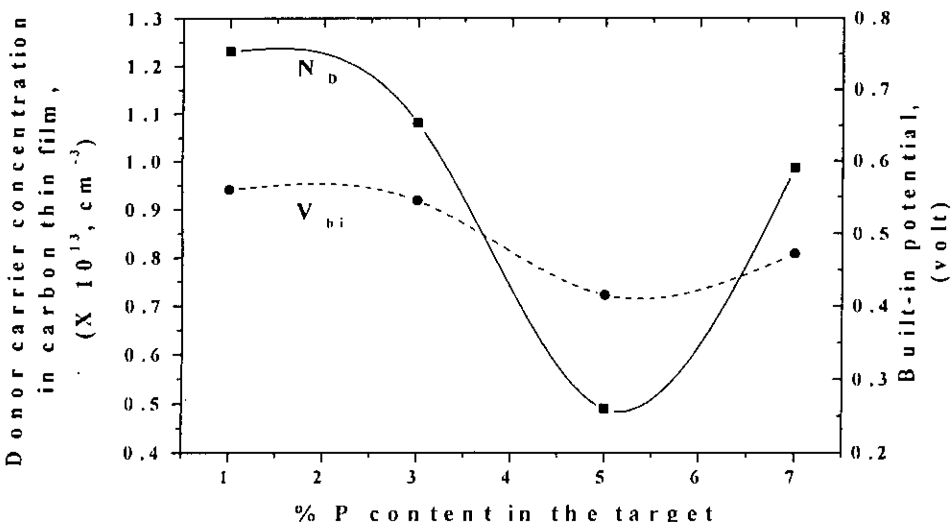

Figure 3.7: Variation of carrier concentration in n-DLC and the built-in potential of the heterojunction with % phosphorus in the target material from where, the films are grown.

The main objective of this work is to calculate the energy band parameters for the n-DLC/p-Si heterojunction grown from targets containing different amounts of P. As the carrier concentration in the p-Si substrate is 1.5×10^{15} cm^{-3}, the activation energy for Si (difference between Fermi energy level and valance band energy level) is considered as 0.3 eV.

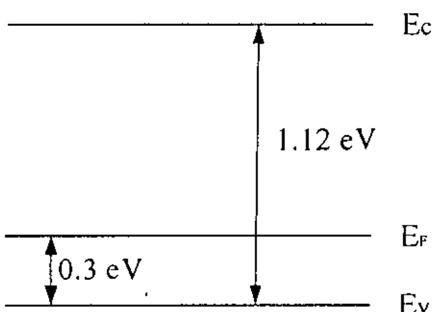

Figure 3.8: Optical band gap and activation energy for silicon.

We next try to calculate the activation energy (difference between Fermi energy level and conduction band energy level) for n-type DLC. To do so, the conductivity data at various temperatures for the heterojuction for different P dopant content are analyzed. This data were also obtained from "Soga Laboratory", Department of Electrical and Electronic Engineering, Nagoya Institute of Technology, Japan. The data are given in Table 3.3.

Table 3.3: Conductivity of the films deposited from the target containing various amounts of phosphorus (1%, 3%, 5% and 7% by mass) for different temperatures

Temperature (° K)	**Conductivity (Ω-cm)$^{-1}$**				
	Undoped	**1% P**	**3% P**	**5% P**	**7% P**
50	2.73E-06	1.67E-06	7.98E-05	0.000566	0.000875
60	2.76E-06	1.67E-06	8.00E-05	0.000566	0.000876
75	2.79E-06	1.67E-06	8.02E-05	0.000567	0.000876
90	2.81E-06	1.67E-06	8.06E-05	0.000567	0.000877
100	2.84E-06	1.67E-06	8.14E-05	0.000567	0.00088
110	2.85E-06	1.75E-06	8.46E-05	0.000567	0.000883
125	2.94E-06	1.83E-06	0.000106	0.000569	0.000896
140	3.53E-06	1.96E-06	0.000124	0.000572	0.000934
150	4.46E-06	2.22E-06	0.000145	0.000591	0.000989
160	5.47E-06	2.51E-06	0.000165	0.000617	0.001035
175	6.50E-06	3.31E-06	0.000185	0.000697	0.00115
190	7.64E-06	3.70E-06	0.000206	0.000733	0.00123
200	9.34E-06	4.30E-06	0.000257	0.000738	0.001326
210	1.14E-05	4.71E-06	0.000292	0.000771	0.001445
225	1.45E-05	6.22E-06	0.000371	0.000833	0.001592
240	1.82E-05	7.41E-06	0.000413	0.000981	0.001905
250	2.29E-05	9.44E-06	0.000455	0.001075	0.002193
260	2.53E-05	1.12E-05	0.000496	0.001218	0.002396
275	3.07E-05	1.53E-05	0.000598	0.001354	0.002838
290	3.72E-05	1.99E-05	0.000689	0.001594	0.003552
300	4.72E-05	2.71E-05	0.000826	0.001762	0.003824
310	5.44E-05	3.11E-05	0.000945	0.001962	0.004283
325	6.60E-05	3.76E-05	0.001053	0.002129	0.004817
340	7.80E-05	5.00E-05	0.001324	0.002428	0.005601
360	0.000117	7.06E-05	0.001672	0.002995	0.006935
375	0.000139	9.16E-05	0.001968	0.003526	0.008308
390	0.000166	0.000123	0.002398	0.004154	0.009927
400	0.000195	0.000144	0.002825	0.005123	0.010538

The temperature (T) dependence of electrical conductivity (σ) is obtained for undoped and P doped DLC films. The logarithmic variation of conductivity with inverse temperature (ln(σ) vs 1/T) is shown in Fig 3.9. Above room temperature, the conduction mechanism is suggested to be in the extended states as ln(σ) vs 1/T is linear. Below the room temperature, the slopes of the ln(σ) vs 1/T plot changes and the change in conductivity with the change in temperature becomes very low. The conduction mechanism for below room temperature and lower temperature range can be attributed to conduction in band tail states and variable range hopping via deep states [8] respectively. At any level of temperature, the conductivity of the film is seen to decrease with addition of a small amount of P (1%) in the target material and then increases sharply for the films deposited from the targets containing 3%, 5% and 7% P. Undoped DLC film is lightly p-type in nature due to the presence of acceptor like defect states and a small amount of P addition compensates or passivates the acceptor-like defect states by ionized atoms from P atoms. Therefore, the conductivity is observed to decrease as the Fermi level (E_F) moves through the mid gap for the film deposited from the target containing 1% P. With further increase of P content in the target material, E_F moves towards the conduction band edge and the conductivity increases.

The activation energy is calculated from slope of the conductivity measured as a function of temperature. The relationship between conductivity and conductivity activation energy (E_a) is given by Eqn. 2.10 of chapter 2.

$$\sigma = \sigma_0 \exp\left(-\frac{E_C - E_F}{kT}\right)$$

$$= \sigma_0 \exp\left(-\frac{E_a}{kT}\right) \quad \text{..............................(3.4)}$$

where, σ_0 is the conductivity prefactor, E_F is the Fermi energy, E_C is the energy of bottom of conduction band, k is the Boltzmann constant and T is the absolute temperature at which the conductivity is measured.

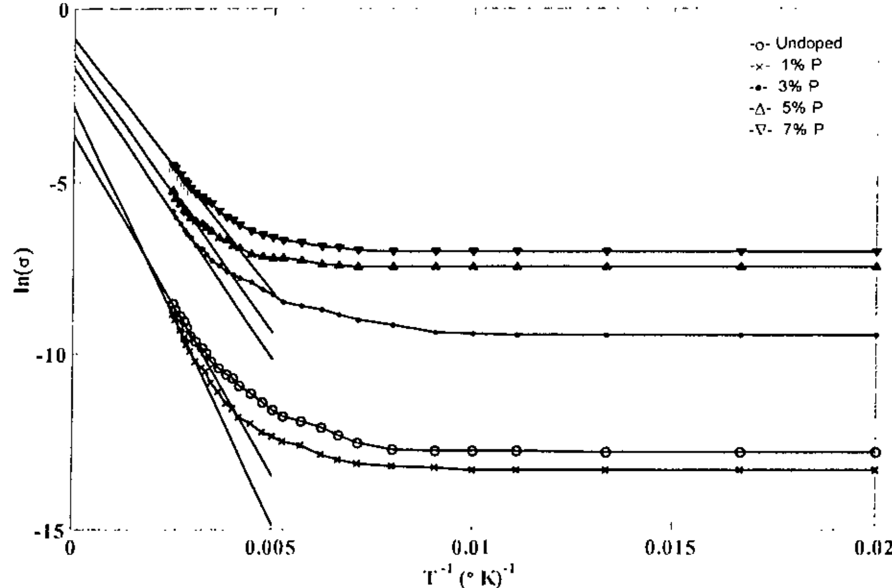

Figure 3.9: ln(σ) vs T^{-1} to calculate activation energy and conductivity prefactor for different phosphorus contents in the target.

Fig. 3.9 shows the ln(σ) vs T^{-1} characteristics for the n-DLC/p-Si heterojunction where, the films are deposited from targets containing 1%, 3%, 5% and 7% P. Near room temperature (300 K), the plot shows linear behavior for each dopant contents. The conduction mechanism in carbon is complex due to presence of tetrahedral and trihedral bonding and anti bonding states. Further, the high density of defects limit the activated conduction mechanism by initiating hopping conduction in the localized states. At low temperatures the conductivity is seen to be almost constant, whereas, with the increase in temperature it is seen that conductivity increases, which indicates that activated conduction mechanism is present there. The slope of the characteristics in this region then gives the room temperature activation energy for the heterojunction deposited from the target containing different dopant contents.

The variation of room temperature activation energy with dopant contents is shown in Fig. 3.10. It is seen that the activation energy for the DLC initially increases and then decreases with the increase in dopant content in the target material. As it is mentioned earlier that the undoped DLC is p-type in nature and addition of small amount of P dopant converts the film to n-type and thus shows an initial increase in

activation energy of DLC. In this case E_F moves towards the mid gap region. Further increase in dopant content moves the Fermi level E_F towards the conduction band edge E_C and thus the value of activation energy decreases.

The value of conductivity prefactor is also calculated. The extrapolation of the linear portion of $\ln(\sigma)$ vs T^{-1} characteristics at high temperature intercepting the $\ln(\sigma)$ axis gives the logarithmic value of conductivity prefactor $\ln(\sigma_0)$ from where the value of conductivity prefactor (σ_0) is calculated. Fig. 3.11 shows the variation of conductivity prefactor with the dopant content in the target material from where the films were grown. The variation shows an increasing trend with the increase in dopant content.

The variation of room temperature conductivity with the dopant content in the target material from where the films were grown is shown in Fig. 3.12. The room temperature conductivity decreases from undoped to 1% P and then increases gradually.

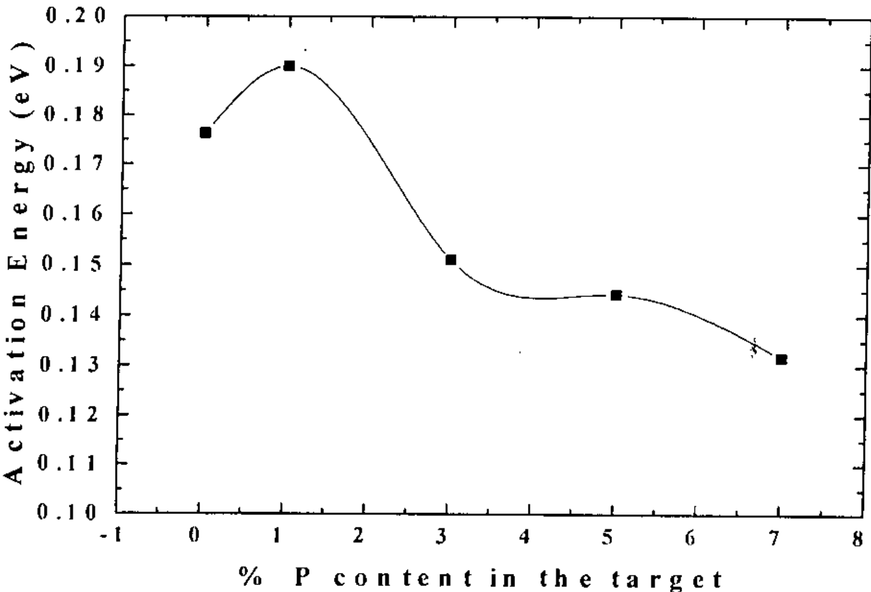

Figure 3.10: Variation of activation energy of DLC with dopant content in the target material.

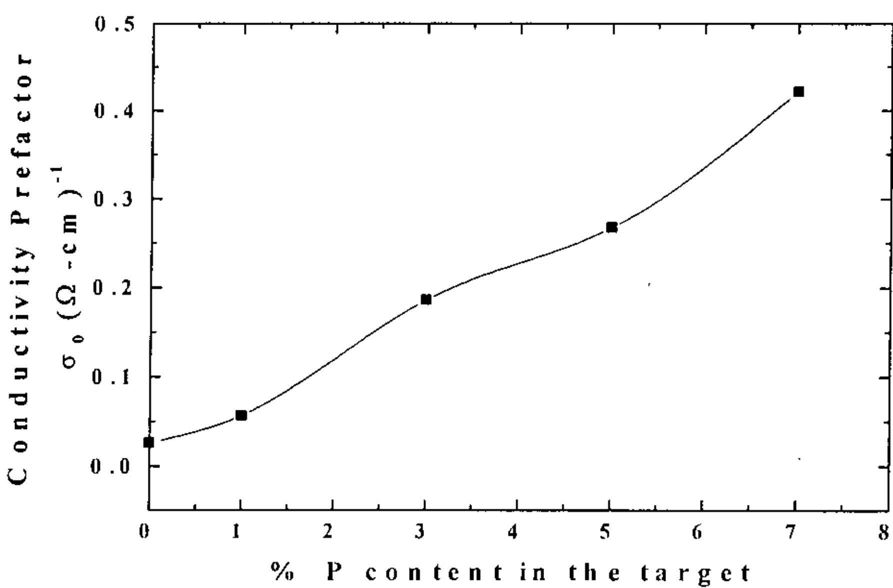

Figure 3.11: Variation of conductivity prefactor with the change in dopant content in the target material.

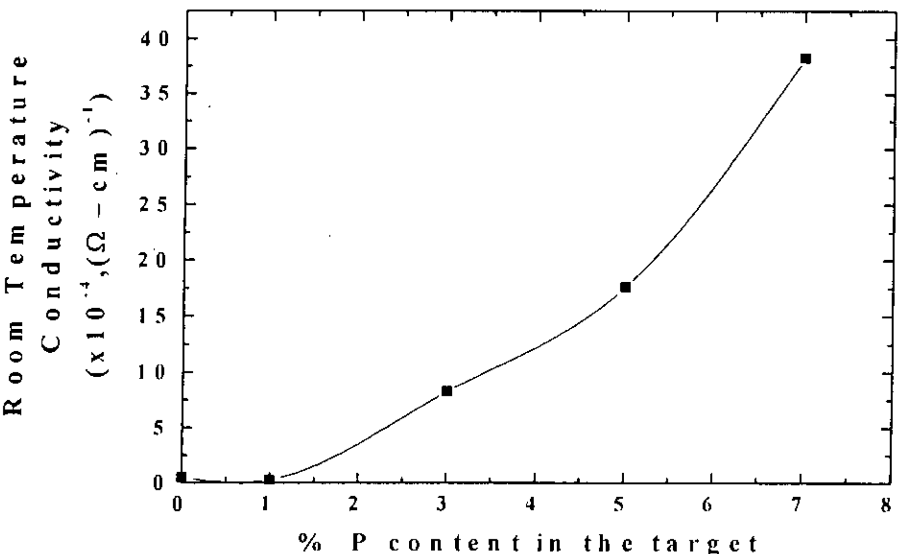

Figure 3.12: Variation of room temperature conductivity with the change in dopant content in the target material.

The values of activation energy, conductivity prefactor and room temperature conductivity from conductivity data analyses for the undoped DLC thin film and for the film deposited from the targets containing 1%, 3%, 5% and 7% P are shown in Table 3.4.

Table 3.4: Values of activation energy, conductivity prefactor and room temperature conductivity for different dopant contents

% P	Activation Energy (eV)	Conductivity Prefactor $(\Omega\text{-cm})^{-1}$	Room Temperature Conductivity $(\Omega\text{-cm})^{-1}$
Undoped	0.18	0.03	4.72×10^{-5}
1	0.19	0.06	2.71×10^{-5}
3	0.15	0.19	8.26×10^{-4}
5	0.14	0.27	1.76×10^{-3}
7	0.13	0.42	3.82×10^{-3}

The optical transmittance and reflectance data are obtained for the carbon thin films grown from the target containing different amounts of P (1%, 3%, 5% and 7% by mass) grown on quartz. Fig. 3.13 shows the variation of optical transmittance with the wavelength. The absorbance is high for photons of energy greater than the band gap. On the other hand, beyond the gap edge the absorbance is very small and the transmittance is high, which indicates that the obtained sample is of low impurity and has few lattice defects.

Fig. 3.14 shows the variation of optical reflectance with the wavelength. For higher wave lengths the carbon thin films show metallic behaviour and thus for higher wavelengths the optical reflectance is high.

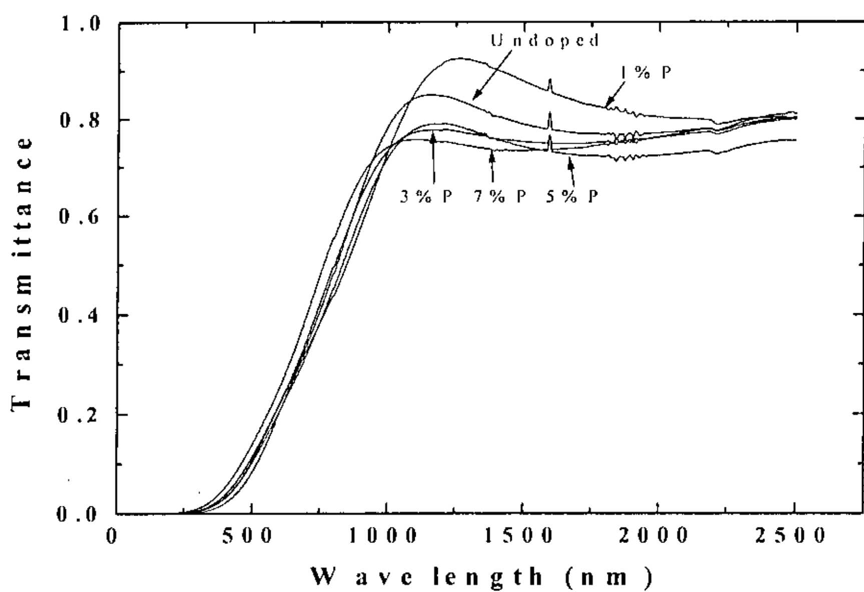

Figure 3.13: Variation of optical transmittance with wavelength.

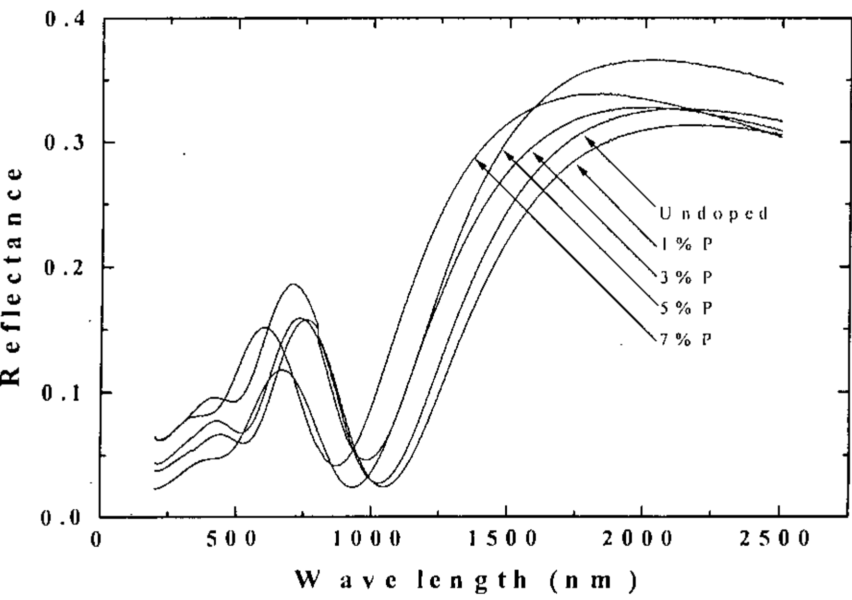

Figure 3.14: Variation of optical reflectance with wavelength.

The absorption coefficient α is determined by using the relation given in Eqn. 2.8,

$$\alpha = \frac{1}{d} \ln \frac{(1-R)^2}{T} \qquad \text{.....(3.5)}$$

where, T is the optical transmittance, R is the optical reflectance and d is the thickness of the film.

From the calculated α, the extinction coefficient k is determined using the equation [63],

$$\alpha = \frac{4\pi k}{\lambda} \qquad \text{.....(3.6)}$$

where, λ is the wavelength.

The variation of the extinction coefficient (k) with photon energy ($h\nu$) is shown in Fig. 3.15. Here ν is the frequency of the incident light. It is seen from the plot that with the increase in photon energy, the value of k increases. This happens as for a fixed mobility gap, with the increase in photon energy, the probability of electron transfer across the mobility gap rises with photon energy. Thus the value of k increases with the increase in photon energy. At high photon energies, extinction coefficient becomes increasingly independent of photon energy.

From the calculated k, the value of refractive index n is calculated from the relation [63],

$$R = \frac{(1-n)^2 + k^2}{(1+n)^2 + k^2} \qquad \text{.....(3.7)}$$

The refractive index of a medium is defined as the ratio of speed of light in free space to its speed in a medium. The variation of refractive index is shown in Fig. 3.16. From the calculated refractive index, the value of relative permittivity is calculated for different photon energies. The relation between refractive index and

relative permittivity is $n = \sqrt{\varepsilon_r}$. The variation of relative permittivity with photon energy is shown in Fig. 3.17.

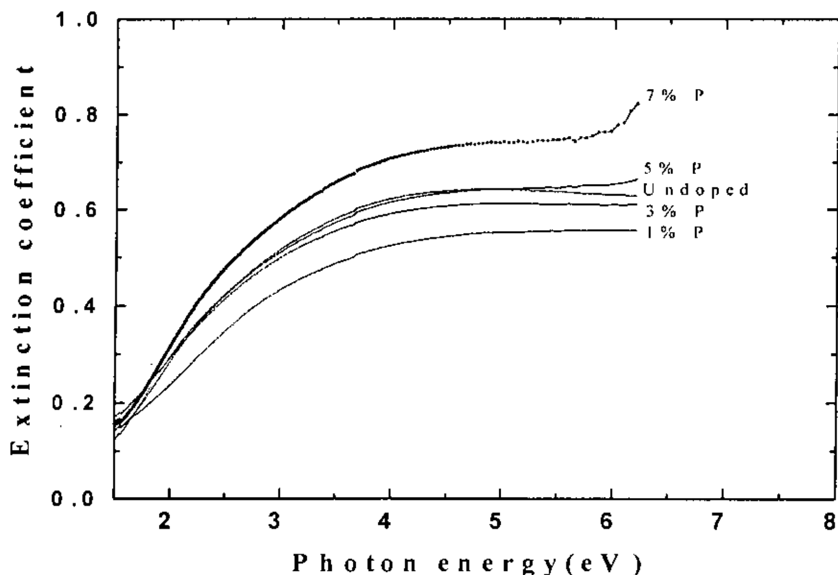

Figure 3.15: Variation of extinction coefficient with photon energy.

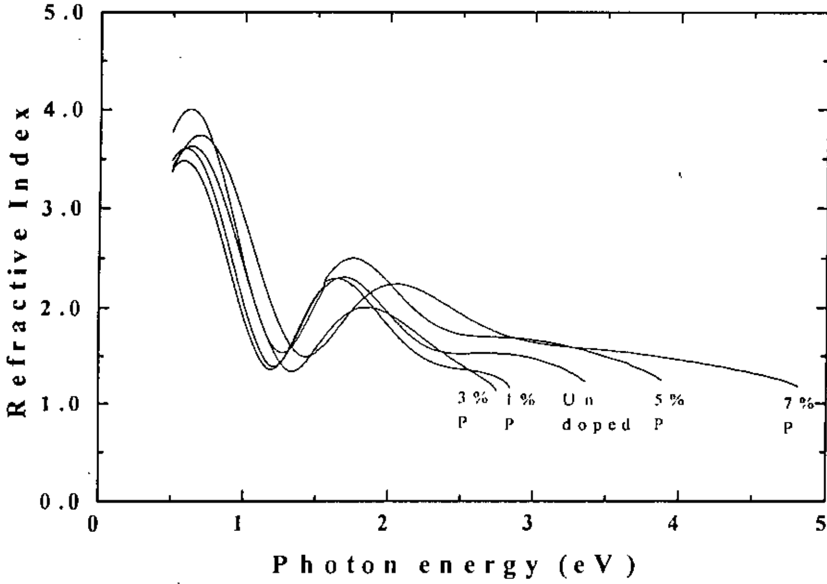

Figure 3.16: Variation of refractive index with photon energy.

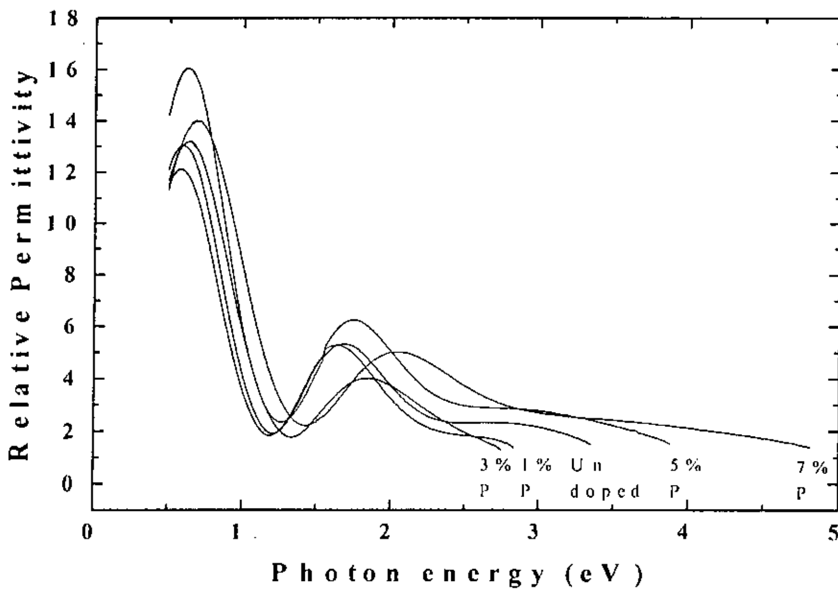

Figure 3.17: Variation of relative permittivity with photon energy.

Then using the values of calculated absorption coefficient and the frequency of the incident light, $(\alpha h\nu)^{1/2}$ is plotted as a function of photon energy ($h\nu$). The optical gap of the carbon thin films obtained from the targets containing different amounts of P(1%, 3%, 5% and 7%) is obtained from the extrapolation of the linear part of the curve, $(\alpha h\nu)^{1/2}$ vs ($h\nu$) at the absorption coefficient α=0, using Tauc relation given in Eqn. 2.9,

$$(\alpha h\nu)^{1/2} = B(E_g - h\nu) \qquad (3.8)$$

where, B is the Tauc parameter.

It is found that the calculated value of optical gap for undoped film is 0.85 eV, which remains almost unchanged for films deposited from the targets containing 1%, 3% and 5% P. For the films deposited from 7% P, it is seen that the value of optical gap decreases and becomes 0.75 eV. The variation of the optical gap with the dopant content in the target material is shown in the Fig. 3.18. The decline in the optical gap

for the films deposited from the target containing 7% P indicates an increase of the fraction of sp^2 bonds due to graphitization of the DLC film. This may happen due to the presence of high P content present in the target material similar to the high nitrogen (N) content induced graphitization in the N doped films [8], [44].

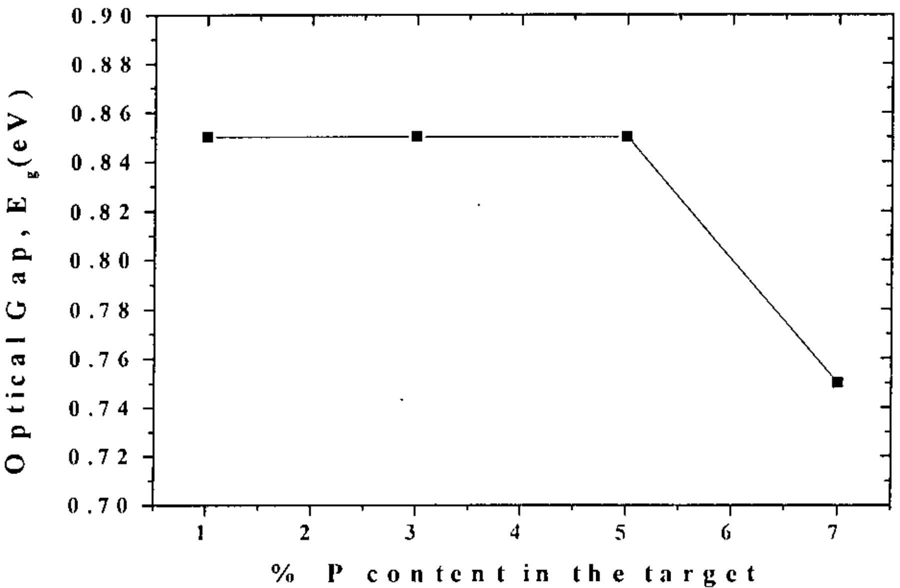

Figure 3.18: Variation of optical gap as a function of %P content in the target.

From Fig. 3.10 it is seen that the value of activation energy decreases with the increase in P content in the target material. This indicates that with the increase in dopant content in the target material, the concentration of donor carriers also increases in the DLC thin film. Thus the Fermi energy level, E_F shift towards the conduction band edge and results a decrease in the value of activation energy. Whereas, the carrier concentration in the film calculated from the C^{-2} vs V characteristics and tabulated in Table 3.2 shows a decreasing trend in carrier concentration for the films deposited from the targets containing 1% P up to 5% P and for 7% P, the carrier concentration increases. Thus there is a difference between the results obtained from the C-V characteristics and the temperature dependent conductivity data analyses obtained for the films.

Though the discrepancy is seen in the results of carrier concentration and the activation energy in the carbon thin film, it is attempted to construct the energy band diagrams for the results obtained above for the DLC films deposited from the targets containing different amounts of P. While constructing the band diagrams, some basic rules are followed. The conduction band discontinuity is always the difference between the electron affinities of the materials constructing the heterojunction as shown in Eqn. 2.1 of chapter 2.

$$\Delta E_c = \chi_1 - \chi_2 \ldots\ldots\ldots\ldots\ldots\ldots\ldots\ldots\ldots\ldots (3.9)$$

where, ΔE_c is the conduction band discontinuity, χ_1 and χ_2 are the electron affinities of the DLC and Si respectively.

Again V_{bi} for the junction is always equal to the differences of work functions of the materials constructing the junction as seen from Fig. 2.7 and Eqn. 2.3 of chapter 2.

$$V_{bi} = \phi_{m2} - \phi_{m1} \ldots\ldots\ldots\ldots\ldots\ldots\ldots\ldots\ldots\ldots (3.10)$$

where, ϕ_{m2} and ϕ_{m1} are the work functions of Si and DLC film respectively.

Considering Eqn. 3.9 and Eqn. 3.10, the energy band diagram is constructed by alligning the Fermi levels of DLC and Si. While constructing the energy band diagram, the activation energy of Si is considered to be 0.3 eV, the value of optical gap of Si to be 1.12 eV. The activation energy of DLC is calculated previously and reported in Table 3.4, which is used to construct the band diagram. The electron affinity of a material can be calculated from photoemission spectroscopy measurements [5]. But the photoemission spectroscopy measurements are not available to us for the carbon thin films. Thus it is attempted to calculate the electron affinity from Fermi level alignment by determining the vacuum energy level using Eqn. 3.10. The calculated energy band parameters are given in Table 3.5. The constructed energy band diagrams for the heterojunctions for films grown from the target containing different amounts of P (1%, 3%, 5% and 7%) are shown in Figs. 3.19, 3.20, 3.21 and 3.22, respectively. The nature of electron affinity with the

variation of dopant content in the target material is shown in Fig 3.23 and the variation of conduction band discontinuity and valance band discontinuity with dopant content is shown in Fig. 3.24.

Table 3.5: Calculated energy band parameters for the constructed energy band diagram

% P	Conduction Band Discontinuity, ΔE_c eV	Valance Band Discontinuity, ΔE_v eV	Work Function, φ_m eV	Electron Affinity, χ eV
1	0.07	0.20	4.27	4.08
3	0.12	0.15	4.28	4.13
5	0.26	0.01	4.42	4.27
7	0.22	0.15	4.36	4.23

From Fig. 3.23 it is found that the electron affinity of the DLC changes with the change in dopant content in the target material. With dopant content 1%, 3% and 5% P in the target material, the film remains diamond like carbon in nature with constant optical gap of 0.85 eV. But for 7% P, the film converts to graphitic in nature with optical gap of 0.75 eV. It is seen that the electron affinity of the film (though the film remains DLC in nature deposited from target containing 1%, 3% and 5% P by mass) changes with the increase in dopant content in the target material, which is not consistent with the theory. It is known that as long as the behaviour of the material remains same, the electron affinity of the material does not depend on the doping on the material. And as the value of electron affinity changes, the value of conduction band discontinuity and valance band discontinuity accordingly changes. For 7% P, the value of the electron affinity, the conduction band and valance band discontinuity can change as the film shows graphitic nature.

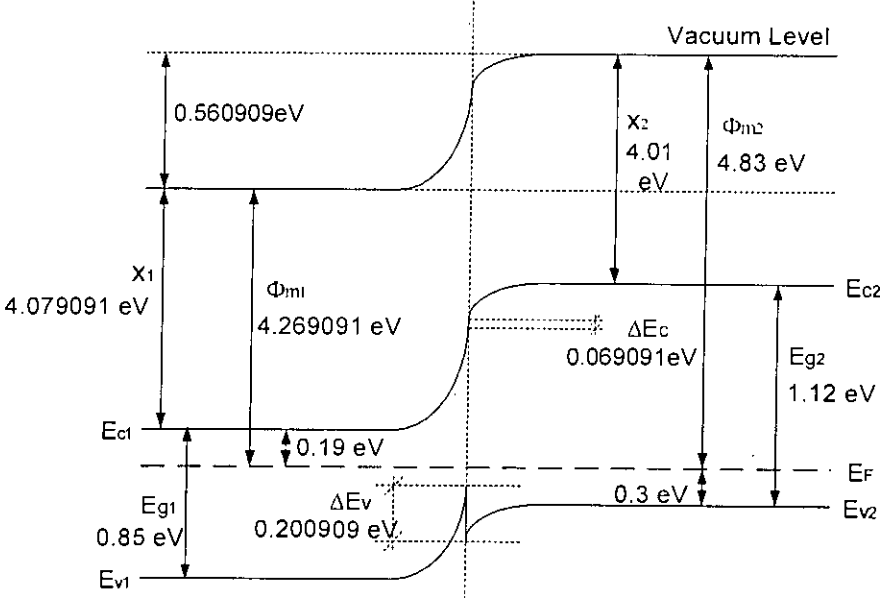

Figure 3.19: Energy band diagram constructed from practical data for heterojunction where, the carbon thin film is deposited from target containing 1% phosphorus.

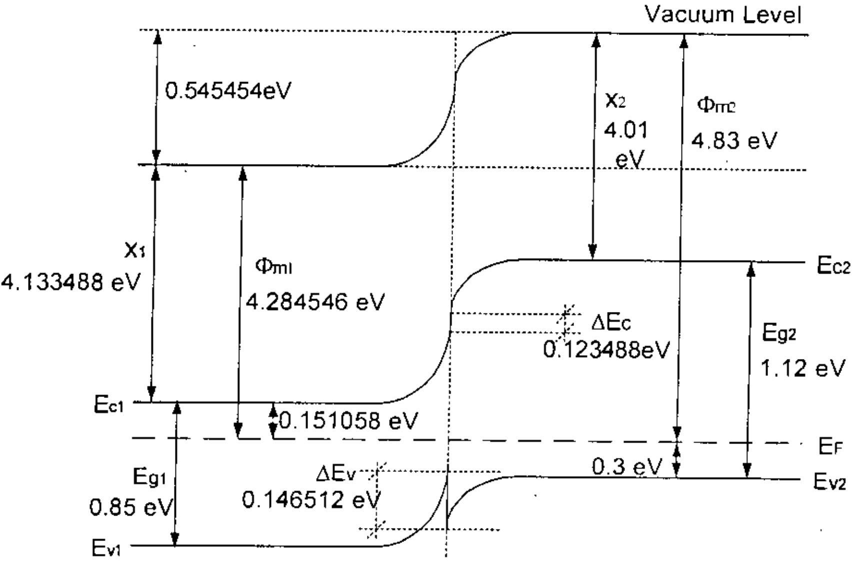

Figure 3.20: Energy band diagram constructed from practical data for heterojunction where, the carbon thin film is deposited from target containing 3% phosphorus.

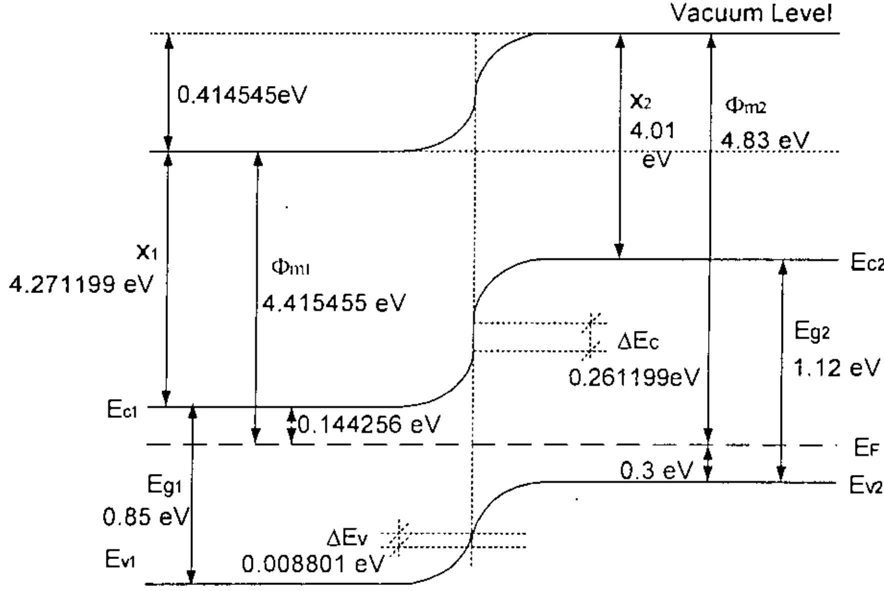

Figure 3.21: Energy band diagram constructed from practical data for heterojunction where, the carbon thin film is deposited from target containing 5% phosphorus.

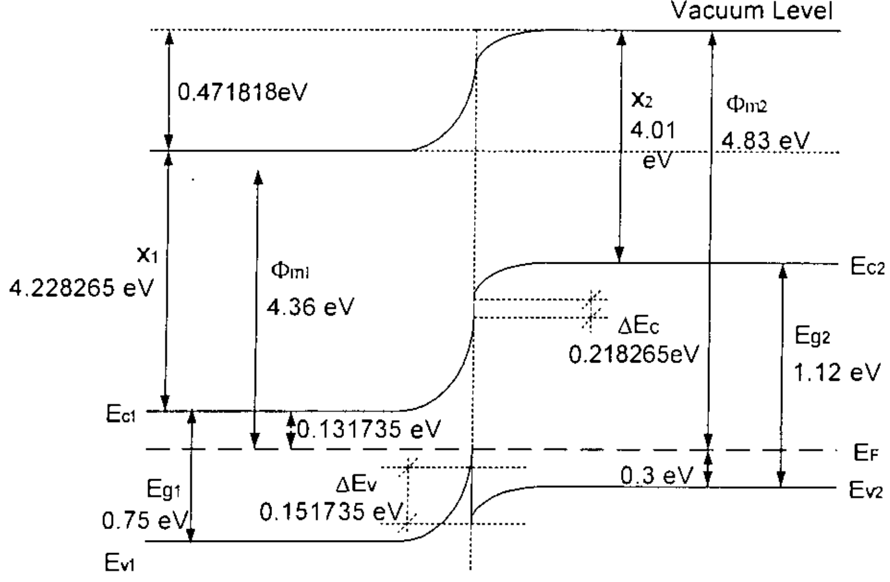

Figure 3.22: Energy band diagram constructed from practical data for heterojunction where, the carbon thin film is deposited from target containing 7% phosphorus.

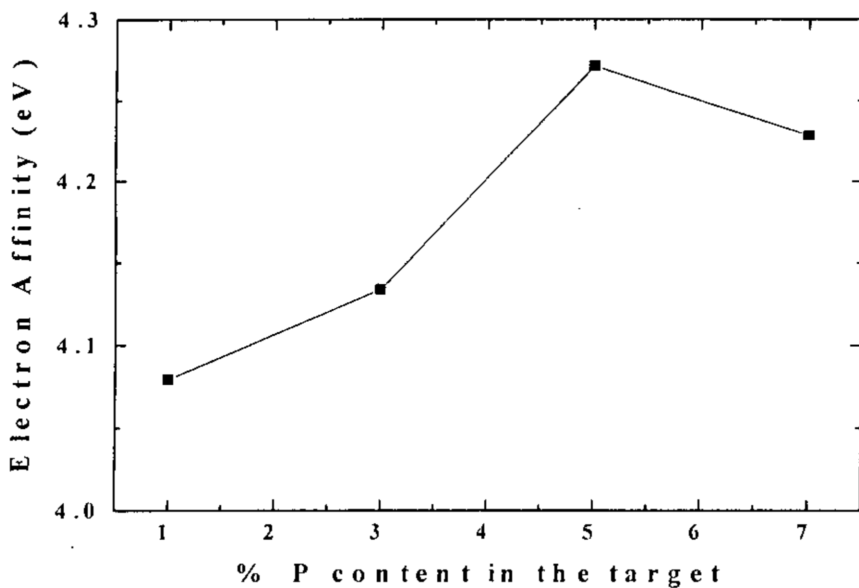

Figure 3.23: Variation of electron affinity for the experimental data with dopant contents in the target material from where the films are grown.

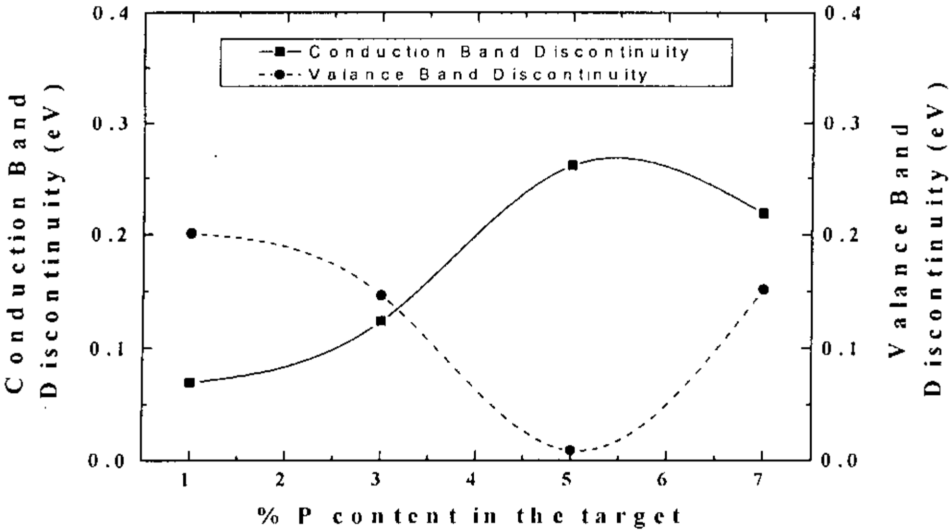

Figure 3.24: Variation of conduction band discontinuity and valance band discontinuity for the experimental data with dopant contents in the target from where the films are grown.

3.2 Analysis of Current Density-Voltage (J-V) Characteristics

It is shown in chapter two that different parameters of heterojunction device are related with the reverse saturation current flowing through the device. Thus the current densities (J) at different voltages (V) for the heterojuction for different P dopant contents are then analyzed.

Fig. 3.25 shows the current density versus voltage (J-V) characteristics for the n-C/p-Si heterostructure, where carbon layer is deposited from the target containing varying amounts of P (1%, 3%, 5% and 7% by mass). The J-V characteristics for the heterojunction show typical diode J-V characteristics.

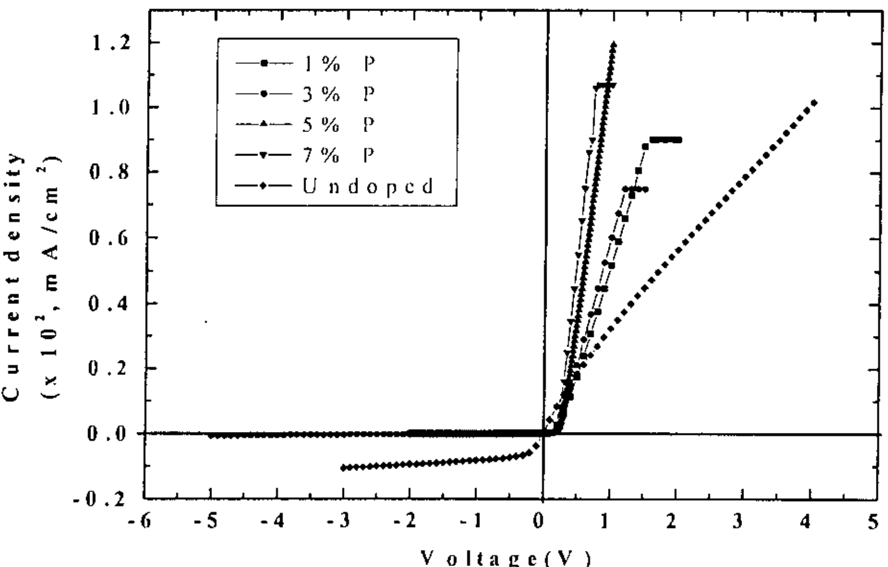

Figure 3.25: Current density-voltage characteristics for the heterojunction for the films grown from targets containing different dopant contents.

From Fig. 3.25 it is seen that after the heterojunction turns on in the forward bias region, for a fixed applied voltage the value of the current density increases gradually with the increase in dopant content in the target material. This indicates that as the

dopant content is increased, the carrier concentration in the heterojunction is also increased. The built-in potential (V_{bi}) is calculated from the J-V characteristics by extrapolating the characteristics to voltage axis for low voltage levels as shown in Fig. 3.26. The values of the built-in potential thus calculated is presented in Table 3.6.

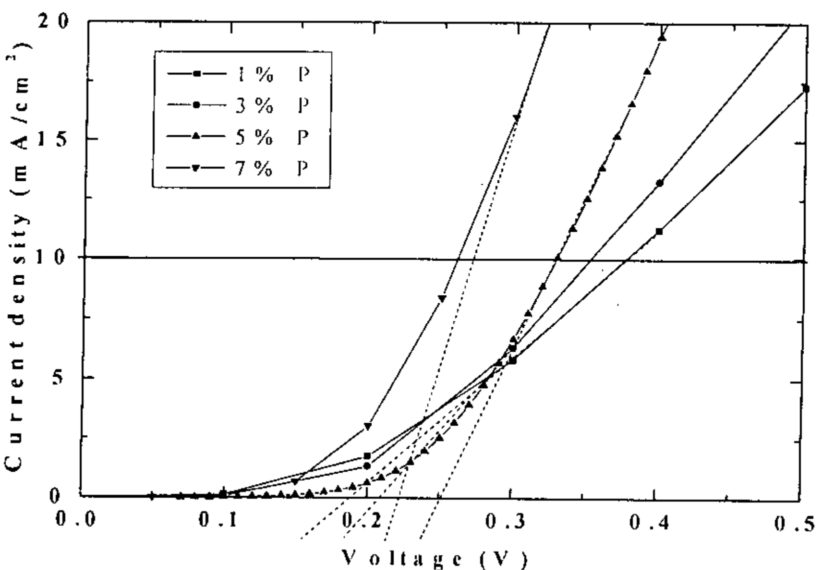

Figure 3.26: Current density-voltage characteristics to calculate the built-in potential for the heterojunction for different dopant contents (1%, 3%, 5% and 7% phosphorus) in the target material.

Table 3.6: Built-in potential calculated from current density-voltage characteristics

% P	Built-in potential of the heterojunction (volt)
1	0.19
3	0.29
5	0.25
7	0.22

The variation of V_{bi} with dopant content in the target material from where the films are grown is shown in Fig. 3.27. If the built-in potential calculated in this way is compared to the built-in potential calculated from C-V characteristics, shown in Table 3.2, it is observed that the value of built-in potential calculated from J-V characteristics is much lower than that calculated from the C-V characteristics. Again the trend of change in built-in potentials are just opposite of each other.

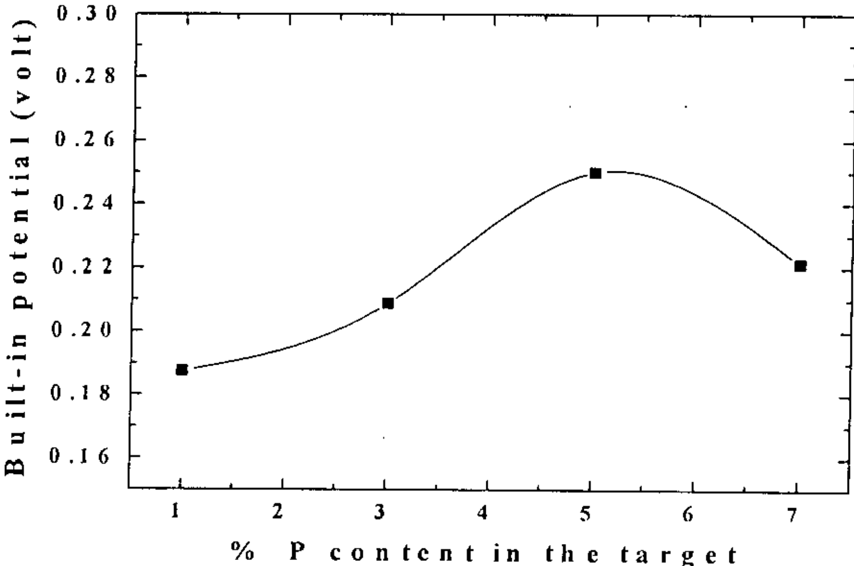

Figure 3.27: Variation of built-in potential calculated from current density-voltage characteristics with dopant content in the target material.

The lower built-in potential for J-V data is due to the presence of reverse current in the junction. Again it is seen from Fig. 3.27 that the built-in potential increases up to dopant content of 5% P in the target material from where the films are grown and then deceases for 7% P. This may happen due to the change in the property of the grown film as from 1% up to 5% P, the film behaves as DLC while for 7% P, the film shows graphitic nature as mentioned earlier.

The forward current in a junction can be expressed by [63],

$$J = J_0(e^{qV/\eta kT}) \quad \text{.................................(3.11)}$$

and thus

$$\ln J = \ln J_0 + qV/\eta kT \quad \ldots\ldots\ldots\ldots\ldots\ldots\ldots\ldots(3.12)$$

where J_0 is the reverse saturation current, q is the charge of electron, V is the applied voltage, k is the Boltzmann's contant, T is the temperature, η is the diode quality factor.

The diode quality factor η actually indicates how ideally the junction behaves. The value of η for an ideal diode is 1. When the value of quality factor is 2, it indicates that recombination limited current flows through the junction. The value of quality factor in between 1 and 2 indicates that the current flowing in the junction comprises both diffusion limited and recombination limited current. As shown in Eqn. 3.12, from the slope of ln(J) vs V characteristics, the diode quality factor η for our heterojunctions can be calculated.

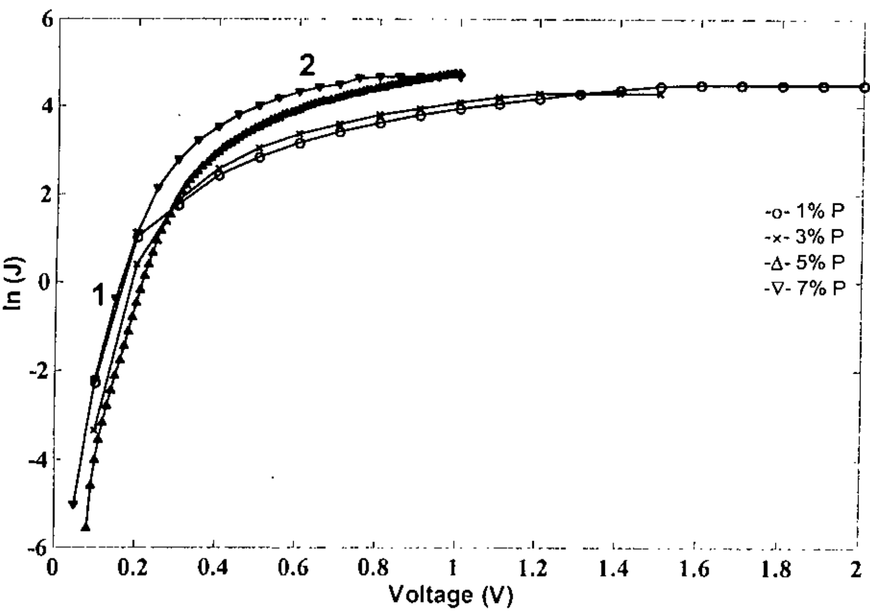

Figure 3.28: ln(J) vs V characteristics to calculate the diode quality factor for films deposited from target containing different dopant contents.

The diode quality factor calculated from the plot of ln(J) vs V is shown in Table 3.7. It is seen from the table that for region 1, i.e., for voltage region $V < 0.25$ volt, the junction behaves like an ideal diode as in this region the value of the diode quality factor is near 1. For region 2, i.e., for voltage region $V > 0.5$ volt, the diode quality factor is seen to increase appreciably. When the value of diode quality factor is 1, it indicated that the current in the junction is diffusion limited. For the applied voltage greater than 0.5 volt, the value of the diode quality factor increases due to the presence of resistive effect in the junction. The nature of current flowing in different regions of current-voltage characteristics for a practical Si diode using Fig. 2.8 is described in chapter 2.

Table 3.7: Calculated diode quality factors from ln(J) vs V characteristics

% P	Region 1 (V < 0.25 volt)	Region 2 (V < 0.5 volt)
	η	η
1	1.18	17.00
3	1.04	17.60
5	1.14	15.22
7	1.06	21.19

98236

Again, the extrapolation of the linear part for the ln(J) vs V characteristics at low voltage region intercepting ln(J) axis gives the value of $\ln(J_0)$, according to Eqn. 3.12 from which the value of J_0 is calculated. The calculated J_0 is given at Table 3.8.

The variation of reverse saturation current (J_0) with the change in dopant content (% P) in the target material from where the films are grown is shown in Fig. 3.30. It is seen that for the films deposited from the targets containing 1%, 3% and 5% P, the reverse saturation current gradually decreases whereas for 7% P it increases. It will be later shown that, the contribution of minority carriers in silicon to the reverse saturation current is negligible compared to the minority carriers in the carbon thin film. Thus only the minority carriers in the carbon thin films contribute to the reverse saturation current of the device. The nature of the variation of reverse saturation

current with the variation of dopant content in the target material will be explained later.

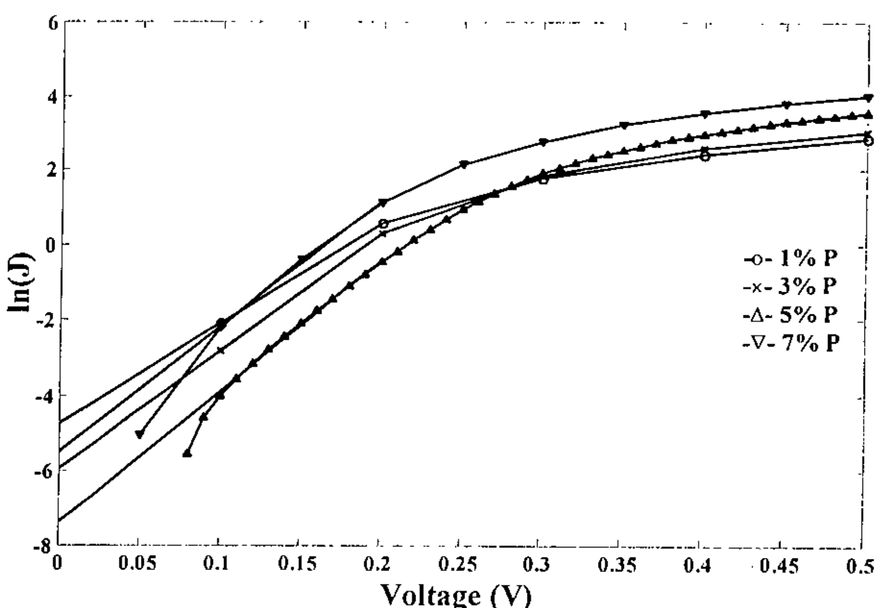

Figure 3.29: Extrapolation of ln(J) vs V characteristics to calculate saturation current.

Table 3.8: Reverse saturation current density for the heterojunctions for the thin films grown from targets containing different dopant contents (1%, 3%, 5% and 7% phosphorus)

% P	Reverse Saturation Current (mA/cm^2)
1	3.36×10^{-3}
3	7.15×10^{-4}
5	6.34×10^{-4}
7	4.21×10^{-3}

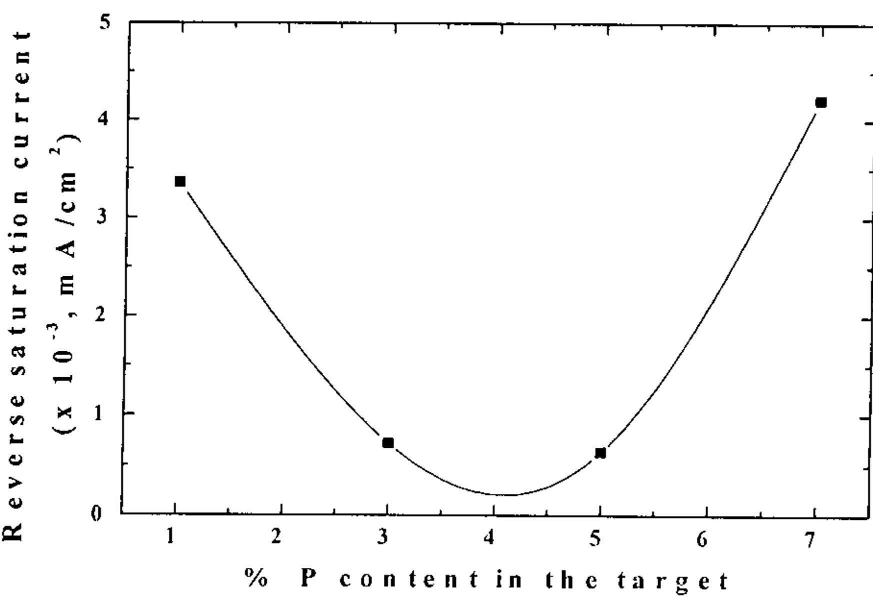

Figure 3.30: Variation of reverse saturation current with dopant content in the target from where the films are grown.

The expression of the reverse saturation current (J_0) for the heterojunction device can be given from Eqn. 2.12 of chapter 2,

$$J_0 = q\left(\frac{D_p}{L_p}\frac{n_{iN}^2}{N_D} + \frac{D_n}{L_n}\frac{n_{iP}^2}{N_A}\right) \quad \text{..........................(3.13)}$$

where,

q is charge of electron

D_p is hole diffusivity in the carbon thin film

D_n is electron diffusivity in the silicon substrate

L_p is hole diffusion length in the carbon thin film

L_n is electron diffusion length in the silicon substrate

n_{iN} is intrinsic carrier concentration in thin film carbon

n_{iP} is intrinsic carrier concentration in silicon substrate

The parameters of Si substrate D_n, L_n, n_{iP} at room temperature are known [63]. The standard values of these parameters are,

$$D_n = \frac{kT}{q}\mu_n = 38.85 \text{ cm}^2/\text{sec}$$

$$L_n = \sqrt{D_n \tau_n} = 9.8552 \times 10^{-5} \text{ cm}$$

$$n_{iN} = 1.6 \times 10^{10} \text{cm}^{-3}$$

and the majority carrier concentration in the p-Si substrate from known resistivity at room temperature is $N_A = 1.5 \times 10^{15}$ cm^{-3}.

Considering all these values, the contributions of minority carriers in Si, i.e., electrons in the reverse saturation current are only 1.076×10^{-8} A/cm^2, which is calculated from part of the contribution of electrons in Si to the reverse saturation current given in Eqn. 3.13. The contribution of electrons in Si to the reverse saturation current is given by $q\frac{D_n}{L_n}\frac{n_{iP}^2}{N_A}$. The contribution of electrons in Si to the total reverse saturation current is much less compared to the total reverse saturation current calculated for the heterojunctions and reported at Table 3.8 and thus can be neglected. Thus, the minority carriers present in the carbon thin films dominate the reverse saturation current of the device.

Here we have calculated the value of reverse saturation current from the extrapolation of the linear part of the plot of ln(J) versus V at the low forward bias region to the ln(J) axis. The reverse saturation current thus found is expressed by the expression given in Eqn. 3.13. However it is also possible to calculate the reverse saturation current from the low reverse bias region of the J-V characteristics. The total reverse current is given by [63],

$$J_R = q\left(\frac{D_p}{L_p}\frac{n_{iN}^2}{N_D} + \frac{D_n}{L_n}\frac{n_{iP}^2}{N_A}\right) + \frac{qn_iW}{\tau_e} \qquad \text{.........................(3.14)}$$

where τ_e is the effective carrier life time.

The first part of Eqn. 3.15 stands for the diffusion component of reverse current in the neutral region and the second part is for the generation current in the depletion region. At low reverse bias, there is always a component of current present due to the generation effect in the depletion region. Thus it is preferable to calculate the reverse saturation current having only the diffusion component of reverse current from the forward J-V characteristics as we have done in this work.

3.3 Results and Discussions

The value of intrinsic carrier concentration in the carbon thin films deposited from the targets containing different dopant contents is not known. It is also possible to calculate the majority carrier concentration in the doped films from the reverse saturation current. It is shown earlier that the contribution of minority carriers in Si to reverse saturation current is negligible and the minority carriers in the carbon thin film are responsible for the reverse saturation current that is present in the heterojunction device. The values of n_{iN} and N_D are fitted to Eqn. 3.13 to give minimum error in the reverse saturation current for each films deposited from the targets containing different amounts of dopant contents (1%, 3%, 5% and 7% P).

Again it is known that for n-type semiconductor [63],

$$E_F - E_i = \frac{kT}{q}\ln\frac{N_D}{n_{iN}} \quad \text{..............................(3.15)}$$

where,

E_F is Fermi energy level

E_i is intrinsic energy level

k is Boltzmann's constant

T is room temperature in K

q is electron charge

From conductivity data analysis, the activation energies for the carbon thin films for different dopant contents in the carbon are previously calculated and given at Table

3.4. The optical gaps of the films are also calculated and are shown in Fig. 3.18. From the values of optical gap and the activation energy, the value of $E_F - E_i$ is calculated. The fitted values of n_{iN} and N_D with the reverse saturation current (J_0) are then fitted with Eqn. 3.15 to give minimum error in $E_F - E_i$. The values for which n_{iN} and N_D gives minimum error in J_0 and $E_F - E_i$ are picked up as correct results of n_{iN} and N_D. The values of n_{iN} and N_D in carbon thin films grown from targets containing different dopant contents (1%, 3%, 5% and 7% P by mass) are reported in Table 3.9. The variations of n_{iN} and N_D in the carbon thin film is shown in Fig. 3.31 and Fig. 3.32 respectively.

Table 3.9: Intrinsic carrier concentration and donor carrier concentration calculated for films deposited from targets containing different dopant contents

% P	Intrinsic carrier concentration in carbon thin film (cm^{-3})	Donor carrier concentration in carbon thin film (cm^{-3})
1	4.60×10^{11}	4.0×10^{15}
3	4.60×10^{11}	1.8×10^{16}
5	4.60×10^{11}	2.3×10^{16}
7	3.17×10^{12}	3.8×10^{16}

It is seen from Fig. 3.31 that the value of intrinsic carrier concentration in carbon thin film increases for 7% P. This happens as for films deposited from target containing 7% P, the optical band gap in the carbon thin film decreases compared to that of other dopant concentrations as shown in Fig. 3.18.

Now from Fig. 3.32, it is observed that the donor carrier concentration in the thin film increases with the increase in dopant content as it was expected earlier. As the conductivity data analysis shows that the activation energy for carbon thin film decreases with the increase in dopant content in the thin film as shown in Fig. 3.10, there must be an increase in carrier concentration in the thin film, which is now found from the analysis of reverse saturation current data and is consistent with our prediction.

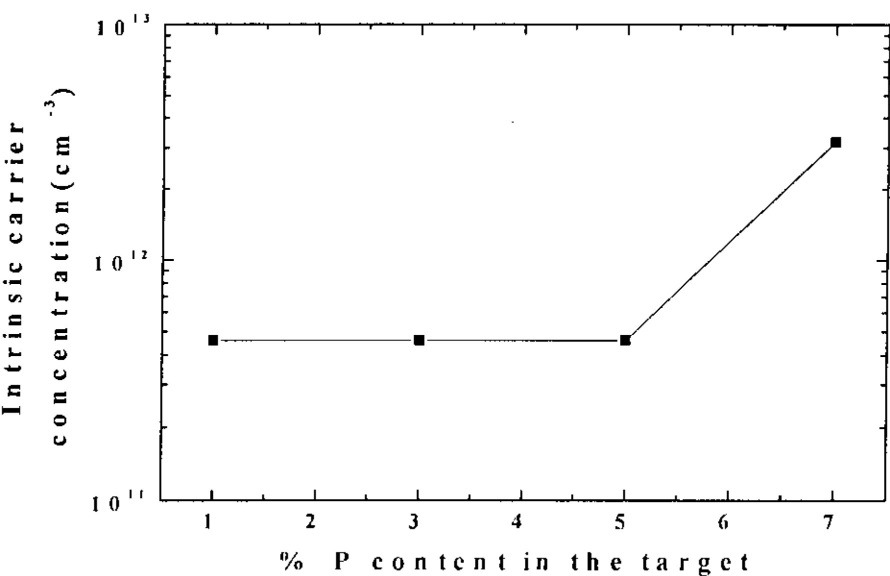

Figure 3.31: Variation of intrinsic carrier concentration in carbon thin film with dopant content in the target material.

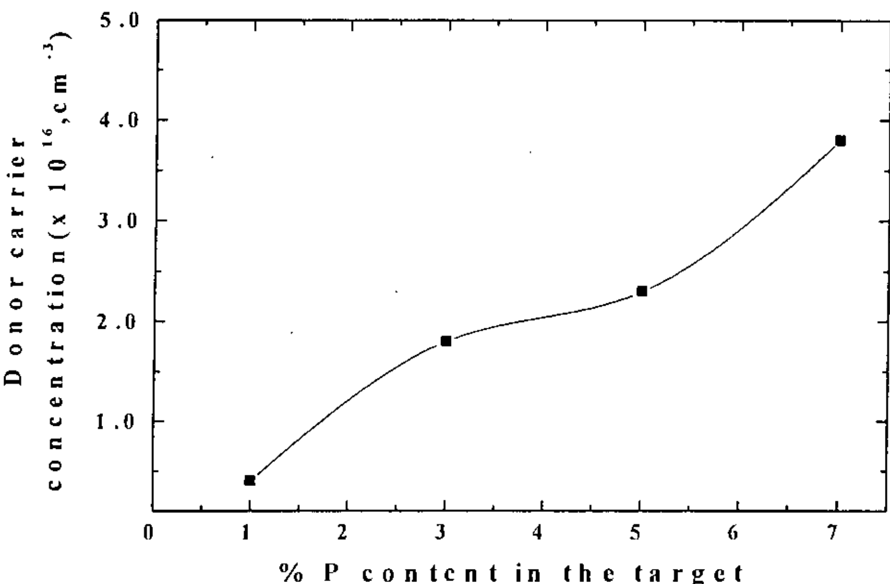

Figure 3.32: Variation of donor carrier concentration in carbon thin film with dopant content in target material.

As the carrier concentration increases in the thin film with the increase in dopant content in the target, the increased carrier compensates the minority carriers more and as a result the reverse saturation current decreases with the increase in dopant content up to 5% P. For 7% P, the reverse saturation current is seen to increase. This may happen as then the optical gap of the carbon thin film decreases from 0.85 eV to 0.75 eV and the film then becomes graphitic in nature.

When the carrier concentration in the carbon thin film is found, it is possible to calculate the electron mobility in the film by using the room temperature conductivity data and the calculated carrier concentration. To calculate the mobility of electron we have to use the equation [63],

$$\sigma = qN_D\mu_n \quad \text{.................................(3.16)}$$

where,

σ = Room temperature conductivity

μ_n = Electron mobility

The electron mobility calculated using Eqn. 3.16 is shown in Table 3.10 and the variation of it with dopant content in the target material is shown in Fig. 3.33.

Table 3.10: Electron mobility calculated from room temperature conductivity and calculated donor carrier concentration

% P	Electron mobility in carbon thin film (cm^2/ V-sec)
1	0.04
3	0.29
5	0.48
7	0.63

It is seen that the value of electron mobility in the carbon thin film is always less than 1 cm^2/V-sec. Due to amorphous nature of the carbon thin film the value of electron mobility is found to be so small.

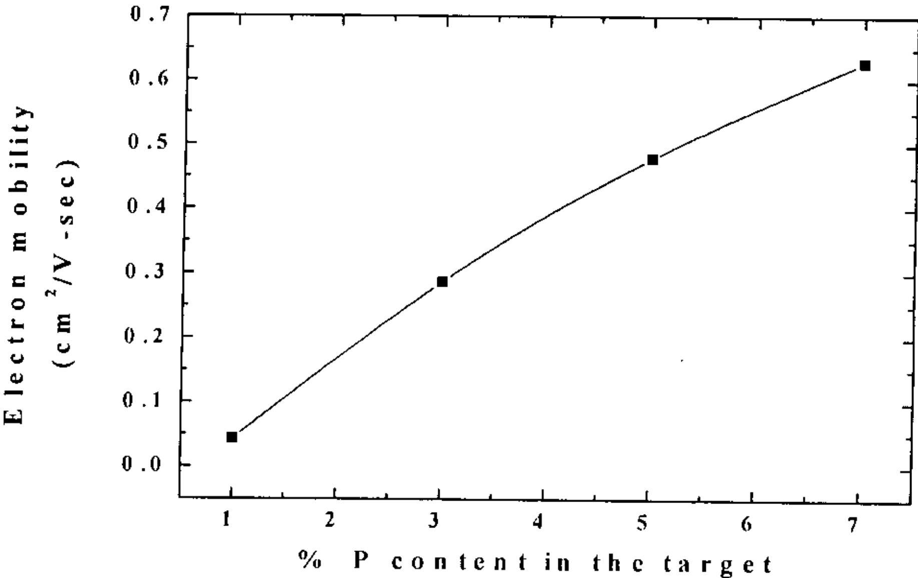

Figure 3.33: Variation of electron mobility in carbon thin film with dopant content in the target.

Various defects in the film that are related to electronic disorder are created due to different bonding configuration and give rise to the gap states around the Fermi level (E_F) of the carbon film. These defects can be either paramagnetic or diamagnetic. Paramagnetic defects can be measured by electron spin resonance (ESR). Fig. 3.34 shows the density of defect states as a function of P content in CC films [57].

It was reported that the defects in the film decrease with the incorporation of P. From Fig. 3.33 it is seen that with the increase in dopant content electron mobility increases. With the increase in carrier concentration, the value of carrier mobility usually decreases. But for our case it is found that with the increase in dopant content in the target material from where the films are grown, the carrier concentration in the film increases as shown in Fig. 3.32 but the electron mobility also increases. As the

defect states in the films decrease with the increase in the dopant content in the target material, the electron mobility increases with the increase in the dopant content.

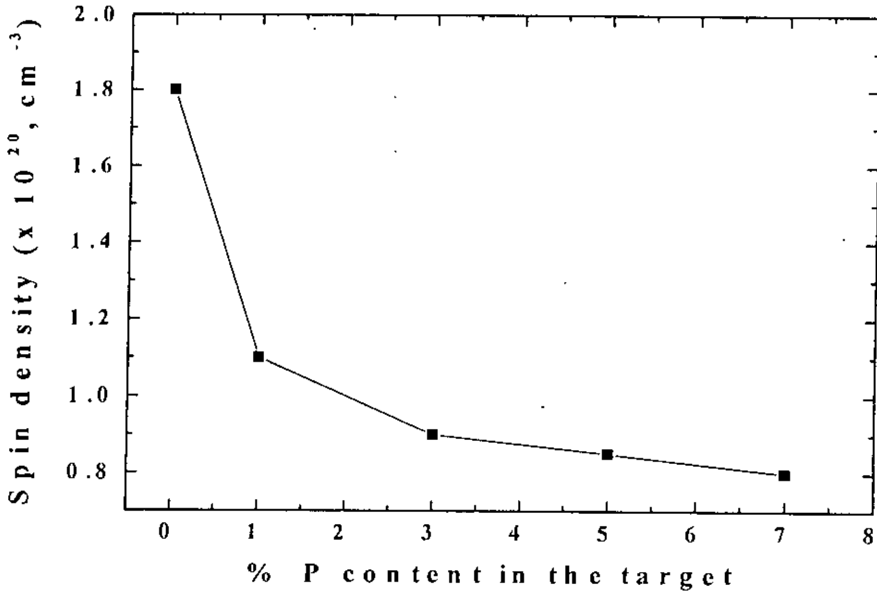

Figure 3.34: Variation of ESR spin density of the carbon film as a function of % P in the target.

While calculating the values of intrinsic carrier concentration and the carrier concentration in thin films grown from targets containing various dopant contents, the value of $\frac{D_p}{L_p}$ is determined to be 4 x 10^5 for 1%, 3% and 5% P and 1x 10^5 for thin films grown for 7% P from fitting with parameters with Eqn. 3.13,

$$J_0 = q\left(\frac{D_p}{L_p}\frac{n_{iN}^2}{N_D} + \frac{D_n}{L_n}\frac{n_{iP}^2}{N_A}\right)$$

The carrier mobility in amorphous materials are always found to be near 1 cm^2/V-cm. Balsi *et al.* [60] reported that the carrier mobility in amorphous hydrogenated silicon (a-Si:H) is near 1 cm^2/V-cm. For amorphous materials hole mobility is always found to be less than the electron mobility in that material. Thus assuming hole mobility in carbon is one tenth of the electron mobility in carbon, it is possible to calculate the value of D_p, L_p and minority carrier life time, τ_p in carbon using the relations [63],

$$L_p = \sqrt{D_p \tau_p} \quad \text{...(3.17)}$$

The calculated parameters are shown in the Table 3.11.

Table 3.11: Calculated diffusion length and minority carrier life time in carbon thin film

% P	Hole mobility, μ_p (cm^2/V-sec)	D_p (cm^2/sec)	L_p (cm)	τ_p (sec)
1	4.23 x 10^{-3}	1.09 x 10^{-4}	2.74 x 10^{-10}	6.85 x 10^{-16}
3	2.87 x 10^{-2}	7.43 x 10^{-4}	1.86 x 10^{-9}	4.64 x 10^{-15}
5	4.79 x 10^{-2}	1.24 x 10^{-3}	3.10 x 10^{-9}	7.75 x 10^{-15}
7	6.29 x 10^{-2}	1.63 x 10^{-3}	1.63 x 10^{-8}	1.63 x 10^{-13}

The variations of hole diffusion length, L_p and the minority carrier (hole) life time τ_p with the variation of dopant content in the thin film is shown in Fig. 3.35 and Fig. 3.36 respectively. It is seen from the figures that with the increase in dopant content in the target from where the films are grown, the diffusion length for the minority carriers increases. This may happen due to the decrease in defect states [Fig. 3.34]. As the diffusion length for the minority carriers increases, there is an increase in minority carrier life time in the thin film with the increase in dopant contents.

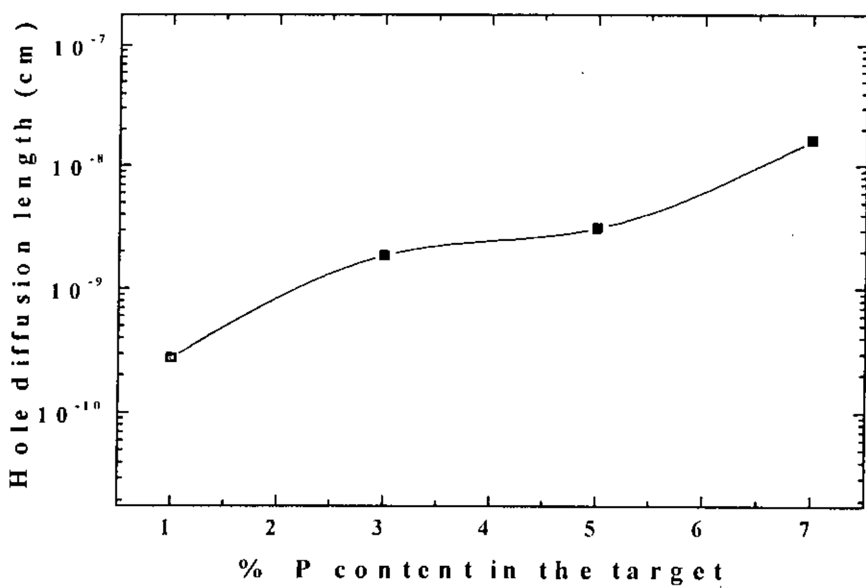

Figure 3.35: Variation of hole diffusion length in carbon thin film with the variation of dopant content in the target.

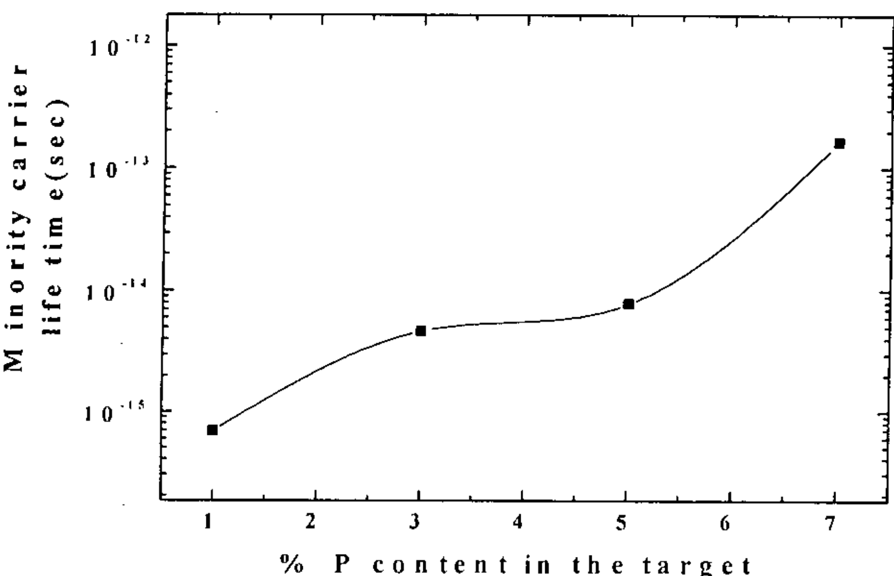

Figure 3.36: Variation of minority carrier life time in carbon thin film with the variation of dopant content in the target.

The calculated values of carrier concentration for the thin film is changed when calculated from J-V reverse saturation characteristics from that calculated from C-V characteristics. For this change in the values of carrier concentration, there will be a change in corresponding built-in potential too. As it is mentioned earlier that the electron affinity of a particular material does not change with the change in dopant concentration to it. Thus the conduction band discontinuity for the heterojunction must remain constant as long as the electron affinities of the materials constructing the heterojunction remain constant. Further, while constructing energy band diagrams by aligning the Fermi levels of carbon thin films and silicon, the relations given in Eqns. 2.1, 2.2 and 2.3 must be satisfied. The activation energy of carbon thin film is calculated before and is given in Table 3.4. The optical gaps of the thin film are calculated from Tauc plot. The activation energy of silicon is considered to be 0.3 eV and the optical gap to be 1.12 eV. Considering the above facts, it is attempted to predict the revised values of the built-in potentials for the heterojunctions and the electron affinity of the thin film carbon. The predicted values thus calculated are reported at Table 3.12.

Table 3.12: Revised built-in potential, electron affinity of carbon thin films, conduction band discontinuity and valance band discontinuity with the variation of dopant content.

%P	Revised built-in potential, V_{bi} (volt)	Electron affinity of carbon thin film (eV)	Conduction band discontinuity, ΔE_c (eV)	Valance band discontinuity, ΔE_v (eV)
1	0.59	4.05	0.04	0.23
3	0.63	4.05	0.04	0.23
5	0.64	4.05	0.04	0.23
7	0.65	4.05	0.04	0.33

The constructed energy band diagrams for n-carbon/p-silicon heterostructure for films deposited from targets containing 1%, 3%, 5% and 7% P are shown in Figs. 2.37, 3.38, 3.39 and 3.40, respectively.

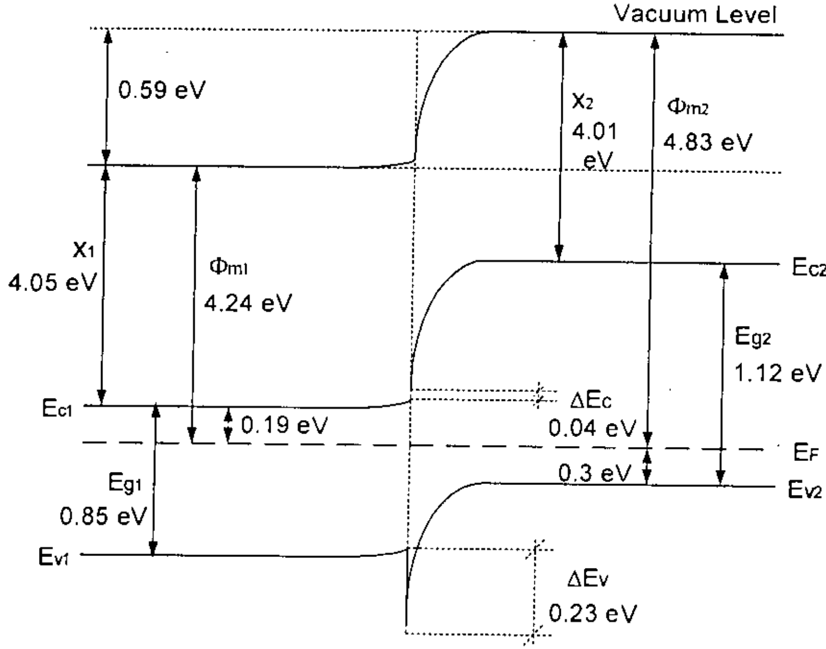

Figure 3.37: Proposed energy band diagram constructed for n-carbon/p-silicon heterojunction where the carbon thin film is deposited from target containing 1% P.

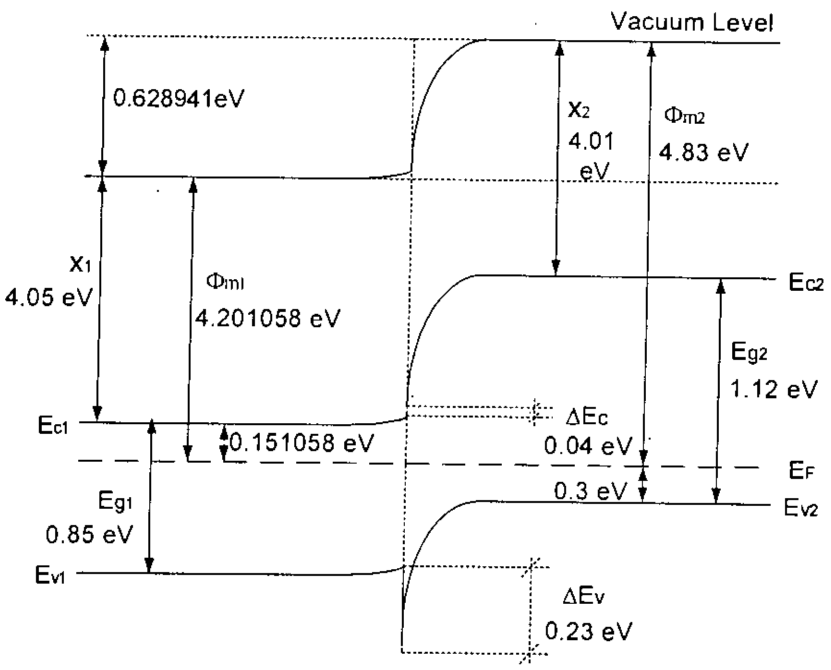

Figure 3.38: Proposed energy band diagram constructed for n-carbon/p-silicon heterojunction where the carbon thin film is deposited from target containing 3% P.

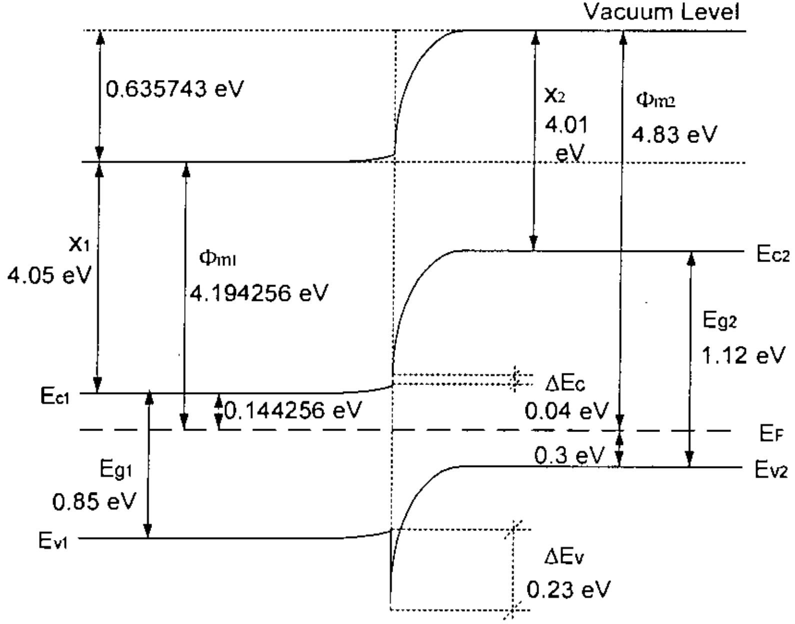

Figure 3.39: Proposed energy band diagram constructed for n-carbon/p-silicon heterojunction where the carbon thin film is deposited from target containing 5% P.

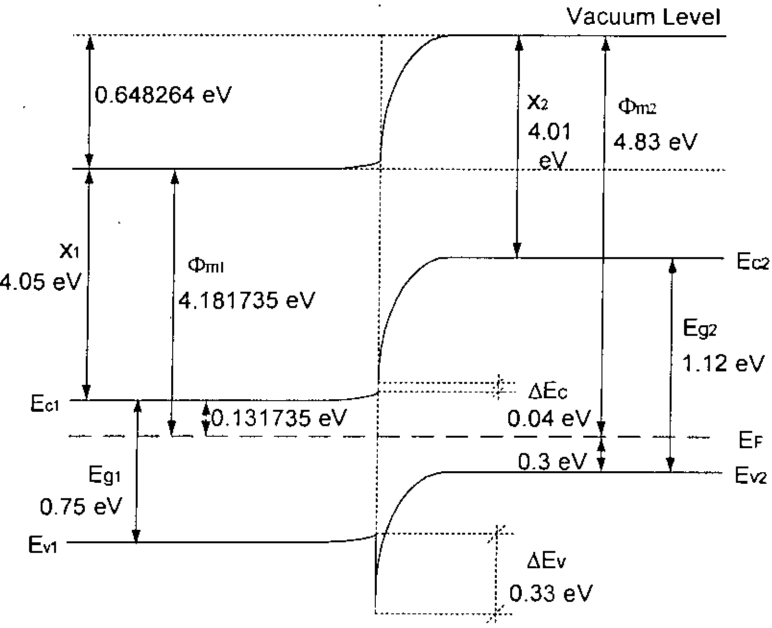

Figure 3.40: Proposed energy band diagram constructed for n-carbon/p-silicon heterojunction where the carbon thin film is deposited from target containing 7% P.

When the revised carrier concentration and built-in potential is calculated, it is then possible to calculate the depletion widths in each materials of the heterojunction for films grown from targets containing different dopant contents using Eqn. 2.4 and Eqn. 2.5 and the total depletion width in the junction for each case.

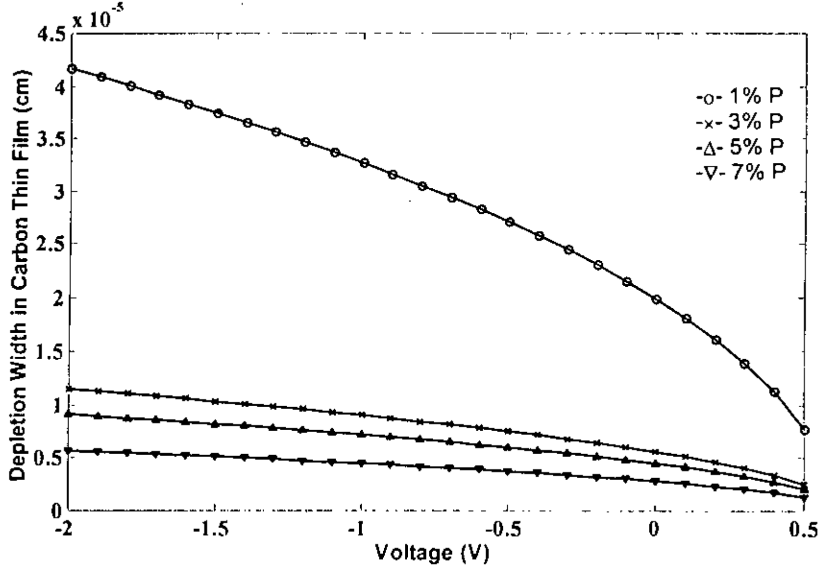

Figure 3.41: Variation of depletion width in carbon thin film with the applied voltage in the junction.

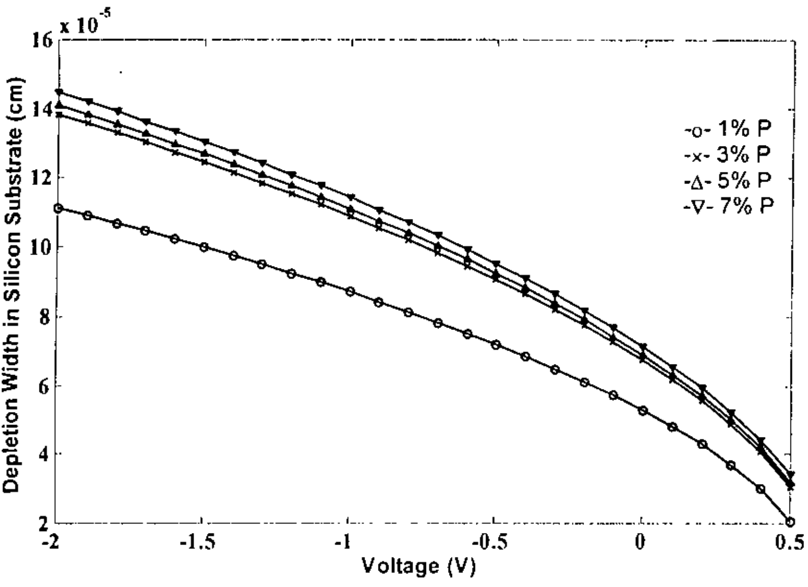

Figure 3.42: Variation of depletion width in silicon substrate with the applied voltage in the junction.

It is now seen from Fig. 3.41 that for all cases, where the carbon thin films are deposited from targets containing different contents of P, for initial reverse bias voltage, the depletion width shows acceptable value, whereas for initial data obtained from C-V characteristics analysis, it is found that for all the cases the value of depletion width in carbon thin film is much greater that the total film thickness even when no voltage is applied to the junction.

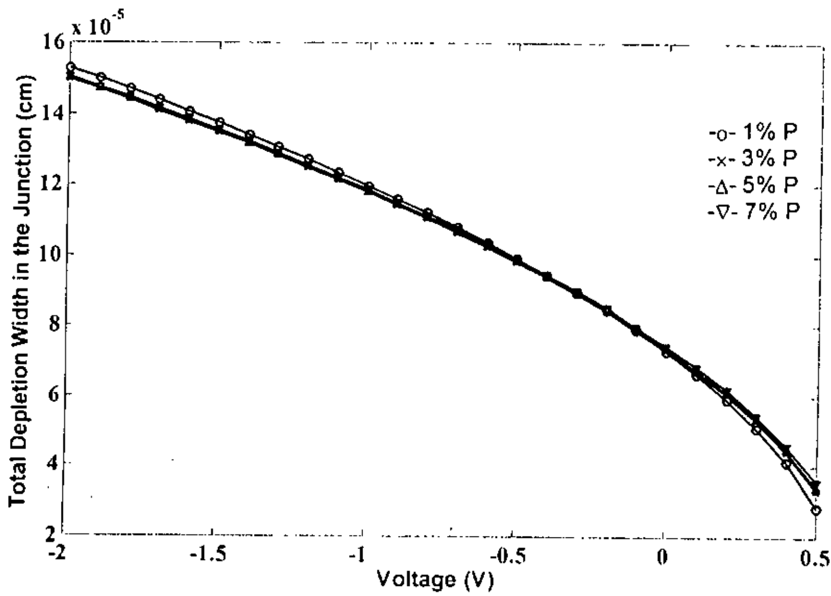

Figure 3.43: Variation of total depletion width in the heterostructure with the applied voltage in the junction.

Fig. 3.44 shows the revised C-V characteristics for the heterostructures determined from the fitted data. In Fig. 3.45, C-V characteristics from both the fitted data and from the experimental results are shown. It is found that the experimental value of capacitance is much less compared to the capacitance calculated from the fitted data. This discrepancy between the experimental and calculated values of capacitance can be due to the presence of additional series capacitance of small value possibly arising from the presence of bulk capacitance, capacitance due to surface charges present in the material. Thus the presence of these capacitances acting in series with the depletion capacitance of the heterojunction reduces the overall device capacitance.

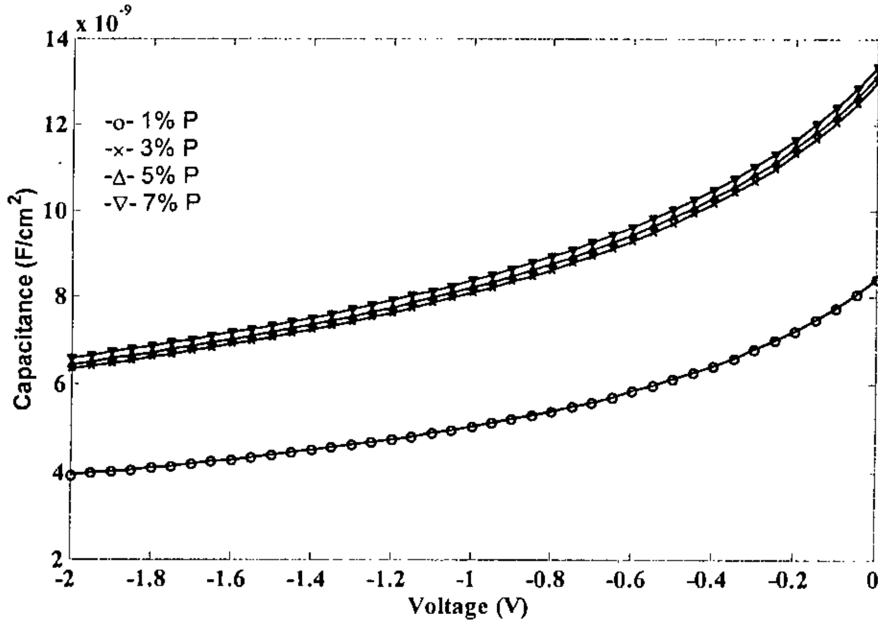

Figure 3.44: Revised C-V characteristics determined from the fitted data.

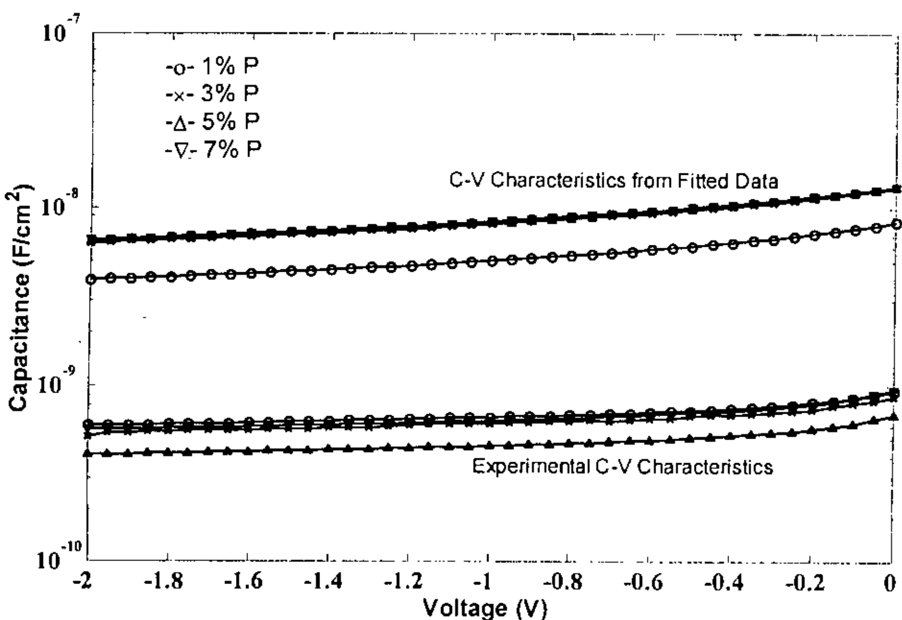

Figure 3.45: C-V characteristics from experiment and from fitted data.

Veerasamy *et al.* [4] deposited n-type (nitrogen doped) tetrahedral amorphous carbon (ta-C) on p-type silicon substrate by filtered catholic vacuum arc deposition method. They determined the energy band diagram for different dopant concentration in the ta-C thin film. The undoped ta-C film was shown to be p-type in nature as determined in this work and arise from the unpaired dangling bonds at the material surface. However, they have ignored the bulk defects while studying the device characteristics. The electron affinity of ta-C was found by them to be in the range of 2.9-3.0 eV from photoemission spectroscopy measurements performed on doped ta-C. The electron affinity of silicon was considered to be equal to 4.01 eV. The findings of Veerasamy *et al.* are shown in Table 3.13.

Table 3.13: Carrier concentration in carbon thin film, conduction band and valance band discontinuity and built-in potential in the heterojunction with the variation in dopant content in the target material [4]

N (at %)	$N_D (10^{15})$ cm^{-3}	ΔE_C eV	ΔE_V eV	V_D volt
0.7	0.35	0.97	-0.19	1.59
1.0	1.09	0.98	-0.26	1.70
1.5	18.2	0.98	-0.27	1.75

It is seen from Table 3.13 that as the dopant content in the ta-C film is increased, the carrier concentration N_D and the built-in potential are also increased. The value of conduction band discontinuity remains constant as it depends on the electron affinity of the materials constructing the heterostructure and not upon the dopant concentration in the materials. Valance band discontinuity then depends on the optical gaps of the of the materials of the heterojunction as given by

$$\Delta E_C + \Delta E_V = E_{g2} - E_{g1}$$

The doping in the silicon substrate was 1.0-1.1 x 10^{15} cm^{-3} and the optical gap was 1.12 eV. From the Table 3.13 it is seen that the values of valance band discontinuity changes. It indicates that with the change in dopant concentration, there was a change in the optical gap in the ta-C film. But in all the cases the value of electron affinity in

ta-C was found to remain constant. The electron affinity determined by Veerasamy for their ta-C was found to be 2.9-3.0 eV. The calculated optical gap was near 2.0 eV. In this heterojunction device, the doping in the film is done by phosphorus instead of nitrogen as was done by Veerasamy. In this case it is found that with the increase in dopant content in the target from where the films are grown, the dopant concentration in the film and the built-in potential are seen to increase as found by Veerasamy. In this case, we determined that the electron affinity of thin film carbon is 4.05 eV. For our film, the optical gap is 0.85 eV for films deposited from target contain 1%, 3%, 5% P and 0.75 eV from target containing 7% P. The conduction band discontinuity for our case is found to be much smaller than that found by Veerasamy and is only 0.04 eV, whereas Veerasamy found that to be 0.98 eV. This happens as the difference of electron affinities of the materials constructing heterostructure for our case is found to be smaller than that found by Veerasamy. And accordingly the value of valance band discontinuity is found for our device.

The electron affinity found in our device shows a higher value compared to the other devices of similar type reported previously [4], [6], [58]. This discrepancy may arise due to the difference in the optical band gaps of the amorphous carbon reported by others and the optical band gap that was determined for our device. Veerasamy *et al.* [4] found the optical gap of ta-C about 2.0 eV and the corresponding electron affinity to be equal to 2.9-3.0 eV. Veerasamy *et al.* [58] reported that for highly tetrahedral amorphous carbon the optical band gap varies from 1.0 eV to 2.5 eV with the variation of sp^2 fraction in the material. They however did not report the value of electron affinity of the material. Chan *et al.* [6] reported that for r.f. plasma enhanced chemical vapour deposited diamond like carbon-diamond have variable optical band gap from 1.2 eV to 4.0 eV which was controlled by the change in deposition condition. Maldei *et al.* [2] used electric arc evaporation system to deposit a-C:H . They reported the optical band gap to be equal to 0.6eV and 1.0 eV for different deposition conditions. But for both the cases, the value of electron affinity was found to be equal to 4.1 eV, which is much higher than that reported by others. For our case, the calculated optical band gap is 0.85 eV for thin film carbon films deposited from target containing 1%, 3% and 5% P and 0.75 eV for the film deposited from

target containing 7% P. Thus the value of optical band gap found here is in the range that reported by Maldei. The value of electron affinity determined for our case is 4.05 eV, which is also comparable to that reported by Maldei.

Veerasamy *et al.* [4] reported that the activation energy in the n-type ta-C deposited on p-type crystalline silicon varies from 0.1 eV to 0.15 eV, which is comparable to the activation energy calculated in this work for n-type carbon thin film as reported in Table 3.4.

The films deposited here are amorphous in nature and for amorphous films the value of carrier mobility is near 1 cm^2/V-sec. Balsi *et al.* [60] reported that the carrier mobility in amorphous hydrogenated silicon (a-Si:H) is near 1 cm^2/V-sec. Thus the calculated values of the electron mobility are consistent with the theoretical value for the amorphous materials.

In Fig 3.45 we have shown the C-V characteristics from fitted data and the experimental data together. The C-V characteristics predicted from experimental fitted data shows a much larger value compared to the experimentally obtained C-V characteristics. Veerasamy *et al.* [4] deposited n-type (nitrogen doped) tetrahedral amorphous carbon (ta-C) on p-type crystalline silicon substrate by filtered cathodic vacuum arc process. They studied the C-V characteristics of the device for different dopant contents in the ta-C thin film. The C-V characteristics obtained by them are shown in Fig 3.46.

It is seen from Fig 3.46 that with the increase in N dopant content in the thin film, the value of the junction capacitance increases. Further the capacitance determined by them was in the order of 10^{-9} F/cm^2. Here in this work, a revised C-V characteristic is proposed from the parameters obtained by fitting with experimental data. The proposed characteristic is shown in Fig 3.44. From that figure, it is observed that the value of the capacitance increases with the increase in dopant concentration in the carbon thin film and thus gives similar pattern of C-V characteristics as was reported by Veerasamy [4]. Further, the values of capacitance of the proposed characteristics

are seen in the order of 10^{-8} F/cm^2 for applied voltage from zero to –0.4 volt and of the order of 10^{-9} F/cm^2 for higher reverse bias voltage applied, which are consistent with the order of capacitance obtained and reported by Veerasamy.

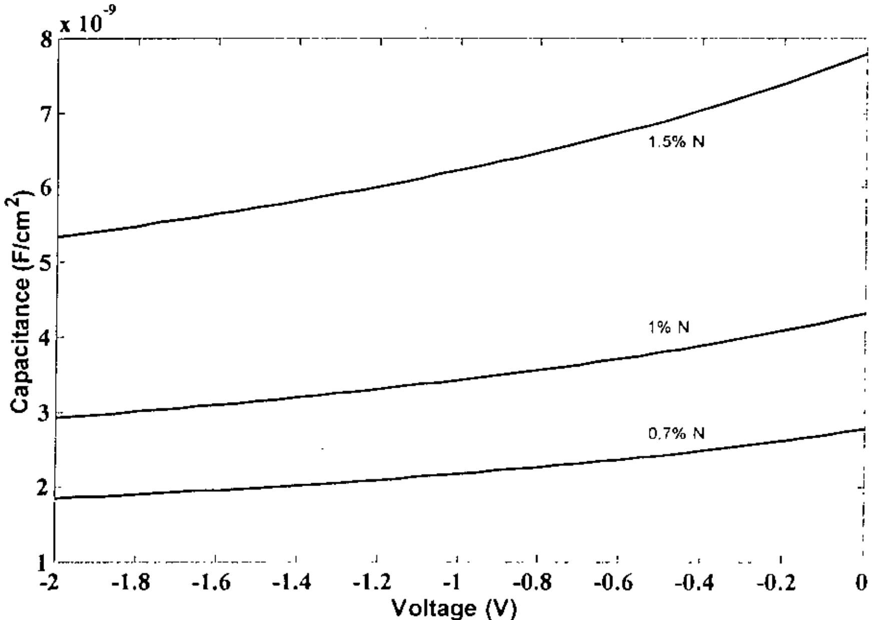

Figure 3.46: Junction capacitance as a function of reverse bias voltage for diodes with different nitrogen-doping levels (0.7, 1.0 and 1.5 at % nitrogen) in the ta-C reported by Veerasamy *et al.* [4].

Then it is attempted to use our approach to determine the donor carrier concentration of the ta-C analyzed by Veerasamy *et al.* [4]. While applying the method it is found that the results do not converge. Then using the value of donor carrier concentration and the value of activation energy determined by them, using Eqn. 3.15, the value of intrinsic carrier concentration is calculated to be equal to only 1.91 cm^{-3}, which is in practical case an unacceptable value. This is why our approach to determine the device parameters failed to converge and there are errors in the parameters determined by Veerasamy *et al.*

Chapter 4

Conclusions

4.1 Conclusions

Carbon has shown potentiality in device fabrication in recent time. Some heterostructure devices based on carbon and silicon (C/Si) have already been fabricated using carbon. Successful doping of carbon is reported by many researchers. But very few efforts have been taken to dope carbon with phosphorus to convert it to n-type material. Very recently, phosphorus doped n-type carbon thin film is grown on p-type silicon substrate. The detailed characteristics of phosphorus doped carbon thin films grown on silicon substrate are yet to be reported. Therefore, the study of this type of device is very important for practical implementations. In this work, we have analyzed the capacitance versus voltage (C-V) characteristics and current density versus voltage (J-V) characteristics using the experimental observations of phosphorus (P) doped camphoric carbon deposited onto p-type silicon (n-C/p-Si) substrate. Ultraviolet visible infrared (UV-VIS-IR) spectroscopy and temperature dependence conductivity data are obtained from the experimental observations of phosphorus (P) doped camphoric carbon deposited onto quartz.

The aim of this work is to determine the energy band parameters of the n-C/p-Si heterostructure. The properties of Si substrate in the heterostructure are already known. To determine the carrier concentration in thin film carbon and the built-in potential of the heterostructure, the C-V characteristics for the films grown from the target containing different amounts of phosphorus by mass are analyzed. It is seen that the carrier concentration in the thin film carbon decreases consecutively for films grown from target containing 1%, 3% and 5% P and then increases for 7% P. The built-in potential determined shows the same trend. Later, from the temperature dependent conductivity data analyses, it is seen that with the increase in dopant content in the target material, the value of activation energy decreases, which indicates that the increase in dopant content activates the carbon thin film in greater amount and the result obtained from C-V characteristics are not consistent with the activation energy in carbon measured from temperature dependent conductivity data analyses. Thus attemp is made to calculate the intrinsic carrier concentration and donor carrier concentration in the carbon thin film by fitting the parameters with the reverse saturation current determined from the J-V characteristics of the heterostructure. The calculated parameters show acceptable trends and are consistent with the activation energy values calculated from the temperature dependent conductivity data analysis. The revised built-in potential is calculated by using the activation energy and data fitting with standard equations and later the energy band diagrams for the heterostructures with carbon thin films grown from targets containing different amounts of dopant contents are proposed.

The extracted results are also correlated with those of reported literatures. It is shown that the value of electron affinity determined for our thin film is consistent with the value reported previously [2]. The values of activation energy of carbon and conductivity data analyses are also consistent with the previously reported results. The electron mobility determined also shows acceptable results with that reported previously for amorphous material. Further, revised C-V characteristics are suggested at the end of this work. The revised C-V characteristics show similar trend and the order of the value of capacitance as reported earlier by Veerasamy *et al.* [4]. Considering the above

similarities, it can be concluded that, the obtained results successfully represent the characteristics of the studied n-C/p-Si heterostructure device.

4.2 Suggestions for Future Works

While constructing the energy band diagram, the influence of interface trap states at the junction between the carbon and silicon are neglected. Sometimes, the junction between carbon and silicon are not sharp and at the interface, silicon-carbon related compounds, specially, silicon-carbide (SiC) is formed. Further, the influence of semiconductor bulk defect states and the influence of the metal-semiconductor junction on the characteristics are not considered here. So there is a scope to work on determination of the influences of all these over the characteristics of the device. While determining minority carrier life time in carbon thin film, we have assumed that the hole mobility in carbon to be one tenth of the electron mobility of the carbon. The accurate value of hole mobility can be determined in the future and accordingly the accurate values of minority carrier life time and hole diffusivity in carbon thin film can be determined. Further, it is seen that there is a large amount of discrepancy in the value of capacitances between the fitted result and the experimental result. A detailed study to explain this discrepancy can be done in future.

References

[1] N. Konofaos and C. B. Thomas, "Characterization of heterojunction devices constructed by amorphous diamond like films on silicon", *Appl. Phys. Lett.*, vol. 61, p. 2805, 1992.

[2] M. Maldei and D. C. Ingram, "Advances in a-C:H based photovoltaic devices", *Proc. of the 13th European Photovoltaic Solar Energy Conf., Nice, France* , pp. 1258-1263, 1995.

[3] F. J. Clough, W. I. Milne, B. Kleinsorge, J. Robertson, G. A. J. Robertson and B. N. Roy, "Tetrahedrally bonded amorphous carbon (ta-C) thin film transistors", *Electron Lett.*, vol. 32, no. 5, pp. 498-499, 1996.

[4] V. S. Veerasamy, G. A. J. Amaratunga, J. S. Park, H. S. Mackenzie and W. I. Milne, "Properties of n-type tetrahedral amorphous carbon (ta-C)/p-type crystalline silicon heterojunction diodes," *IEEE Trans. Electron Devices*, vol. 42, no. 4, pp. 577-585, 1995.

[5] J. Robertson, "Hard amorphous (diamond-like) carbons", *Prog. Solid St. Chem.*, vol. 21, pp.199-333, 1991.

[6] K. K. Chan, S. R. P. Silva and G. A. J. Amaratunga, "Electron properties of semiconducting diamon-like carbon-diamond", *Thin Solid Films*, vol. 212, pp. 232-239, 1992.

[7] N. Konofaos and C. B. Thomas, "Characterization of heterojunction devices constructed by amorphous diamond like films on silicon", *J. Appl. Phys*, Vol 81, no. 4, pp. 6238-6245, 1997.

[8] S. M. Mominuzzaman, Kalaga Murali Krishna, Tetsuo Soga, "Optical absorption and electrical conductivity of amorphous carbon thin films from Camphor: A natural source", *Jpn. J. Appl Phys.*, Vol 38, Pt 1, No 2A, pp 658-663, February 1999.

[9] S. M. Mominuzzaman, T. Soga, T. Jambo and M. Umeno, "Diamond-like carbon by pulsed laser deposition from a camphoric target: effect of phosphorus incorporation", *Diamond and Related Materials,* Vol 10, pp. 1839-1842, 2001.

[10] S. M. Mominuzzaman, "Preparation and characterization of semiconducting carbon thin films and their application to photovoltaic cell", Ph.D Thesis, Department of Electrical and Electronic Engineering, Nagoya Institute of Technology, Japan, 2001.

[11] Kirk and Othmer, "Encyclopedia of chemical technology", Wiley, New York, Vol. 4, pp. 556, 1980.

[12] V. S. Veerasamy, G. A. J. Amaratunga, C. A. Davis, A. E. Timbs, W. I. Milne and D. R. Mackenzie, "n-type doping of highly tetrahedral diamond-like amorphous carbon", *J.Phys: Conden. Matter*, vol. 5, pp. L169-L174, 1993.

[13] G. A. J. Amaratunga, D. E. Segal and D. R. Mackenzie, "Amorphous diamond-Si semiconductor heterojunctions", *Appl. Phys. Lett.*, Vol. 59, pp. 69-71, 1991.

[14] S. Aisenberg and R. Chabot, *J App Phys*, Vol. 42, pp. 2953, 1971.

[15] E. G. Spencer, P. H. Schmidt, D. C. Joy and F. J. Sansalone, "Ion-beam-deposited polycrystalline diamondlike films", *Appl. Phys. Lett.*, Vol. 29, pp. 118-120, 1976.

[16] C. Weissmantel, *Thin Film Solids*, Vol. 63, pp. 315, 1979.

[17] J. C. Angus, P. Koidl and S. Domitz, "Plasma deposited thin films", Ed J. Mort (CRC Press), 1986.

[18] P. Koidl, C. Wild, B. Dischler, J. Wagner and M. Ramsteiner, *Mat Sci Forum*, Vol. 51, pp. 41, 1990.

[19] J. C. Angus and C. C. Hayman, *Science* Vol. 241, pp. 913, 1988.

[20] J. C. Angus, "Amorphous hydrogenated carbon films", ed P. Koidl and P. Oelhafen, *Proc EMRS*, Vo. 17, pp. 179 (Les Editions de Physique, Paris, 1987).

[21] J. Robertson and E. P. O'Reilly, "Electronic and atomic structure of amorphous carbon", *Phys. Rev. B*, Vol. 35, pp. 2946–2957, 1987.

[22] B. Meyerson and F. W. Smith, *Solid State Commun*, Vol. 34, pp. 531, 1980.

[23] W. E. Spear and P. G. LeComber, *Solid State Commun*, Vol. 17, pp. 1193, 1976.

[24] D. I. Jones and A. D. Stewart, *Phil Mag B*, Vol. 46, pp. 423, 1982.

[25] O. Amir and R. Kalish, "Properties of nitrogen-doped amorphous hydrogenated carbon films", *J Appl Phys*, Vol. 70, pp. 4958-4962, 1991.

[26] S. Orzeszko, W. Bala, F. Fabisiak and F. Rozploch, *Phys Stat Solidi*, Vol. 81, pp. 579, 1984.

[27] J. Hauser, *J Non-Cryst Solids*, Vol. 23, pp. 21, 1977.

[28] N. Wada, P. J. Gaczi and S. A. Solin, *J Non-Cryst Solids*, Vol. 35, pp. 543, 1980.

[29] H. Pan, M. Pruski, B. C. Gerstein, F. Li and J. S. Lannin "Local coordination of carbon atoms in amorphous carbon", Phys. Rev. B, Vol. 44, pp. 6741–6745, 1991.

[30] D. Dasgupta, F. Demichelis, C. F. Pirri, and A. Tagliaferro, "pi bands and gap states from optical absorption and electron-spin-resonance studies on amorphous carbon and amorphous hydrogenated carbon films", Phys. Rev. B Vol. 43, pp. 2131–2135, 1991.

[31] M. Vogel, O. Stenzel, R. Petrich, G. Schaarschmidt and W. Scharff, "The position of the fundamental absorption edge and activation energies for thermally activated electrical conductivity in amorphous carbon layers", *Thin Solid Films*, Vol. 227, pp. 74-89, 1992.

[32] M. Vogel, O. Stenzel, W. Gruenewald and A. Barna, *Thin Solid Films*, Vol. 209, pp. 195, 1992.

[33] J. Ullmann and G. Schimdt, *Diamond Relat. Mater.*, Vol. 1, pp. 321, 1992.

[34] V. S. Veerasamy, G. A. J. Amaratunga, C. A. Davis, W. I. Milnes and P. Hewitt, "Electronic density of states in Highly tetrahedral amorphous carbon", *Solid-State Electronics*, Vol. 37, No. 2, pp 319-326, 1994.

[35] R. Zeisel, H. Sternschulte, C. E. Nebel and M. Stutzmann, "Characterization of implantation damage in semiconducting diamond", *Appl. Phys. Lett.*, Vol. 74, pp. 1875-1876, 1999.

[36] E. Liu, X. Shi, L. K. Cheah, Y. H. Hu, H. S. Tan, J. R. Shi, B. K. Tay, "Electrical behaviour of metal/tetrahedral amorphous carbon/metal structure", Solid-State Electronics, Vol. 43, pp. 427-434, 1999.

[37] V. S. Veerasamy, J. Yuan, G. A. J. Amaratunga, W. I. Milnes, K. W. R. Gilkes, M. Weiler and L. M. Brown, "Nitrogen doping of highly tetrahedral amorphous carbon", *Physical Review B*, Vol. 48, No. 24, pp. 954-959, 1993.

[38] M. Weiler, S. Sattal, T. Giessen, K. Jung and H. Ehrhard, "Preparation and properties of highly tetrahedral hydrogen doped amorphous carbon", *Physical Review B.*, Vol. 53, No. 3, pp. 1594-1608, 1996.

[39] K. Mukhopadhyay, K. M. Krisna and M. Sharon, "Fullerencs from camphor: A natural source", *Phys. Rev. Lett.*, Vol. 72, pp. 3182-3185, 1994.

[40] M. Sharon, K. Mukhopadhyay, I. Mukhopadhyay and K. M. Krisna, *Carbon*, Vol. 34, pp. 251, 1996.

[41] N. Savvides and B. Window, *J. Vac. Sci. Technol.*, Vol. A3, pp. 2386, 1985.

[42] M. C. Polo, J. Cifre, G. Sánchez, R. Aguiar, M. Varela, and J. Esteve, "Pulsed laser deposition of diamond from graphite targets", *Appl. Phys. Lett.*, Volume 67, Issue 4, pp. 485-487, 1995.

[43] S. M. Mominuzzaman, T. Soga, T. Jimbo and M. Umeno, "Camphoric carbon soot: a new target for deposition of diamond-like carbon films by pulsed laser ablation", *Thin Solid Films*, Vol. 376, pp. 1-4, 2000.

[44] S. M. Mominuzzaman, H. Ebishu, T. Soga, T. Jimbo and M. Umeno, "Phosphorus doping and defect studies of diamond like carbon films by pulsed laser deposition using camphoric carbon target", *Diamond and related materials*, Vol. 10, pp. 984-988, 2001.

[45] C. Z. Wang and K. M. Ho, "The electronic structure of diamond-like amorphous carbon", *J. Phys. Condens. Matter*, Vol. 6, pp. L239, 1994.

[46] W. Shockley, *U.S. Patent 2*, Vol. 569, pp. 347, 1951.

[47] H. Kroemer, "Theory of a Wide-gap emitter for transistors", *Proc. IRE*, Vol. 45, pp. 1535, 1957.

[48] W. G. Oldham and A. G. Milnes, "Interface states in abrupt semiconductor heterojunctions", *Solid State Electron.*, Vol. 7, pp. 153, 1964.

[49] R. L. Anderson, "Experiments on Ge-GaAs heterojunctions", *Solid-State Electronics*, Vol. 5, pp. 341-351, 1962.

[50] J. P Donnelly and A. G. Milnes, "The capacitance of p-n heterojunctions including the effects of interface states", *IEEE Transactions on Electron devices*, Vol. ED-14, No. 2, pp. 63-68, 1967.

[51] G. A. J. Amaratunga, V. S. Veerasamy, C. A. Davis and et al., *J. Non-Cryst. Solids*, Vol. 164, pp. 1119, 1993.

[52] M. Alaluf, L. Klibanov and N. Croitoru, *Diamond Related Mater.*, Vol. 5, pp. 1497, 1996.

[53] L. K. Cheah, X. Shi, J. R. Shi, E. J. Liu and S. R. P. Silva, *J. Non-Cryst. Solids*, Vol. 242, pp. 40, 1998.

[54] D. Chen, A. Wei, S. P. Wong and S. Peng, *Diamond Related Mater.*, Vol. 8, pp. 1130, 1999.

[55] M. T. Kuo, P. W. May, A. Gunn, M. N. R. Ashfold and R. K. Wild, *Diamond Related Mater.*, Vol. 9, pp. 1222, 2000.

[56] Experimental data of n-DLC/p-Si heterojunction obtained from "Soga Laboratory", Department of Electrical and Electronic Engineering. Nagoya Institute of technology, Japan.

[57] Md. Shofiqul Islam, "Spectral photoresponse characteristics of n-carbon/p-silicon heterostructure", M.Sc. Engg Thesis, pp. 48-54, Department of Electrical and Electronic Engineering, Bangladesh University of Engineering and Technology, 2002.

[58] V. S. Veerasamy and J. Robertson, "Preparation and properties of highly tetrahedral hydrogenated amorphous carbon", *Physical Review B*, Vol. 53, No. 3, pp. 1594-1608, 1996.

[59] J. J. Hauser, *J. Non-Cryst Solids*, Vol. 23, pp. 21, 1977.

[60] M. Balsi, I. Ciancaglioni, V. Cimagalli, F. Galluzzi, "Optoelectronic Cellular Neural Networks Based on Amorphous Silicon Thin Film Technology", *Proc. of Third IEEE Int. Workshop on Cellular Neural Networks and their Applications (CNNA-94)*, Rome, Italy, Dec. 18-21, 1994, pp. 399-403.

[61] J. L. Moll, "The evaluation of the theory of the current-voltage characteristics of p-n junctions", *Proc IRE*, Vol. 46, pp. 1076, 1958.

[62] K. C. Palinginis, A. Ilie, B. Kleinsorge, W. I. Milnes and J. D. Cohen, "Characterization of tetrahedrally bonded amorphous carbon via capacitance techniques", *Mat. Res. Soc. Symp. Proc.*, Vol. 508, pp. 197-202, 1998.

[63] S.M. Sze, "Physics of Semiconductor Devices", Wiley Eastern Limited, New Delhi, India, 1979.